UNIVERSITY OF MICHIGAN
AUG 14 1951
ENGINEERING LIBRARY

JOURNAL OF THE AERONAUTICAL SCIENCES

VOLUME 18 AUGUST, 1951 NUMBER 8

CONTENTS

Nonsteady Supersonic Flow About Pointed Bodies of Revolution.....WILLIAM H. DORRANCE 505

Determination of Rocket-Motor Heat-Transfer Coefficients by the Transient Method.....STANLEY GREENFIELD 512

Aerodynamics of a Supersonic Rectangular Wing Striking a Sharp-Edged Gust.....THEODORE R. GOODMAN 519

Similarity Laws for Slender Bodies of Revolution in Hypersonic Flows.....STANFORD E. NEICE AND DORRIS M. EHRET 527

A Superposition Method for Calculating the Aeroelastic Behavior of Swept Wings.....R. B. BROWN, K. F. HOLTBY, AND H. C. MARTIN 531

Transient Loading of Wide Delta Airfoils at Supersonic Speeds.....JOHN W. MILES 543

Comparison of Theoretical and Experimental Results for the Turbulent Boundary Layer in Supersonic Flow Along a Flat Plate.....CARLO FERRARI 555

Readers' Forum: "Turbulent Diffusion from a Source in Turbulent Shear Flow," by J. O. Hinze; "Note on Sphere Drag Data," by Frederick S. Sherman; "Effective End Restraint of Columns by Frequency Measurements," by Harold Lurie; "Comment on the Calculation of Deflections of Indeterminate Structures," by Carlos Thalau; "Note on 'Heat Transfer by Laminar Flow from a Rotating Plate,'" by Arthur N. Tifford.....565–568

Published by the

INSTITUTE OF THE AERONAUTICAL SCIENCES, INC.

JOURNAL OF THE AERONAUTICAL SCIENCES

Editor: HUGH L. DRYDEN, *Director, N.A.C.A.*

Associate Editor: ROBERT R. DEXTER *Managing Editor:* BERNEICE H. JARCK

Editorial Committee

Aerodynamics

Francis Clauser
Howard Emmons
R. Paul Harrington
R. T. Jones
Carl Kaplan
W. B. Klemperer
John G. Lee
H. W. Liepmann
C. C. Lin
H. F. Ludloff
John R. Markham
Clark B. Millikan
Shatswell Ober
W. Bailey Oswald
Allen E. Puckett
Elliott G. Reid
H. J. F. Reid
Russell Robinson
G. B. Schubauer
W. R. Sears
John Stack
Theodore von Kármán
Richard von Mises

Flight Testing

W. K. Ebel
R. R. Gilruth
Melvin N. Gough
Robert Stanley
E. G. Stout

Meteorology

C. F. Brooks
D. M. Little
E. J. Minser
F. W. Reichelderfer
H. C. Willett

Structures and Materials

W. B. Bleakney
E. W. Conlon
J. P. Den Hartog
L. H. Donnell
E. C. Hartmann
N. J. Hoff
E. E. Lundquist
C. F. Nagel, Jr.
J. S. Newell
Alfred S. Niles
W. Ramberg
E. Reissner
F. R. Shanley
H. W. Sibert
C. R. Strang
S. Timoshenko
H. S. Tsien
Chi-Teh Wang

Rotating Wing Aircraft

Robert Coleman
K. H. Hohenemser
Bartram Kelley
Ralph McClarren
R. H. Miller
R. H. Prewitt
Igor I. Sikorsky

Physiologic Problems

H. G. Armstrong
Louis H. Bauer
Eugene Du Bois
W. Randolph Lovelace, II
Ross A. MacFarland
A. D. Tuttle

Flight Propulsion

George W. Brady
Frank W. Caldwell
L. S. Hobbs
E. E. Johnson
Joseph Keenan
R. P. Kroon
Arthur Nutt
Hans Reissner
Abe Silverstein
C. Fayette Taylor
E. S. Taylor
P. Taylor
E. S. Thompson
H. S. Tsien

Aircraft Design

W. E. Beall
W. K. Ebel
Hall L. Hibbard
Richard Hutton
C. L. Johnson
I. M. Laddon
C. J. McCarthy
Fred E. Weick
Robert J. Woods

Air Transport

Charles Froesch
J. A. Herlihy
R. D. Kelly
Otto E. Kirchner
Jerome Lederer
John C. Leslie
R. Dixon Speas

Instruments

Allan G. Binnie
W. G. Brombacher
Charles H. Colvin
B. M. Craig
C. S. Draper
S. G. Eskin
O. E. Esval
W. L. Howland
George H. Purcell
C. F. Savage
O. Hugo Schuck
L. N. Schwien
C. L. Seward, Jr.
L. D. Statham
R. C. Sylvander
D. K. Warner
P. F. Weber
Elmer P. Wheaton

Vibration and Flutter

Lee Arnold
M. A. Biot
William Bollay
Chieh-Chien Chang
Martin Goland
J. P. Den Hartog

Fuels and Oils

D. P. Barnard
J. H. Doolittle
Graham Edgar
R. T. Goodwin
S. D. Heron
A. M. Rothrock

SUBSCRIPTION RATES

JOURNAL OF THE AERONAUTICAL SCIENCES, Published Monthly.—United States and Possessions: 1 Year, $12.00; Single Copies, $1.50. Foreign Countries Including Canada (American Currency Rate): 1 Year, $13.00; Single Copies, $1.50.

AERONAUTICAL ENGINEERING REVIEW, Published Monthly.—United States and Possessions: 1 Year, $3.00; Single Copies, $0.50. Foreign Countries Including Canada (American Currency Rates): 1 Year, $3.50; Single Copies, $0.50.

Notices of change of address should be sent to the Institute at least 30 days prior to actual change of address.

Manuscripts for publication, proofs, and all correspondence should be addressed to the Editorial Office of the JOURNAL.

Correspondence regarding subscriptions may be addressed to Publication Office, 20th and Northampton Sts., Easton, Pa., or to the Editorial Office of the JOURNAL OF THE AERONAUTICAL SCIENCES, 2 East 64th Street, New York 21, New York.

Copyright, 1951, by the Institute of the Aeronautical Sciences, Inc.

Entered as Second Class Matter at the Post Office, Easton, Pa., May 1, 1937. Acceptance for mailing at a special rate of Postage provided for in the Act of August 24, 1912. Authorized April 29, 1937.

JOURNAL OF THE AERONAUTICAL SCIENCES

VOLUME 18 AUGUST, 1951 NUMBER 8

Nonsteady Supersonic Flow About Pointed Bodies of Revolution

WILLIAM H. DORRANCE*

University of Michigan, Willow Run Research Center

(I) Summary

The general velocity potential for a slender pointed body of revolution oscillating periodically in a supersonic uniform stream is presented. The solution is shown to reduce in the limit to the sum of the well-known stationary source-sink and doublet solutions when the frequency of oscillation approaches zero. Stability derivatives for low-frequency oscillations are determined by making use of the potential expression obtained by expanding the oscillating velocity potential in powers of reduced frequency, retaining only the first-order terms in reduced frequency. In particular, the following four cases of steady and nonsteady supersonic motion are treated: (1) harmonic pitching about a point x_0; (2) harmonic normal oscillations in pitch; (3) steady pitching about a point x_0; and (4) steady angle of attack. Equations for the slender body theory normal force and pitching moment stability derivatives are also determined.

Two types of bodies of revolution are examined to demonstrate how the aerodynamic stability derivates may be varied by changing the contour of the body. "Flaring" the aft end of the body is shown to increase the lift, as well to increase the aerodynamic damping moment of a finless body.

(II) Symbols and Nomenclature

c = local velocity of sound

C_n = normal force coefficient

$C_m q_0 SL$ = pitching moment about x_0 (positive in stall)

$C_{n_{\dot\alpha}}, C_{m_{\dot\alpha}}$ = $\partial C_n/\partial(\dot\alpha L/U_0), \partial C_m/\partial(\dot\alpha L/U_0)$ [dimensionless nonsteady pitching stability derivatives]

$C_{n_{\dot w}}, C_{m_{\dot w}}$ = $\partial C_n/\partial(\dot w L/U_0^2), \partial C_m/\partial(\dot w L/U_0^2)$ [dimensionless normal acceleration stability derivatives]

C_{n_q}, C_{m_q} = $\partial C_n/\partial(qL/U_0), \partial C_m/\partial(qL/U_0)$ [dimensionless steady pitching stability derivatives]

$C_{n_\alpha}, C_{m_\alpha}$ = $\partial C_n/\partial\alpha, \partial C_m/\partial\alpha$ [steady aerodynamic coefficients]

C_p = $-2[(\varphi_{2x}/U_0) + (\varphi_{2t}/U_0^2)]$ [incremental lifting pressure coefficient]

$\overline{f(s)}$ = $\int_0^\infty \exp\{-sx\} f(x)\,dx$ [Laplace transform of $f(x)$]

$K_0(z)$ = modified Bessel function of second kind with modulus z

k = $(M/\beta)(\omega r/U_0)$ [reduced frequency]

L = length of body of revolution

M = free-stream Mach Number

p = local static pressure

q_0 = free-stream dynamic pressure

q = steady pitching velocity (Fig. 2c)

$R(x)$ = locus of surface of body of revolution

S = reference area

$S(x)$ = cross-sectional area of body of revolution at station x

t = time, sec.

U_0 = free-stream speed

$\vec{V}$ = local velocity

$w(x, t)$ = upwash velocity (Fig. 1)

x_0 = center of rotation of pitching motion

x, r, θ = cylindrical coordinates

X, Y, Z = body stability axes through x_0

α = angle of attack

β = $\sqrt{M^2 - 1}$ compressibility parameter

γ = ratio of specific heats

φ_0 = free stream velocity potential

$\varphi, \varphi_1, \varphi_2$ = perturbation velocity potentials

Φ = total velocity potential

ω = frequency of periodic motion

(III) Introduction

Attention has been directed lately to the problem of dynamic stability of low aspect ratio high-speed aircraft.[1, 2] The problem of determining the static and dynamic aerodynamic force and moment stability derivatives of low aspect ratio wings at supersonic speeds has been treated by many investigators.[3–9] Little consideration beyond first approximations has been given to the corresponding problems for bodies of revolution.[10] The dynamic stability derivatives for such bodies become of prime importance for finless missiles and missile configurations having relatively low area, low aspect ratio surfaces.

It is the purpose of this paper to present the general potential for the harmonic motion of a slender pointed body of revolution in a steady supersonic stream. Fol-

Received November 20, 1950. Revised and received March 2, 1951.

* Aerodynamics Group Leader.

lowing this, the doublet potential for low-frequency harmonic oscillations is demonstrated. The slender body theory doublet potentials are also determined. Example solutions for a body of revolution are calculated to illustrate the variation of the stability derivatives with Mach Number in a limited supersonic Mach Number range. It is shown how the stability derivatives can be modified considerably by varying the contour of the body of revolution.

The solutions for steady pitching and steady angle of attack are also presented for comparison purposes.

(IV) Fundamental Solutions

The well-known linearized potential equation for compressible nonsteady flow is, in cylindrical coordinates (Fig. 1),

$$\beta^2\varphi_{xx} - \varphi_{rr} - \frac{1}{r^2}\varphi_{\theta\theta} - \frac{1}{r}\varphi_r + \frac{1}{c^2}\varphi_{tt} + \frac{2M}{c}\varphi_{xt} = 0 \quad (1)$$

The solutions with which this paper is concerned will satisfy Eq. (1). As such, these solutions are all subject to the usual limitations of the linearized theory. The solution sought in this paper is

$$\varphi_2 = \varphi_1 \cos\theta \quad (2)$$

where φ_1 is the solution to the equation

$$\beta^2\varphi_{xx} - \varphi_{rr} - \frac{1}{r}\varphi_r + \frac{1}{c^2}\varphi_{tt} + \frac{2M}{c}\varphi_{xt} = 0 \quad (3)$$

Direct substitution of Eq. (2) into Eq. (1) will verify this. Here, the perturbation potential representing the body is composed of

$$\varphi = \varphi_1 + \varphi_2 \quad (4)$$

The potential φ_1 is axially symmetric with respect to the x-axis and cannot yield "lifting" velocity perturbations (except as a product with the φ_2 potential velocity perturbations). The potential φ_2, being odd with respect to the plane $\theta = \pi/2$, will yield the desired lifting velocity perturbations.

(*a*) *The Nonsteady Source-Sink Potential*

Let

$$\varphi_1 = -\eta(x, r) \exp\left\{i\omega[t - (Mx/c\beta^2)]\right\} \quad (5)$$

in Eq. (3). There results

$$\eta_{rr} + \frac{1}{r}\eta_r - \beta^2\eta_{xx} - \frac{\omega^2}{c^2\beta^4}\eta = 0 \quad (6)$$

Further, make use of the Laplace transformation, and let

$$\overline{\eta(s, r)} = \int_0^\infty \exp\left\{-sx\right\} \eta(x, r)dx \quad (7)$$

If

$$\eta(0, r) = (\partial\eta/\partial x)\ (0, r) \equiv 0$$

appropriate to pointed bodies, operating upon Eq. (6) with Eq. (7) yields

$$\frac{d^2\bar{\eta}}{dr^2} + \frac{1}{r}\frac{d\bar{\eta}}{dr} - \beta^2\left(s^2 + \frac{\omega^2}{c^2\beta^4}\right)\bar{\eta} = 0 \quad (8)$$

The desired solution to Eq. (8) is the modified Bessel function of the second kind.

$$\bar{\eta} = K_0\left\{\beta r[s^2 + (\omega^2/c^2\beta^4)]^{1/2}\right\} \quad (9)$$

Using transform pair (871.5) of reference 11 we obtain

$$\left.\begin{aligned}\eta(x, r) = \frac{\cos\left[(\omega/c\beta^2)\ (x^2 - \beta^2r^2)^{1/2}\right]}{(x^2 - \beta^2r^2)^{1/2}}\\ x - \beta r > 0\end{aligned}\right\} \quad (10)$$

The point source solution to Eq. (3) is obtained through Eqs. (5) and (10).

$$\left.\begin{aligned}\varphi_1 = -\frac{\exp\left\{i\omega\ [t - (Mx/c\beta^2)]\right\} \cos\left[(\omega/c\beta^2)\ (x^2 - \beta^2r^2)^{1/2}\right]}{(x^2 - \beta^2r^2)^{1/2}}\\ x - \beta r > 0\end{aligned}\right\} \quad (11)$$

If the sources are distributed along the x-axis at points ξ according to $f(\xi)$, then Eq. (11) becomes

$$\left.\begin{aligned}\varphi_1 = -\exp\left\{i\omega t\right\} \int_0^{x-\beta r} \frac{f(\xi) \exp\left\{-\dfrac{i\omega M}{c\beta^2}(x - \xi)\right\} \cos\left\{\dfrac{\omega}{c\beta^2}\left[(x - \xi)^2 - \beta^2r^2\right]^{1/2}\right\} d\xi}{\left[(x - \xi)^2 - \beta^2r^2\right]^{1/2}}\\ x - \beta r > \xi\end{aligned}\right\} \quad (12)$$

If $\omega = 0$, as in the steady source-sink solution, then Eq. (12) becomes the easily recognized form

$$\varphi_1 = -\int_0^{x-\beta r} \frac{f(\xi)d\xi}{\left[(x - \xi)^2 - \beta^2r^2\right]^{1/2}} \qquad x - \beta r > \xi \quad (13)$$

(*b*) *The Nonsteady "Doublet" Potential*

Eqs. (2) and (12) are now employed to obtain the desired supersonic nonsteady doublet potential. This differentiation is accomplished by first substituting

$$u = \cosh^{-1}[(x - \xi)/\beta r]$$

to eliminate the improper integral, which is then easily differentiated and results in Eq. (24). This may be converted to the original form by

$$\xi = x - \beta r \cosh u$$

so that the resulting doublet potential is

$$\varphi_2 = \exp\{i\omega t\} \cos\theta \left\{ \frac{\omega}{rc\beta^2} \int_0^{x-\beta r} f(\xi) \exp\left\{ -\frac{i\omega M}{c\beta^2}(x-\xi) \right\} \sin\left\{ \frac{\omega}{c\beta^2}[(x-\xi)^2 - \beta^2 r^2]^{1/2} \right\} d\xi + \right.$$
$$\int_0^{x-\beta r} \frac{f'(\xi)(x-\xi) \exp\left\{ -\frac{i\omega M}{c\beta^2}(x-\xi) \right\} \cos\left\{ \frac{\omega}{c\beta^2}[(x-\xi)^2 - \beta^2 r^2]^{1/2} \right\} d\xi}{r[(x-\xi)^2 - \beta^2 r^2]^{1/2}} +$$
$$\left. \frac{i\omega M}{c\beta^2 r} \int_0^{x-\beta r} \frac{f(\xi)(x-\xi) \exp\left\{ -\frac{i\omega M}{c\beta^2}(x-\xi) \right\} \cos\left\{ \frac{\omega}{c\beta^2}[(x-\xi)^2 - \beta^2 r^2]^{1/2} \right\} d\xi}{[(x-\xi)^2 - \beta^2 r^2]^{1/2}} \right\} \quad (14)$$

If, in Eq. (14), $\omega = 0$, the recognized steady doublet potential results:

$$\varphi_2 = \frac{\cos\theta}{r} \left\{ \int_0^{x-\beta r} \frac{f'(\xi)(x-\xi)d\xi}{[(x-\xi)^2 - \beta^2 r^2]^{1/2}} \right\} \quad (15)$$
$$x - \beta r > \xi$$

Eq. (14) is the desired nonsteady doublet solution to Eq. (1). The balance of this paper will be devoted to presenting particular solutions to Eq. (1) appropriate to: (1) harmonic pitching about a point x_0; (2) harmonic normal oscillations in pitch; (3) steady pitching about a point x_0; and (4) steady angle of attack. All of these situations can be treated by making use of Eq. (14) and its derivatives.

(*c*) *Boundary Conditions*

The boundary conditions for the steady or nonsteady supersonic flow about a body of revolution specify that the velocity component normal to the surface of the body at the surface must be zero. That is, if

$$r = R(x) \qquad (0 \leqq x \leqq L) \quad (16)$$

is the locus of the surface of the body in all meridian planes, then the boundary condition is (Fig. 1)

$$(\partial\varphi_2/\partial r)_{r=R\to 0} = -w(x, t) \cos\theta \quad (17)$$

in general. Eq. (17) takes a different form for each of the four steady and nonsteady motions previously mentioned.

(*1*) *Harmonic Pitching About the Point* x_0.—In this case

$$\alpha(t) = \alpha_0 \exp\{i\omega t\}$$

and from Fig. 2a and Eq. (17)

$$\left(\frac{\partial\varphi_2}{\partial r}\right)_{R\to 0} = -\{U_0\alpha_0 + i\omega(x - x_0)\alpha_0\} \exp\{i\omega t\} \cos\theta \quad (18a)$$

(*2*) *Harmonic Normal Oscillations in Pitch.*—From Fig. 2b and Eq. (17),

$$(\partial\varphi_2/\partial r)_{R\to 0} = -w_0 \exp\{i\omega t\} \cos\theta \quad (18b)$$

(*3*) *Steady Pitching About the Point* x_0.—From Fig. 2c and Eq. (17),

$$(\partial\varphi_2/\partial r)_{R\to 0} = -\alpha_0 U_0 \cos\theta - q(x - x_0) \cos\theta \quad (18c)$$

The capital letters X and Z in Fig. 2c denote the body stability axes. The point x_0 is the center of gravity, and the steady pitching velocity is taken in the conventionally defined sense.

(*4*) *Steady Angle of Attack.*—From Fig. 2d and Eq. (17),

$$(\partial\varphi_2/\partial r)_{R\to 0} = -U_0 \alpha \cos\theta \quad (18d)$$

This case has been treated in the literature[12, 13] and will not be dwelt upon in any great detail in this paper other than to compare it with the other solutions.

Eqs. (14) and (15), together with Eq. (18), are now used to specify the function $f(\xi)$. The value of $(\partial\varphi_2 \div \partial r)_{R\to 0}$ is obtained by the same limiting process as in references 12 and 13 so that

$$(\partial\varphi_2/\partial r)_{R\to 0} = [-f(x)/R^2] \exp\{i\omega t\} \cos\theta \quad (19)$$

The function $f(\xi)$ is now determined through Eqs. (18) and (19) for all of the cases treated in this paper.

(V) Normal Force and Pitching Moment Coefficients

The steady and nonsteady pressure coefficients can be obtained from the general Bernoulli equation,

$$\Phi_t + \frac{V^2}{2} + \int_{p_T}^{p} \frac{dp}{\rho} = F(t)$$

$\Phi = \varphi_0 + \varphi_1 + \varphi_2$ is substituted into the Bernoulli equation, and terms are dropped in keeping with the process used to obtain Eq. (1). Keeping only terms odd with respect to the plane $\theta = \pi/2$ results in the approximate "lifting" pressure coefficient,

$$C_p = -2\left[(\varphi_{2_x}/U_0) + (\varphi_{2_t}/U_0^2)\right] \tag{20}$$

If normal force coefficient and moment coefficient are defined as

$$C_n = \frac{-2}{S}\int_0^L \int_0^\pi C_p R \cos\theta \, d\theta \, dx$$

and

$$C_m = \frac{-2}{SL}\int_0^L \int_0^\pi C_p \, R(x_0 - x)\cos\theta \, d\theta \, dx$$

because C_p is proportional to $\cos\theta$, it follows that

$$C_n = -\frac{\pi}{S}\int_0^L \left(\frac{C_p}{\cos\theta}\right) R \, dx \tag{21}$$

and

$$C_m = C_n \frac{x_0}{L} + \frac{\pi}{SL}\int_0^L \left(\frac{C_p}{\cos\theta}\right) Rx \, dx \tag{22}$$

we are now in a position to obtain the lift and pitching moment coefficients for the four motions discussed in Section (IV).

(VI) The Low-Frequency Oscillations and Steady Motion

The task of obtaining solutions for the nonsteady supersonic flow about bodies of revolution using Eq. (14) is simplified for the case of low-frequency oscillations. It can be shown by expanding Eq. (14) into powers of reduced frequency that, for harmonic frequencies of the order of $c\beta/L$, the nonsteady potential can be represented by the first-order terms in k with an error of about 5 per cent or less. For bodies of the order of 20 to 30 ft. in length in the Mach Number range of 1.5 to 2.5, the first-order terms in k in Eq. (14) would represent the nonsteady potential for harmonic frequencies of the order of 35 to 115 rad. per sec. within about 5 per cent. Before proceeding to this expansion process, circumvent the improper integrals in Eq. (14) by introducing the dummy variable u through the substitution

$$\cosh u = (x - \xi)/\beta r \tag{23}$$

If Eq. (23) is substituted into Eq. (14), there results

$$\varphi_2 = -\cos\theta \exp\{i\omega t\}\left[\beta \int_{\cosh^{-1}(x/\beta r)}^{0} f'(x - \beta r\cosh u)\exp\left\{\frac{-i\omega M r}{c\beta}\cosh u\right\}\cos\left(\frac{\omega r}{c\beta}\sinh u\right)\cosh u \, du + \right.$$
$$\frac{\omega}{c\beta}\int_{\cosh^{-1}(x/\beta r)}^{0} f(x - \beta r\cosh u)\exp\left\{\frac{-i\omega M r}{c\beta}\cosh u\right\}\sin\left(\frac{\omega r}{c\beta}\sinh u\right)\sinh u \, du +$$
$$\left.\frac{i\omega M}{c\beta}\int_{\cosh^{-1}(x/\beta r)}^{0} f(x - \beta r\cosh u)\exp\left\{\frac{-i\omega M r}{c\beta}\cosh u\right\}\cos\left(\frac{\omega r}{c\beta}\sinh u\right)\cosh u \, du\right] \tag{24}$$

Carrying out the expansion into powers of k, we obtain

$$\varphi_2 = -\cos\theta \exp\{i\omega t\}\left[\beta\int_{\cosh^{-1}(x/\beta r)}^{0} f'(x - \beta r\cosh u)\cosh u \, du - iM\beta k \times \right.$$
$$\left.\int_{\cosh^{-1}(x/\beta r)}^{0} f'(x - \beta r\cosh u)\, du + 0(k^2)\right] \tag{25}$$

If $k = 0$ in Eq. (25), the well-known steady potential results,

$$\varphi_2 = -\beta\cos\theta\int_{\cosh^{-1}(x/\beta r)}^{0} f'(x - \beta r\cosh u)\cosh u \, du \tag{26}$$

Eqs. (25) and (26) will be used to obtain the four nonsteady and steady solutions with which we are concerned.

(*a*) *Harmonic Pitching About the Point* x_0

The equation for the distribution function $f(\xi)$ is obtained from Eqs. (18a) and (19),

$$f(\xi) = [S(\xi)/\pi]\,[U_0\alpha_0 + i\omega(x - x_0)\alpha_0] \tag{27}$$

Eq. (27) is substituted into Eq. (25) and Eq. (25) is substituted into Eq. (20) to obtain the pressure coefficient on the body.

$$C_p = \frac{2\cos\theta}{\pi}\left[\left(\alpha\beta - \frac{\beta\dot{\alpha}x_0}{U_0}\right)\frac{\partial I_1}{\partial x} + \frac{\dot{\alpha}\beta}{U_0}\frac{\partial I_2}{\partial x} + 2\frac{\dot{\alpha}\beta}{U_0}I_1 - \frac{\dot{\alpha}M^2R}{U_0}\frac{\partial I_4}{\partial x} + 0(k^2)\right] \tag{28}$$

The integrals I_n appearing in Eq. (28) are presented in the Appendix. These integrals will also appear in the remaining expressions for the steady and nonsteady pressure coefficients to be determined. Eq. (28) is now substituted into Eqs. (21) and (22) to obtain the desired derivatives,

$$C_{n\dot{\alpha}} = \frac{-2}{SL}\int_0^L \left[2\beta\left(I_1 + \frac{1}{2}\frac{\partial I_2}{\partial x}\right) - M^2R\frac{\partial I_4}{\partial x} - \beta x_0\frac{\partial I_1}{\partial x}\right]R\,dx \tag{29}$$

$$C_{m\dot{\alpha}} = \frac{x_0}{L}C_{n\dot{\alpha}} + \frac{2}{SL^2}\int_0^L \left[2\beta\left(I_1 + \frac{1}{2}\frac{\partial I_2}{\partial x}\right) - M^2R\frac{\partial I_4}{\partial x} - \beta x_0\frac{\partial I_1}{\partial x}\right]Rx\,dx \tag{30}$$

The slender body theory expression for pressure coefficient is obtained by substituting Eq. (18a) into Eq. (19) and integrating with respect to R to obtain $(\varphi_2)_{R\to 0}$. The resulting expression is then combined with Eqs. (20), (21), and (22) to obtain

$$C_{n\dot{\alpha}} = 2\frac{S(L)}{S}\left[\left(1 - \frac{x_0}{L}\right) + \frac{\text{vol.}}{LS(L)}\right] \tag{31}$$

and

$$C_{m\dot{\alpha}} = -2[S(L)/S]\,[1 - (x_0/L)]^2 \tag{32}$$

(*b*) ***Harmonic Normal Oscillations in Pitch***

From Eqs. (18b) and (19), we have

$$f(\xi) = [S(\xi)/\pi]\,w_0 \tag{33}$$

Eq. (33) is used in Eqs. (25), (20), (21), and (22), respectively, to yield

$$C_{n\dot{w}} = \frac{-2}{SL}\int_0^L \left(\beta I_1 - M^2R\frac{\partial I_4}{\partial x}\right)R\,dx \tag{34}$$

and

$$C_{m\dot{w}} = C_{n\dot{w}}\frac{x_0}{L} + \frac{2}{SL^2}\int_0^L \left(\beta I_1 - M^2R\frac{\partial I_4}{\partial x}\right)Rx\,dx \tag{35}$$

The corresponding slender body theory expressions are

$$C_{n\dot{w}} = 2(\text{vol.}/SL) \tag{36}$$

and

$$C_{m\dot{w}} = 2\frac{S(L)}{S}\left[\frac{x_0}{L}\frac{\text{vol.}}{S(L)L} - \frac{\int_0^L S(x)\,x\,dx}{L^2S(L)}\right] \tag{37}$$

(*c*) ***Steady Pitching About the Point*** x_0

Eqs. (18c) and (19) yield

$$f(\xi) = [S(\xi)/\pi]\,q(\xi - x_0) \tag{38}$$

Substitution of Eq. (38) into Eq. (26) and the resulting equation into Eq. (20) and thence to Eqs. (21) and (22) gives

$$C_{nq} = \frac{-2\beta}{SL}\int_0^L \left(I_1 + \frac{\partial I_2}{\partial x} - x_0\frac{\partial I_1}{\partial x}\right)R\,dx \tag{39}$$

and

$$C_{mq} = \frac{x_0}{L}C_{nq} + \frac{2\beta}{SL^2}\int_0^L \left(I_1 + \frac{\partial I_1}{\partial x} - x_0\frac{\partial I_1}{\partial x}\right)xR\,dx \tag{40}$$

The corresponding slender body theory expressions are

$$C_{nq} = 2[S(L)/S]\,[1 - (x_0/L)] \tag{41}$$

and

$$C_{mq} = -2\frac{S(L)}{S}\left[\left(1 - \frac{x_0}{L}\right)^2 + \frac{x_0}{L}\frac{\text{vol.}}{S(L)L} - \frac{\int_0^L S(x)\,x\,dx}{L^2S(L)}\right] \tag{42}$$

(*d*) ***Steady Angle of Attack***

From Eqs. (18d) and (19),

$$f(\xi) = [S(\xi)/\pi]\,U_0\alpha \tag{43}$$

Then, from Eqs. (43), (26), (20), (21), and (22),

$$C_{n\alpha} = \frac{-2\beta}{S}\int_0^L \left(\frac{\partial I_1}{\partial x}\right)R\,dx \tag{44}$$

$$C_{m\alpha} = \frac{x_0}{L}C_{n\alpha} + \frac{2\beta}{LS}\int_0^L \left(\frac{\partial I_1}{\partial x}\right)xR\,dx \tag{45}$$

The slender body theory results are

$$C_{n\alpha} = 2[S(L)/S] \tag{46}$$

and

$$C_{m\alpha} = 2\frac{S(L)}{S}\left[\frac{x_0}{L} + \frac{\text{vol.}}{LS(L)} - 1\right] \tag{47}$$

This completes the list of steady and nonsteady stability derivatives. These equations will be demonstrated in the next section for two different bodies of revolution.

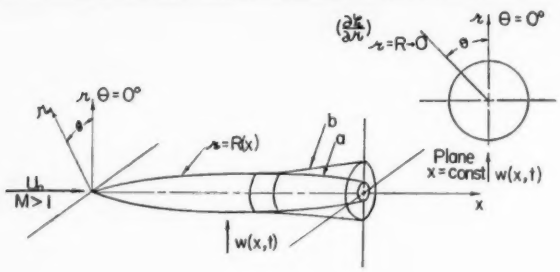

FIG. 1 CYLINDRICAL COORDINATES & ORIENTATION of BODY of REVOLUTION

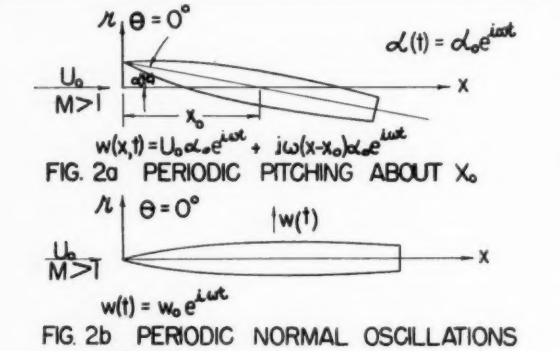

FIG. 2a PERIODIC PITCHING ABOUT X_0

FIG. 2b PERIODIC NORMAL OSCILLATIONS

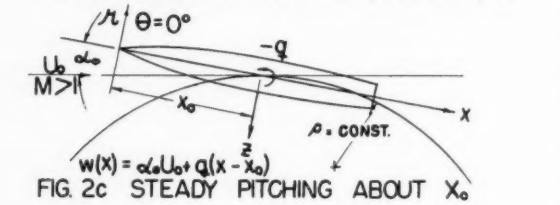

FIG. 2c STEADY PITCHING ABOUT X_0

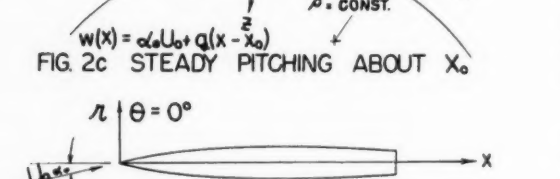

FIG. 2d STEADY ANGLE OF ATTACK

(VII) Example Results for Two Bodies of Revolution

The equations obtained in the previous section will now be applied to the two bodies shown in Fig. 1. The stability derivatives for body (a) of Fig. 1 will be obtained using both the first order in frequency equations and the slender body theory. Following this, it will be shown how modifying the shape of body (a) to body (b) changes the stability coefficients.

Body (a) of Fig. 1 is generated by revolving a parabolic arc about the x axis. The equation of this parabolic arc is

$$R = 0.02\,(10x - x^2) \qquad (0 \leqq x \leqq 8) \qquad (48)$$

Body (b) incorporates the nose of body (a) with a short cylindrical section and a slightly "flaring" rear section. The equations for the locus of the surface of body (b) are

$$R = 0.02(10x - x^2) \qquad (0 \leqq x \leqq 5) \quad (49a)$$

$$R = 0.50 \qquad (5 \leqq x \leqq 6) \quad (49b)$$

$$R = 0.08715x - 0.0229 \qquad (6 \leqq x \leqq 8) \quad (49c)$$

The point of rotation x_0 for the steady and nonsteady pitching derivative was taken to be $x_0 = 4.78$ for both bodies. This point was chosen as being typical for certain rocket-propelled missiles.

Fig. 3 presents the values of $C_{n\dot{\alpha}}$ and $C_{m\dot{\alpha}}$ for body (a) using Eqs. (29), (30), (31), and (32). The limitations of the slender body theory in predicting the magnitude and variation with Mach Number of these stability coefficients is apparent. This depends, of course, on the validity of the first order in frequency theory.

Figs. 4, 5, and 6 present values of $C_{n\dot{w}}$, $C_{m\dot{w}}$, $C_{n\alpha}$, $C_{m\alpha}$, C_{nq}, and C_{mq} for body (a) using both theories. The remarks above relative to the two theories also apply to these results.

An interesting result of these calculations is obtained by comparing Figs. 3 and 6, which present the nonsteady and steady pitching derivatives, respectively. In dynamic stability analyses the steady pitching derivatives C_{nq} and C_{mq} are often used rather than the nonsteady derivatives $C_{n\dot{\alpha}}$ and $C_{m\dot{\alpha}}$. If this procedure were followed for body (a), both the magnitudes of the derivatives and the variation of the pitching moment derivative with Mach Number would be in error in the Mach Number range of Figs. 3 and 6. In both cases, however, the sign of the pitching moment derivative is such as to indicate a damping moment due to a pitching angular velocity.

The slender body theory derivatives for both bodies are given in Table 1 and indicate qualitatively the effects of changing the shape of body (a) to that of body (b). All coefficients are based on the same reference area—the cross-sectional area at $x = 5$.

Table 1 shows that body (b) has increased lift over that of body (a). It is also apparent from the values of $C_{m\alpha}$ that the static center of pressure has moved rearward with changing body (a) to body (b). Thus, body

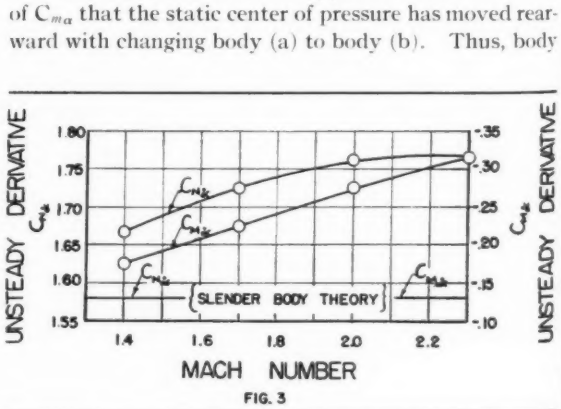

FIG. 3

(b) has an improved margin of static stability over that of body (a).

Both bodies possess steady and nonsteady damping in pitching about x_0. However, body (b) shows an increase in both C_{m_q} and $C_{m_{\dot{\alpha}}}$ over those values appropriate to body (a). Thus, body (b) has greater damping in pitch than body (a).

The above discussion indicates briefly how the aerodynamic properties of bodies of revolution can be modified by varying the shape of the body. In general, it can be stated that increasing the base area of a body of revolution will improve its steady and nonsteady lift and pitching moment characteristics in the supersonic range of Mach Numbers.

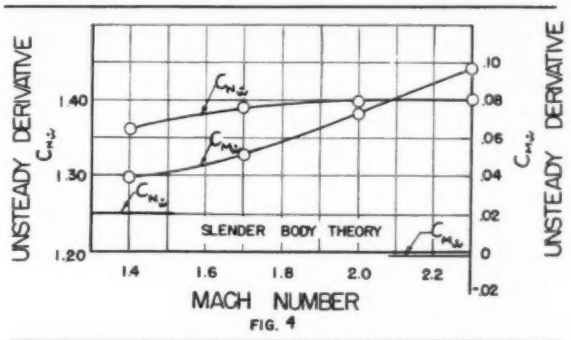

FIG. 4

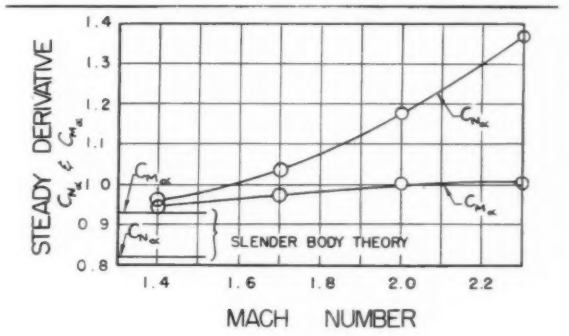

FIG. 5

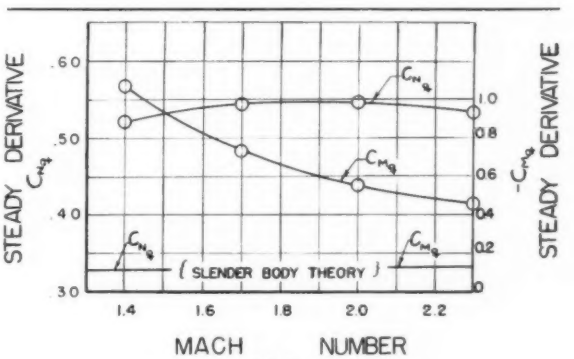

FIG. 6

(VIII) References

[1] Donovan, A. F., Flax, A. H., and Cheilek, H. A., *Stability and Control of Supersonic Aircraft*, Institute of the Aeronautical Sciences, Preprint No. 136, January, 1948.

[2] Mazurkiewicz, H. G., and Spath, R. M., *The Stability and Response of an Aerodynamic Missile in Plane Motion*, University of Michigan Memorandum No. 37, December, 1949.

[3] Ribner, H. S., *The Stability Derivatives of Low-Aspect-Ratio Triangular Wings at Subsonic and Supersonic Speeds*, N.A.C.A. T. N. No. 1423, 1947.

[4] Ribner, H. S., and Malvestuto, F. S., Jr., *Stability Derivatives of Triangular Wings at Supersonic Speeds*, N.A.C.A. T.N. No. 1572, 1948.

[5] Moeckel, W. E., and Evvard, J. C., *Load Distributions Due to Steady Roll and Pitch for Thin Wings at Supersonic Speeds*, N.A.C.A. T.N. No. 1689, 1948.

[6] Malvestuto, F. S., Jr., and Margolis, K., *Theoretical Stability Derivatives of Thin Sweptback Wings Tapered to a Point with Sweptback and Sweptforward Trailing Edges for a Limited Range of Supersonic Speeds*, N.A.C.A. T.N. No. 1761, 1949.

[7] Miles, J. W., *On Damping in Pitch for Delta Wings*, Journal of the Aeronautical Sciences, Vol. 16, No. 9, pp. 574–576, September, 1949.

[8] Moskowitz, B., and Moeckel, W. E., *First-Order Theory for Unsteady Motion of Thin Wings at Supersonic Speeds*, N.A.C.A. T.N. No. 2034, 1950.

[9] Stewart, H. J., and Li, Ting-Yi, *Periodic Motions of a Rectangular Wing Moving at Supersonic Speed*, Journal of the Aeronautical Sciences, Vol. 17, No. 9, pp. 529–539, September, 1950.

[10] Miles, J. W., *Unsteady Flow Theory in Dynamic Stability*, Readers' Forum, Journal of the Aeronautical Sciences, Vol. 17, No. 1, pp. 62–63, January, 1950.

[11] Campbell, G. A., and Foster, R. M., *Fourier Integrals for Practical Applications*, Bell Telephone System Technical Publications, Monograph B-584, p. 113, September, 1931.

[12] Tsien, H., *Supersonic Flow over an Inclined Body of Revolution*, Journal of the Aeronautical Sciences, Vol. 5, No. 12, pp. 480–484, October, 1938.

[13] Laitone, E. V., *The Linearized Subsonic and Supersonic Flow About Inclined Slender Bodies of Revolution*, Journal of the Aeronautical Sciences, Vol. 14, No. 11, pp. 631–642, November, 1947.

Appendix

The Integrals I_n (n = 1, 2, 3, 4) Appearing in the Steady and Nonsteady Pressure Coefficients

Certain integrals appear in any or all of the expressions for pressure coefficient derived in this paper. These integrals are:

(*Continued on page 542*)

Table 1
Slender Body Theory Stability Derivatives

Body	C_{n_α}	C_{m_α}	C_{n_q}	C_{m_q}	$C_{n_{\dot{\alpha}}}$	$C_{m_{\dot{\alpha}}}$	$C_{n_{\dot{\beta}}}$	$C_{m_{\dot{\beta}}}$
(a)	0.82	0.93	0.33	−0.13	1.58	−0.13	1.25	−0.002
(b)	3.63	0.15	1.47	−0.48	3.08	−0.59	1.61	−0.114

Determination of Rocket-Motor Heat-Transfer Coefficients by the Transient Method*

STANLEY GREENFIELD†
North American Aviation, Inc.

SUMMARY

An experimental procedure has been developed to measure gas-film heat-transfer coefficients in rocket-motor combustion chambers and nozzles. The procedure utilizes the transient temperature rise of the uncooled segmented walls of a rocket motor to determine the rate of heat transfer.

This "transient method" was used to determine axial variation of film heat-transfer coefficients of gases at temperatures up to 3,000°F. flowing through a de Laval-type supersonic nozzle at rates typical of rocket-motor operation. Experimentation results of 107 tests are presented.

Forty-nine tests were conducted with high-pressure air at 1,400°F. and at mass velocities varying between 1.4×10^5 and 6.8×10^5 lbs. per ft.^{2} hour. The remaining 58 tests were conducted on an oxygen-ethyl alcohol rocket motor of 1,000-lb. nominal thrust by passing the combustion gases through the test nozzle at flow rates of between 3.5×10^5 and 11.3×10^5 lbs. per ft.^{2} hour and at estimated temperatures of 3,000°F.

Experimental values of nozzle gas-film heat-transfer coefficients both for the rocket-motor and the lower temperature tests were satisfied by the relation

$$h_g = 0.029\,(G^{0.8}/D^{0.2})\,c_p u^{0.2}$$

NOMENCLATURE

- A = area (inside surface of nozzle segment), sq.ft.
- D = diameter (inside nozzle at segment axial midpoint), ft.
- G = mass velocity (at midpoint of segment), lbs. per ft.^{2} hour
- c_p = specific heat, B.t.u. per lb., °F.
- h = film heat-transfer coefficient, B.t.u. per ft.^{2} hour, °F.
- q = rate of heat flux per unit area, B.t.u. per ft.^{2} hour
- t = temperature, °F.
- θ = time, hours
- u = viscosity, combustion gases, lbs. per ft. hour
- L^* = characteristic chamber length; volume of the combustion chamber to the nozzle throat divided by the cross-section area of the throat, in.

Subscripts

- g = gas
- w = wall, inner segment
- a = average, segment

INTRODUCTION

AS THE FIELD OF ROCKET-MOTOR DESIGN advances from rule-of-thumb to a more scientific quantitative basis of calculation, the need is apparent for reliable engineering values of axial variation of gas-film heat-transfer coefficients over the motor internal surfaces.

Although several methods have been proposed for such measurements, two procedures appear to be used most frequently. The first of these requires careful measurement of the steady-state temperature rise of the motor coolant as it flows around a given area of motor wall. To observe axial variation of heat transfer, the chambers and nozzles are constructed in several short axial sections that are individually cooled. However, the increasingly difficult task of measuring precisely the small coolant temperature rise and our preliminary knowledge of the coolant-film heat-transfer coefficient limit this method as a means for calculating combustion gas-film coefficients.

The second procedure uses the difference of temperature at two or more precise points within the wall of the motor at the same instant of time, from which the heat-transfer rate and the gas-film heat-transfer coefficient may be calculated. The shortcomings of measuring accurately the temperature at a given point in a metal wall are well known in the field of pyrometry, and achievement of this goal represents a cardinal task.

A method of measuring the gas-film heat-transfer coefficient suggested by the work of London, Nottage, and Boelter[2] appeared to possess substantial advantage in its simplicity and direct approach. Briefly, these authors utilized the transient temperature decrease of a thermal capacitor discharging into a fluid stream to determine gas-film coefficients with results that were in substantial agreement with those obtained by means of other orthodox steady-state procedure.

Following this principle of the transient method, a procedure has been developed and a copper rocket-motor nozzle has been designed and fabricated for gas-film coefficient studies in a 1,000-lb. thrust rocket motor. The construction of the nozzle was such that it permitted measurements in five axial sections, and, in addition, with minor alterations, two to four circumferential positions could be evaluated in each axial section; a maximum of 20 measurements.

Presented at the 1950 Heat Transfer and Fluid Mechanics Institute, Los Angeles, June 28-30, 1950.

*The author wishes to express his thanks to Joseph Friedman, formerly of North American Aviation, Inc., for his assistance and guidance in the execution of this paper.

† Propulsion Specialist, Aerophysics Laboratory.

Prior to testing the heat-transfer nozzle (H.T.N.) on a rocket motor, it was felt desirable to check the various thermocouple installations and attendant instrumentation and to judge the efficacy of the transient method under similar yet more controllable flow conditions than those provided by the rocket motor. Therefore, a series of tests was made first on equipment that supplied heated, high-velocity air. The results of this lower temperature work served as a guide for the rocket-motor tests that followed.

Test Equipment

Heat-Transfer Nozzle (H.T.N.)

The copper nozzle, shown in Fig. 1, was designed and fabricated for installation on a liquid oxygen-ethyl alcohol, 1,000-lb. thrust rocket motor to measure gas-film heat-transfer coefficients at five positions along the axis of the nozzle.

From Fig. 2, it will be seen that the internal nozzle geometry for a 1,000-lb. thrust motor at 300 lbs. per sq. in. absolute chamber pressure was machined out of a bar of electrolytic copper, and five $^1/_{16}$-in. wide circumferential grooves were cut from the outside surface to within $^1/_4$ in. of the inside surface. These grooves acted as insulators between five rings of copper, which, in turn, served as thermal capacitors for the heat rejected to the inside surface by the rocket combustion gases.

A study of circumferential variation of the gas-film coefficients is possible by cutting these rings into circumferential segments; however, the scope of this work covers only the five axial segments described above.

The segmented nozzle was installed for test on two pieces of equipment which delivered gases at 1,400° and 3,000°F., respectively.

Low-Temperature Test Equipment

Heated, high-pressure air was furnished by the exhaust of a high-pressure kerosene-air burner, which ordinarily supplies the working fluid for a jet pump. This installation of the H.T.N. is shown in Figs. 3 and 4. Air, flowing at velocities varying between 1 and 3 lbs. per sec. at 80 to 100 lbs. per sq.in., was burned with ANF 58 (jet-engine fuel) to yield gases at a maximum temperature of 1,700° F. The flow of air was measured with a calibrated flat-plate orifice, and the flow of fuel was measured with a rotatmeter; the gas temperature was sensed by an unshielded chromel-alumel thermocouple placed at the centerline of the first straightening section (see Fig. 3).

During the first 37 tests, the straightening sections (15.7 in. in length and 3.3 in. inside diameter) were water-cooled. During the remaining twelve tests, the straightening sections were uncooled. They were fabricated from Type 347 stainless steel with $^1/_4$-in. thick cylindrical walls. No shielding or insulation was installed on these uncooled chambers.

Fig. 1. Copper segmented heat-transfer nozzle.

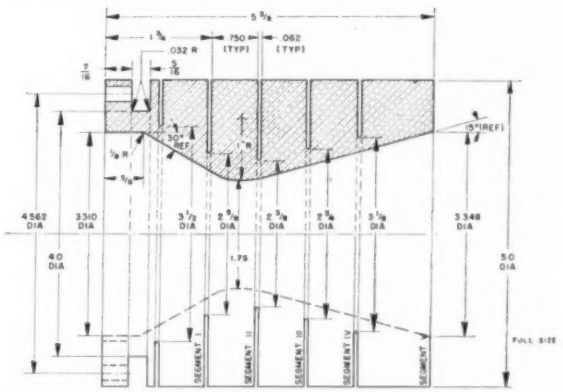

Fig. 2. Detailed cross section of the heat-transfer nozzle.

High-Temperature Test Equipment

A fixed injector and chamber configuration was used throughout the 58 rocket-motor tests. The propellants used were liquid oxygen and 92.5 per cent ethyl alcohol.

The injector was chosen for use in these tests from previous experience, which showed that average heat transfer to the nozzle, reproducible performance between runs at the same mixture ratio, and smooth burning through a wide range of mixture ratios and motor L^* could be expected. The specific thrust at

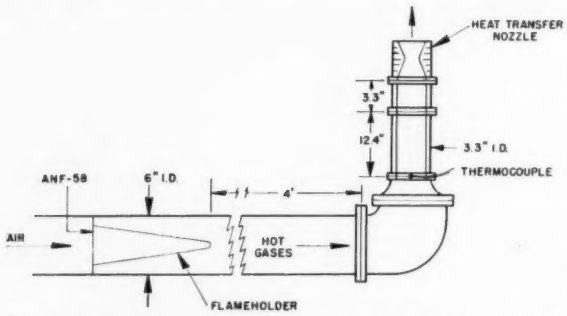

FIG. 3. Diagrammatic sketch of segmented nozzle installation for operation at low temperature.

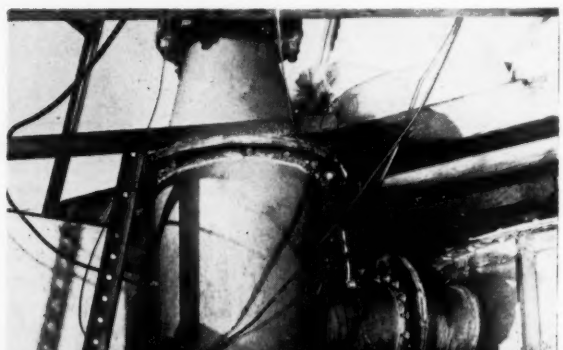

FIG. 4. View of equipment for low-temperature tests.

300 lb. per sq.in. absolute chamber pressure with this injector was usually 85 per cent of the theoretical at optimum mixture ratio.

A conventional rocket-motor chamber, with L^* of 48 in., was used in all of these heat-transfer experiments. The cylindrical chamber was water-cooled through a helical cooling passage. A nominal chamber pressure of 300 lbs. per sq.in. absolute was used in all rocket tests.

The assembly of the rocket motor is shown in Fig. 5 during Run N15.

APPLICATION OF THE TRANSIENT METHOD

The method of evaluation of heat-transfer coefficients as described by London, et al.,[2] was used in principle for the analysis of the data of this report.

The circular segments of the H.T.N. acted as thermal capacitors insulated axially from each other by an air gap and essentially insulated on the outside surface by the surrounding air. Heat was transferred from the combustion gases through the gas film to the inner wall of the segment and then conducted in a radial direction through the segment body. The axial variation of the heat transferred in an individual segment was not considered. The average temperature rise of the segment with time reflected the amount of heat which was absorbed by the capacitor. All heat transfer is assumed by forced convection only.

The rate equation for flow of the unit heat flux, q, through the gas film is

$$q = h_g(t_g - t_w) \tag{1}$$

and the energy balance on the thermal capacitor may be expressed as

$$q = (W_{cp}/A)\ (dt_a/d\theta) \tag{2}$$

Combining the energy balance and rate equation results in

$$h_g = [W_{cp}/A\ (t_g - t_w)]\ (dt_a/d\theta) \tag{3}$$

Description of Terms

The terms W and A are geometric or physical properties of the copper segments which are readily measured. These segment constants are listed in Table 1. The value of the specific heat for copper at the segment average temperature was used in calculations of all tests.

The rate of change of segment average temperature with respect to time, $dt_a/d\theta$, is the slope of the tangent to the average temperature-time curve as shown in Fig. 10. These temperatures were sensed with iron-constantan thermocouples and were recorded on appropriate automatic recording instruments.

In order to minimize the effect of radiation losses from the H.T.N. outside surfaces, tangents were taken at the earliest time in the test after steady operating conditions had been obtained. Calculations showed that the effect of radiation loss on the values of the heat-transfer coefficients was less than 1 per cent when the tangent data were taken at the 5th sec. of oper-

TABLE 1
Physical Constants of the Heat-Transfer Nozzle Segments

Segment Number	Segment Weight, W, Lbs.	Segment Inner Area, A, Sq.Ft.
I	3.5	0.049
II	4.1	0.031
III	3.9	0.034
IV	3.6	0.042
V	4.8	0.081

ation in the rocket tests and at the 20th sec. of operation in the low-temperature equipment.

The thermocouple within each axial segment was installed at the location of the segment average temperature as calculated from Schmidt plots of the nozzle wall. Procedures outlined by Schmidt[3] and Perry and Berggren[4] were followed in the preparation of these temperature gradient plots, wherein a scale distortion of the abscissa is required to apply the Schmidt method to plane radial heat flow. The segments of the H.T.N. were considered to be finite hollow cylinders, and Perry and Berggren have shown that the use of a logarithmic scale in plotting equal finite increments of cylinder radius makes possible the graphical application of the Schmidt method to cylindrical systems in the same fashion as to slabs and with equal precision.

The area beneath the curve of temperature versus radial thickness of the nozzle wall segment was graphically integrated and averaged for the position of the average temperature after the radial thickness coordinate was weighted to account for the variation of the mass of metal with respect to thickness. The graphical integration described, therefore, is essentially a summation and an average of the heat content of the segment. The positions of segment average heat content and temperature at a particular instant of time are alike.

For these Schmidt plots the values of specific heat and thermal conductivity of copper used were assumed constant at values corresponding to the average temperature experienced by the metal segment during the test. The gas-film coefficient was arbitrarily calculated from Eq. (4j) of McAdams,[1] and a gas temperature of 4,500°F. was used. In the event experimental values of the gas-film coefficient radically disagreed with this selection, a reiteration process would be applied on the Schmidt Plot using the experimental values of h_g and t_g.

The temperature of the gas, t_g, which affects heat transfer across the gas film, was a variable factor dependent upon the test equipment and the position in the nozzle. At the three segments in the divergent portion of the nozzle, the gas temperatures were considered to be equal to that of an adiabatic wall alongside the same fluid as the segment wall. The temperature of the adiabatic wall was computed from the main-stream conditions and a recovery factor from a curve given by Kaye, Keenan, and McAdams.[5] The heat-transfer coefficient was insensitive to variations in the selected value of the recovery factor because the difference between segment wall temperature and adiabatic wall temperature was relatively large. It was appreciated, nevertheless, that the recovery factors measured by Kaye, et al., would not apply directly to the flow conditions in a supersonic nozzle, however, application of a recovery factor was considered necessary and no more correct information was available.

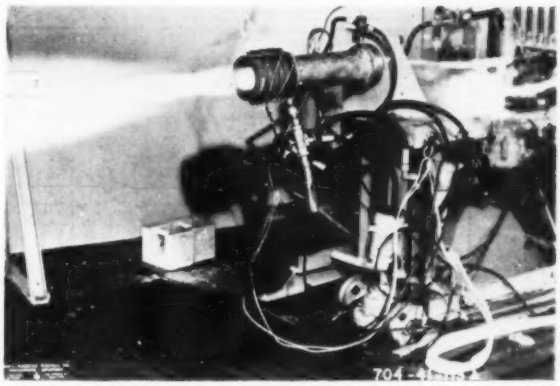

FIG. 5. A view of a typical rocket-motor heat-transfer test.

For the two segments in the convergent portion of the nozzle and the throat, the stagnation or total temperature of the gas was taken as t_g. At these segments the gas velocity was equal to a maximum of only the speed of sound and the recovery factor was therefore of little significance.

The value of the main-stream gas temperature in the rocket motor, equal to the stagnation temperature in the nozzle, can be calculated from thermodynamic data when complete chemical equilibrium and uniform mixing of the propellant gas components are assumed. Test runs of rocket motors showed, however, that these assumptions were not strictly correct and that the effective combustion temperature, as judged by rocket-motor specific thrust, was lower than the calculated thermodynamic value. A well-known thermodynamic relation showed rocket-motor specific thrust proportional to the square root of the absolute combustion temperature. It was assumed that variations of the ratio of specific heats and molecular weight were negligible and that the square-root relation of measured specific thrust of the rocket motor was used to calculate the effective combustion temperature.

Combustion temperature of the gases from the low-temperature equipment was sensed with an unshielded chromel-alumel thermocouple. Corrections were applied to the measured gas temperature to account for radiation loss and recovery factor at the thermocouple.

For the rocket-motor tests, temperatures of the inner wall of the H.T.N., t_w, adjacent to the combustion gases at each axial segment were estimated from the Schmidt plots. The temperature difference between the inner wall and the position of the segment average was obtained by multiplying the ratio of experimental gas temperature used in the Schmidt plots, 4,500°F., by the inner wall-to-segment average temperature drop as given by the Schmidt plot at 5 sec. time. This approximation was considered to be valid within the accuracy of the results, since the experimental and

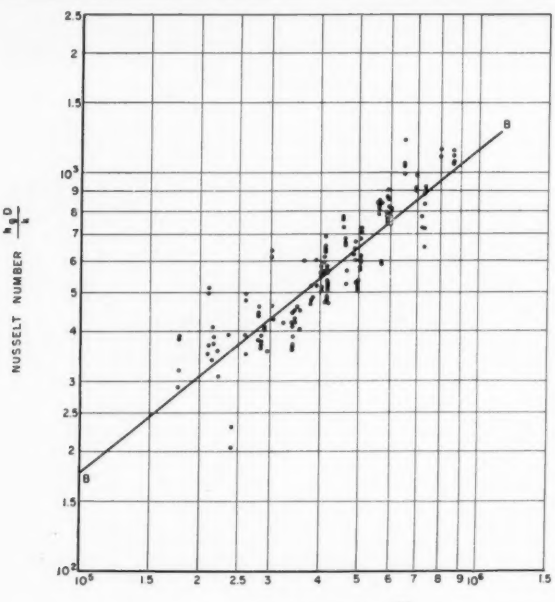

NUSSELT NUMBER VS REYNOLDS NUMBER
COOLED STRAIGHTENING SECTIONS
GAS TEMPERATURE – 1400°F

FIG. 6.

assumed values of the gas-film coefficient checked closely.

Wall temperatures in the nozzle during the low-temperature ram-jet equipment tests were extrapolated linearly from the temperature drop that was recorded between two thermocouples at different depths in the throat segment. One temperature was taken at a depth of $^1/_2$ in. to measure average segment temperature, and another was taken 1 in. in from the outside surface. The validity of this linear extrapolation of the temperature at the wall was supported by the low values of the gas-film coefficient and the gas temperature during these tests.

DISCUSSION OF RESULTS

Low-Temperature Tests

It will be recalled these tests were conducted to achieve a degree of familiarity with the heat-transfer equipment and to evaluate better the effectiveness of the transient method. The low-temperature equipment provided control in variation of temperature and flow, conditions not easily obtained in a rocket motor.

The complete series was conducted at a gas temperature of 1,400°F. (total temperature) and a gas flow rate varying between 1 and 3 lbs. per sec. Two factors were considered of importance in selecting these conditions: (1) The equipment operators could reach steady burning conditions most quickly, and (2) the gas Reynolds Numbers in the nozzle were of the same order of magnitude as those in rocket tests.

Results are shown plotted in Figs. 6 and 7 in the form of Nusselt and Reynolds Numbers based on inside diameter at the axial midpoint of each segment as the characteristic dimension. The physical properties of the gas were assumed to be essentially that of air at 1,400°F., since the amount of fuel burned with air to form the hot combustion gases was far below stoichiometric and represented less than 5 per cent of the total gas flow. The data is presented in two groups corresponding to cooled and uncooled upstream chamber conditions. No correction is applied to account for the maximum 3 per cent heat loss from the gases to the walls of the straightening sections.

The inlet chamber conditions for the data of Fig. 6 closely approached that of a cooled rocket motor, and it was noted that a straight-line correlation of 85 per cent of the experimental points was obtained within ±15 per cent. This scatter of the experimental data could be anticipated by considering the nonuniform flow field at the inlet to the heat-transfer nozzle. After passing through a 90° elbow and a 6- to 3.3-in. inside diameter transition section, the 4.7 diameter lengths of straightening section could not be expected to establish reproducible gas velocity and temperature profiles at the nozzle entrance. Additional calming lengths would have been desired but could not be installed because of space limitation.

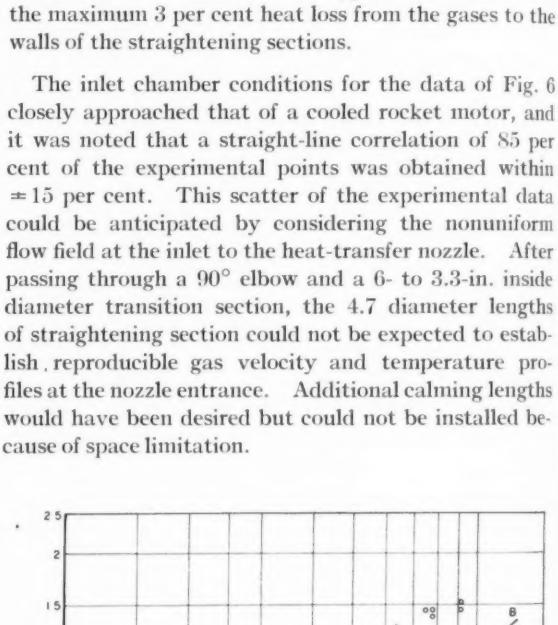

NUSSELT NUMBER VS REYNOLDS NUMBER
UNCOOLED STRAIGHTENING SECTIONS
GAS TEMPERATURE – 1400°F

FIG. 7.

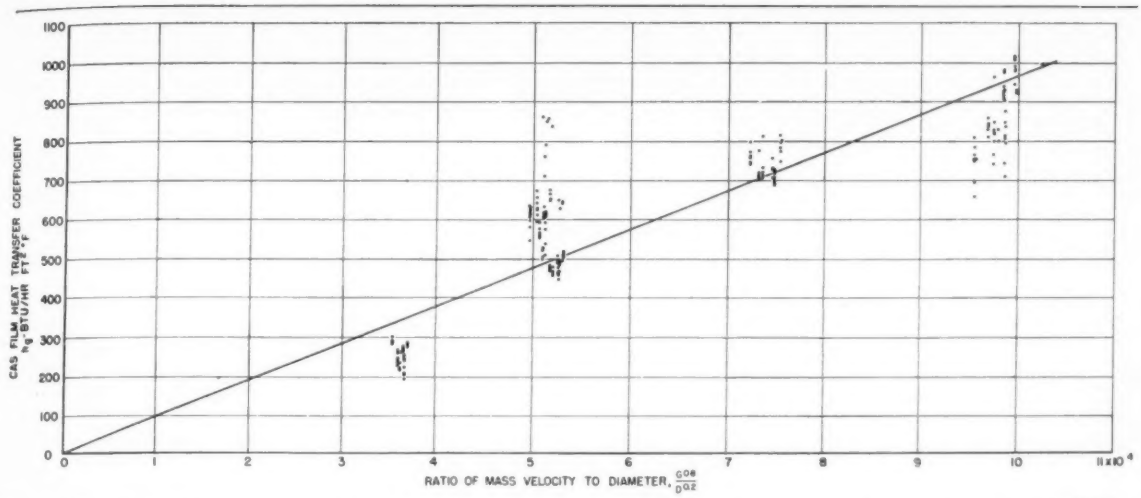

FIG. 8. Rocket-motor nozzle heat-transfer coefficient vs. ratio of mass velocity to diameter. (High-temperature studies, 3,000°F.)

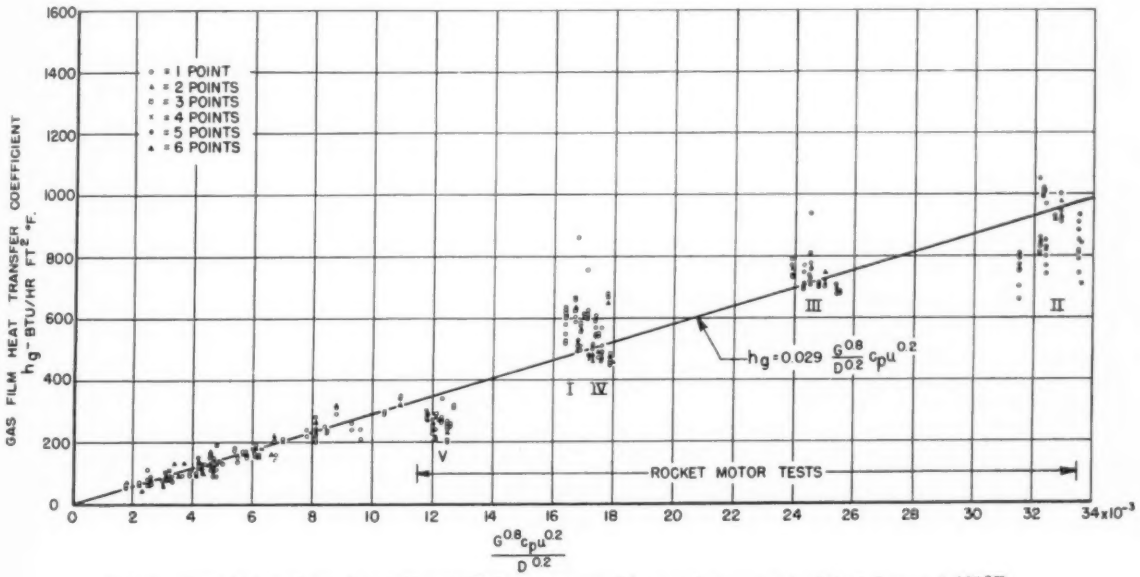

FIG. 9. Correlation of nozzle gas-film coefficients measured in a rocket motor to data taken at 1,400°F.

The conditions in an uncooled rocket motor were simulated in a second series of twelve tests when the straightening sections were uncooled. The data of these runs are plotted as Nusselt Numbers vs. Reynolds Numbers in Fig. 7 showing line B-B as in Fig. 6. The values of Nusselt Number show a trend parallel to, but about 50 per cent higher than, the line B-B. Inspection of the Nusselt Numbers of the individual nozzle segments showed the highest values for Segment I (see Fig. 2), with progressively lower values at Segments II and III and, finally, values corresponding to B-B for Segments IV and V. The higher trend in Nusselt Numbers is attributed to the nature of the nozzle inlet gas temperature profile during this test series. The stainless-steel metal surfaces of the uncooled straightening section adjacent to the gases quickly reached an elevated temperature causing the combustion gases in and near the wall boundary layer to reach a higher average temperature as compared to previous tests with cooled straightening sections. In effect, a discontinuity of metal surface temperature occurred at the entrance of the nozzle where lower surface temperatures were expected on the highly conductive copper. The result would be a higher apparent value of Nusselt Number at the leading segment with subsequent decrease in the effect as the gas temperature profile became adjusted to the new boundary conditions in the nozzle.

The correlation of data, particularly that taken with cooled straightening sections, and the reproducibility

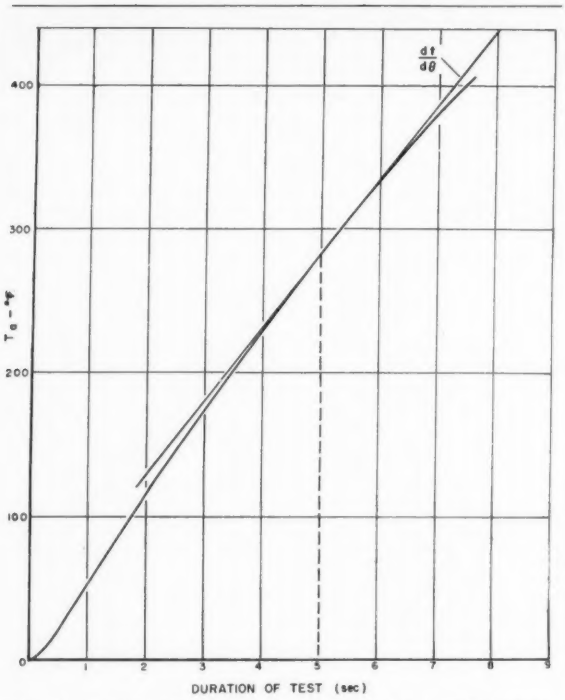

FIG. 10. Typical temperature-time relation for a rocket-motor test showing tangent at 5 sec.

of test results reflected satisfactory operation of the segmented copper nozzle with its attendant instrumentation and furthermore asserted the potentiality of the transient method for measurement of gas-film heat-transfer coefficients in a rocket motor.

High-Temperature Rocket-Motor Tests

Correlation of the rocket-motor heat-transfer data was attempted through plots of dimensionless groupings, Nusselt and Reynolds Numbers, based on inside diameter of the nozzle, and length along the nozzle wall, as the characteristic dimension, D. The points fell in a nonuniform fashion, however, and it was not possible to fit a representative continuous curve or line to the result. Probable source of this poor correlation lies in the lack of accurate values for the thermal conductivity and viscosity of the combustion gases. At the time of this report, the author is unaware of reliable extrapolation of transport properties of gas mixtures or experimental measurements of conductivity and viscosity at temperatures as high as 3,000°F.

Because of their inaccuracy, the use of dimensionless groups was set aside for the present in favor of a more elementary plot. A straight-line relation of data was obtained by plotting the segment gas-film coefficients versus the ratio $G^{0.8}/D^{0.2}$ as shown in Fig. 8, with D the inside diameter at the midpoint of the segment. The validity of such a plot was further demonstrated by the correlation of the rocket data with the data from the low-temperature tests at 1,400°F. (see Fig. 9). The specific heat and the viscosity of the combustion gases at the recovery temperature were applied to the ratio $G^{0.8}/D^{0.2}$ of Fig. 8 in order to adjust for the difference in temperature of the two sets of data. The gas viscosity entered only to the two-tenths power for this application and the effect of inaccurate values was minimized. The specific heat of the gas mixture at the higher temperature was readily calculable and probably accurate to within 5 per cent.

The equation of the straight line in Fig. 9 is

$$h_g = 0.029\ (G^{0.8}/D^{0.2})\ c_p \mu^{0.2} \qquad (4)$$

and it is noted that 75 per cent of the rocket-motor test points are satisfied by the above equation with ±15 per cent. The data generally fell into five groups, numbered in Fig. 9, corresponding to the five segments of the nozzle (see Fig. 2).

Heat losses from an individual segment radially to the atmosphere and axially to an adjoining segment through the $^1/_4$-in. web at the inside wall have been shown through preliminary calculations to be less than 2 per cent and were neglected in this report. There is an additional heat loss through forced convection caused by a movement of air over the nozzle induced by the action of the jet flame. Experimental checks of the magnitude of this convection loss have not been made at this time, since initial estimates showed an effect less than 2 per cent. The total of the error in the values of gas-film heat-transfer coefficients as a result of the above three heat losses was estimated to be not more than 5 per cent. However, the consistently low values of the gas-film coefficient in the exit Segment V have been in part attributed to the excessive amount of turbulence over the outer and end surfaces of this particular portion of the nozzle. Therefore, an experimental evaluation of the convection loss is planned at an early date to corroborate the preliminary calculations.

The less than 3 per cent decrease of gas temperature due to transfer of heat to the cooled rocket chamber walls is neglected. The effect of change in rocket motor mixture ratio on the nozzle gas-film coefficients has not been emphasized, since, at the present time, information for all the mixture ratios investigated is not complete enough to make definite conclusions.

The information presented here illustrates an initial phase of a series of rocket-motor heat-transfer measurements that are anticipated with the oxygen-alcohol propellant system using the transient method.

It is appreciated that application of the data reported here to rocket-motor-nozzle heat transfer in general is limited, since a fixed injector and L^* configuration were used throughout.

When further test data are recorded with a variety of injectors and motor L^*, a more complete picture of the heat-transfer field will be available to rocket motor designers.

(*Continued on page 526*)

Aerodynamics of a Supersonic Rectangular Wing Striking a Sharp-Edged Gust

THEODORE R. GOODMAN*

Cornell Aeronautical Laboratory, Inc.

ABSTRACT

The method of C. S. Gardner for solving nonsteady finite wing problems at supersonic speeds is briefly described. An expression for the pressure is derived in terms of the velocity potential in the transformed variables used by Gardner. Nonsteady wing problems are solved, according to Gardner, by solving two three-dimensional boundary-value problems. In the case of the sharp-edged gust, the first problem is a symmetrical finite wing problem, and the second is an antisymmetrical problem based on the solution to the first problem. Expressions are derived for the pressure in the various regions on the wing, and these are shown to be conical. Finally, the pressures are integrated, and formulas are given for the lift and leading-edge moment as functions of time, aspect ratio, and Mach Number.

INTRODUCTION

THE METHOD PRESENTED RECENTLY by Gardner[1] for solving nonsteady finite wing problems at supersonic speeds is particularly adaptable to the wing of rectangular plan form. This method, which reduces a nonsteady finite wing problem to two "steady" finite wing problems, will be used here to solve for the pressures on a rectangular wing striking a sharp-edged gust.

The problem of a sharp-edged gust on an infinite wing at supersonic speeds has been solved by Schwarz[2] and others.[3–6] Moreover, Miles has solved the problem for a rectangular wing.[7] The method he uses, however, permits him to derive only the chordwise lift distribution. The actual pressure at a point is not given. Not only are the pressures required in certain applications, but physical insight is gained into the nature of the behavior of a sharp-edged gust interacting with a wing tip when the local pressure at a point is known.

THE METHOD OF GARDNER

Without deriving the method, its essential points will be presented here. With rectilinear coordinates x, y, z fixed on the wing (x in the downstream direction and y in the spanwise direction), the boundary-value problem satisfied by ϕ (the perturbation velocity potential) is, for (x, y) in W,

$$\lim_{z \to 0+} \phi_z = \lim_{z \to 0-} \phi_z = Uf_x(x, y, t) + f_t(x, y, t) \qquad (1)$$

for $x < 0$

$$\phi(x, y, z, t) \equiv 0 \qquad (2)$$

$$(M^2 - 1)\phi_{xx} - \phi_{yy} - \phi_{zz} + \frac{2M}{c}\phi_{xt} + \frac{1}{c^2}\phi_{tt} = 0 \qquad (3)$$

where W is the projection of the wing in the xy-plane, $z = f(x, y, t)$ describes the surface of the wing, c is the velocity of sound, and M is the Mach Number of the free stream ($M = U/c$).

This boundary-value problem involves four independent variables. Gardner's method reduces the problem to two boundary-value problems, each one of which involves only three independent variables.

First, transform the variables x and t to the variables x' and t', where

$$\left.\begin{aligned} x' &= x(M^2 - 1)^{-1/2} \\ t' &= [Mx - (M^2 - 1)ct](M^2 - 1)^{-1/2} \end{aligned}\right\} \qquad (4)$$

Let $g = Uf_x + f_t$. Now drop the primes on the transformed variables, x' and t'. Then Eqs. (1), (2), and (3) become, for a rectangular tip, for $y > 0$,

$$\lim_{z \to 0+} \phi_z = \lim_{z \to 0-} \phi_z = g(x, y, t) \qquad (5)$$

(where $g \equiv 0$ for $x < 0$), and for

$$x < 0, \qquad \phi \equiv 0 \qquad (6)$$

$$\phi_{xx} - \phi_{yy} - \phi_{zz} - \phi_{tt} = 0 \qquad (7)$$

Gardner's method consists in introducing the variable ξ and the quantities ψ and χ. With a slight modification of Gardner's presentation, χ satisfies the following boundary-value problem, for $\xi \geq 0$,

$$\chi_{xx} - \chi_{tt} - \chi_{\xi\xi} = 0 \qquad (8)$$

for $\xi = 0$,

$$\chi = g(x, y, t) \qquad (9)$$

for $x < 0$,

$$\chi \equiv 0 \qquad (10)$$

ψ satisfies the boundary-value problem

$$\psi_{\xi\xi} - \psi_{yy} - \psi_{zz} = 0 \qquad (11)$$

for $y > 0$,

$$\lim_{z \to 0+} \psi_z = \lim_{z \to 0-} \psi_z = \chi(\xi, x, y, t) \qquad (12)$$

for $\xi > x$,

$$\psi \equiv 0 \qquad (13)$$

Received January 17, 1951.

* Aerodynamic Research Department.

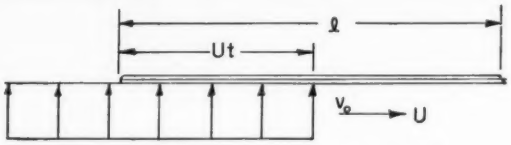

FIG. 1. Wing section entering vertical gust.

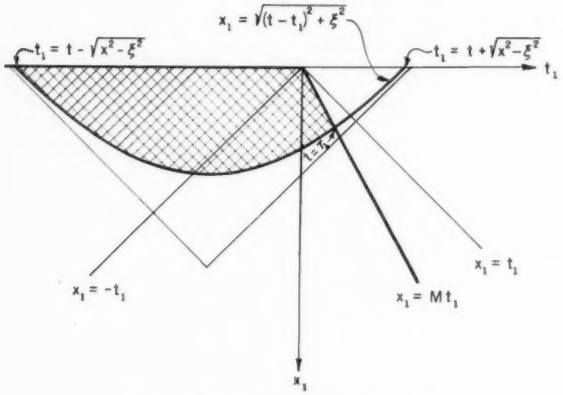

FIG. 2. Regions of the x - t "wing."

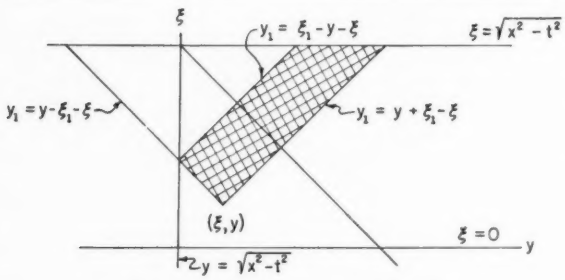

FIG. 3. The second problem—part 1.

The velocity potential is found by setting $\xi = 0$, such that

$$\phi(x, y, z, t) = \psi(0, x, y, z, t) \tag{14}$$

The pressure in terms of physical xt variables is given by

$$p = \rho[(\partial\phi/\partial t) + U(\partial\phi/\partial x)] \tag{15}$$

In terms of the transformed variables the pressure is

$$p = \frac{\rho U}{M\sqrt{M^2 - 1}}\left(\frac{\partial\phi}{\partial t} + M\frac{\partial\phi}{\partial x}\right) \tag{16}$$

THE FIRST PROBLEM

From Fig. 1 it is seen that, in terms of physical x, t variables, the boundary condition is

$$\left.\begin{aligned} g &= v_0 \quad \text{for} \quad x < Ut \\ g &= 0 \quad \text{for} \quad x > Ut \end{aligned}\right\} \tag{17}$$

In terms of transformed variables [Eqs. (4)],

$$\left.\begin{aligned} g &= v_0 \quad \text{for} \quad x > Mt \\ g &= 0 \quad \text{for} \quad x < Mt \end{aligned}\right\} \tag{18}$$

It is convenient to define a quantity σ such that

$$\partial\sigma/\partial\xi = \chi \tag{19}$$

σ satisfies the wave equation [Eq. (8)], and then Eq. (9) becomes

$$\partial\sigma/\partial\xi = g(x, y, t) \tag{20}$$

The boundary-value problem defined by Eqs. (8), (20), and (10) can be thought of as a "symmetrical" supersonic "wing" problem in x, t, ξ space, where x is in the "downstream" direction, t is in the "spanwise" direction, and ξ is normal to the wing as shown in Fig. 2.

The solution for σ can be obtained in terms of simple sources

$$\sigma = -\frac{1}{\pi}\int\int_{\tau}\frac{v_0\, dx_1\, dt_1}{[(x - x_1)^2 - (t - t_1)^2 - \xi^2]^{1/2}} \tag{21}$$

where τ is the shaded region shown in Fig. 2 provided x, t, ξ lies within the "Mach cone" from the apex of the "wing." Call this phase (2). If x, t, ξ lies to the right of the Mach cone, then $\sigma = 0$. If x, t, ξ lies to the left of the Mach cone, σ must be "two-dimensional"—i.e., independent of t. Call this phase (1). Then, clearly,

$$\sigma_2 = \sigma_1 \quad \text{on Mach cone left} \tag{22}$$

$$\sigma_2 = 0 \quad \text{on Mach cone right} \tag{23}$$

where the subscripts refer to the phase.

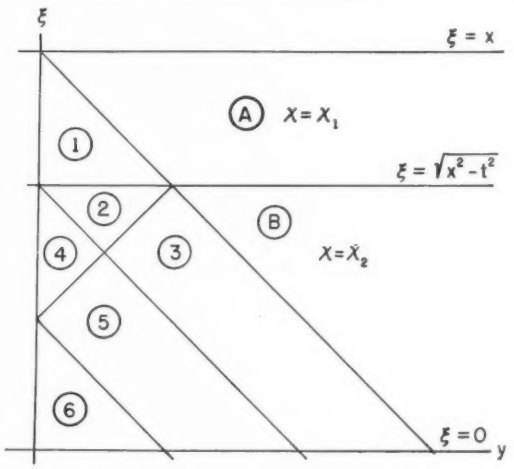

FIG. 4. The second problem—part 2.

Phase (1)

Putting in the limits of integration on Eq. (21), there is found, for σ_1,

$$\sigma_1 = -\frac{v_0}{\pi}\int_{t-\sqrt{x^2-\xi^2}}^{t+\sqrt{x^2-\xi^2}} dt_1 \int_0^{x-\sqrt{(t-t_1)^2+\xi^2}} \frac{dx_1}{\sqrt{(x-x_1)^2-(t-t_1)^2-\xi^2}} \tag{24}$$

Performing this double integration there is obtained

$$\sigma_1 = v_0(\xi - x) \tag{25}$$

Phase (2)

To obtain the proper region τ in Eq. (19), use the result of integrating Eq. (24) and subtract the extraneous area from Fig. 2; then we obtain

$$\sigma_2 = v_0(\xi - x) + \frac{v_0}{\pi}\int_0^{\tau_1} dt_1 \int_0^{Mt_1} \frac{dx_1}{\sqrt{(x-x_1)^2-(t-t_1)^2-\xi^2}} + \frac{v_0}{\pi}\int_{\tau_1}^{t+\sqrt{x^2-\xi^2}} dt_1 \int_0^{x-\sqrt{(t-t_1)^2-\xi^2}} \frac{dx_1}{\sqrt{(x-x_1)^2-(t-t_1)^2-\xi^2}} \tag{26}$$

where

$$\tau_1 = [Mx - t - \sqrt{(x-Mt)^2 + (M^2-1)\xi^2}]/(M^2-1) \tag{27}$$

Performing the x_1 integration, there is obtained

$$\sigma_2 = v_0(\xi - x) - \frac{v_0}{\pi}\int^{\tau_1} \cosh^{-1}\frac{x - Mt_1}{\sqrt{(t-t_1)^2+\xi^2}}\,dt_1 + \frac{v_0}{\pi}\int_0^{t+\sqrt{x^2-\xi^2}} \cosh^{-1}\frac{x}{\sqrt{(t-t_1)^2+\xi^2}}\,dt_1 \tag{28}$$

It will be seen later that, in order to find the pressure on the wing, σ itself is not necessary but only the combination $\sigma_t + M\sigma_x$. We therefore proceed to find this quantity.

$$\frac{\partial\sigma_2}{\partial t} + M\frac{\partial\sigma_2}{\partial x} = -Mv_0 - \frac{v_0}{\pi}\int_0^{\tau}\left(\frac{\partial}{\partial t} + M\frac{\partial}{\partial x}\right)\cosh^{-1}\frac{x-Mt_1}{\sqrt{(t-t_1)^2+\xi^2}}\,dt_1 - \frac{v_0}{\pi}\cosh^{-1}\frac{x-M\tau_1}{\sqrt{(t-\tau_1)^2+\xi^2}} \times \left(\frac{\partial}{\partial t} + M\frac{\partial}{\partial x}\right)\tau_1 + \frac{v_0}{\pi}\int_0^{t+\sqrt{x^2-\xi^2}}\left(\frac{\partial}{\partial t} + M\frac{\partial}{\partial x}\right)\cosh^{-1}\frac{x}{\sqrt{(t-t_1)^2+\xi^2}}\,dt_1 \tag{29}$$

But

$$[(\partial/\partial t) + M(\partial/\partial x)]\tau_1 = 1 \tag{30}$$

Also

$$\int_0^{t+\sqrt{x^2-\xi^2}} \frac{\partial}{\partial t}\cosh^{-1}\frac{x}{\sqrt{(t-t_1)^2+\xi^2}}\,dt_1 = -\int_0^{t+\sqrt{x^2-\xi^2}} \frac{\partial}{\partial t_1}\cosh^{-1}\frac{x}{\sqrt{(t-t_1)^2+\xi^2}}\,dt_1 \tag{31}$$

The last integral in Eq. (20) is easily evaluated, and so there is obtained

$$\frac{\partial\sigma_2}{\partial t} + M\frac{\partial\sigma_2}{\partial x} = -\frac{v_0}{\pi}\int_0^{\tau_1} \frac{[(Mt-x)(t-t_1) + M\xi^2]\,dt_1}{\sqrt{(x-Mt_1)^2-(t-t_1)^2-\xi^2}[(t-t_1)^2+\xi^2]} - \frac{v_0}{\pi}\cosh^{-1}\frac{x-M\tau_1}{\sqrt{(t-\tau_1)^2+\xi^2}} + \frac{v_0}{\pi}\cosh^{-1}\frac{x}{\sqrt{t^2+\xi^2}} - \frac{Mv_0}{\pi}\cos^{-1}\frac{t}{\sqrt{x^2-\xi^2}} \tag{32}$$

The substitutions

$$t - t_1 = \xi\tan\theta$$

and

$$v = (x - Mt)\cos\theta + M\xi\sin\theta$$

make the first term readily integrable. Finally, there is obtained

$$(\partial\sigma_2/\partial t) + M(\partial\sigma_2/\partial x) = -(Mv_0/\pi)\cos^{-1}(t/\sqrt{x^2-\xi^2}) \tag{33}$$

From Eq. (25) there is found

$$(\partial\sigma_1/\partial t) + M(\partial\sigma_1/\partial x) = -Mv_0 \tag{34}$$

On the Mach cone right ($t = \sqrt{x^2 - \xi^2}$), Eq. (23) is satisfied; on the Mach cone left ($t = -\sqrt{x^2 - \xi^2}$), Eq. (22) is satisfied.

The Second Problem

There are two parts to the second problem. Part 1 occurs when $t > 0$; part 2, when $t < 0$. Let us solve part 1 first.

Part 1 can be solved with sources by Evvard's method[8] when $0 < y < \sqrt{x^2 - t^2}$. When $y > \sqrt{x^2 - t^2}$, the solution becomes two-dimensional—i.e., independent of y. In all cases we shall let $z \to 0$ so that we find solutions on the wing only. We obtain ϕ directly by letting $\xi = 0$. The solution for $y > \sqrt{x^2 - t^2}$ is obtained by integrating over the entire fore "Mach cone" as shown in Fig. 3.

$$\phi = -\frac{1}{\pi}\int_0^{\sqrt{x^2-t^2}} d\xi_1 \int_{y-\xi_1}^{y+\xi_1} \frac{\chi_2(\xi_1, x, t)dy_1}{\sqrt{\xi_1^2 - (y - y_1)^2}} \tag{35}$$

$$= \int_0^{\sqrt{x^2-t^2}} \chi_2(\xi_1, x, t)\, d\xi_1 \tag{36}$$

Using Eqs. (19) and (23) we obtain

$$\phi = -\sigma_2(0, x, t) \tag{37}$$

From Eq. (33) we find

$$(\partial\phi/\partial t) + M(\partial\phi/\partial x) = (Mv_0/\pi)\cos^{-1}(t/x) \tag{38}$$

Now we obtain the solution for $y < \sqrt{x^2 - t^2}$ by using Evvard's method[8] and integrating over the shaded region shown in Fig. 3. Again setting $\xi = 0$, we obtain, for ϕ,

$$\phi = -\sigma_2(0, x, t) + \frac{1}{\pi}\int_y^{\sqrt{x^2-t^2}} \chi_2\, d\xi_1 \int_{y-\xi_1}^{\xi_1 - y} \frac{dy_1}{\sqrt{\xi_1^2 - (y - y_1)^2}} \tag{39}$$

After some manipulation there is obtained

$$\phi = -\sigma_2(0, x, t) + \frac{\sqrt{y}}{\pi}\int_y^{\sqrt{x^2-t^2}} \frac{\sigma_2(\xi_1, x, t)\, d\xi_1}{\xi_1\sqrt{\xi_1 - y}} \tag{40}$$

From Eqs. (33) and (23) we obtain (dropping the subscript on ξ)

$$\frac{\partial\phi}{\partial t} + M\frac{\partial\phi}{\partial x} = \frac{Mv_0}{\pi}\cos^{-1}\frac{t}{x} - \frac{Mv_0}{\pi}\sqrt{y}\int_y^{\sqrt{x^2-t^2}} \frac{\cos^{-1}(t/\sqrt{x^2 - \xi^2})d\xi}{\xi\sqrt{\xi - y}} \tag{41}$$

We now proceed to part 2 ($t < 0$).

In part 2, for $x > \xi > \sqrt{x^2 - t^2}$, $\chi = \chi_1$; whereas in part 1, for $x > \xi > \sqrt{x^2 - t^2}$, $\chi = 0$. The regions induced in the second problem are shown and labeled for convenient reference in Fig. 4. Except for region (1), Evvard's method becomes cumbersome, and for the other regions the writer's method[9, 10] will be used instead.

Let us first find the solution in region (B). This may be found by simple sources. Setting $\xi = 0$, we obtain

$$\phi = \frac{-1}{\pi}\int_0^{\sqrt{x^2-t^2}} d\xi_1 \int_{y-\xi_1}^{y+\xi_1} \frac{\chi_2(\xi_1, x, t)\, dy_1}{\sqrt{\xi_1^2 - (y - y_1)^2}} - \frac{1}{\pi}\int_{\sqrt{x^2-t^2}}^{x} d\xi_1 \int_{y-\xi_1}^{y+\xi_1} \frac{\chi_1(\xi_1, x, t)\, dy_1}{\sqrt{\xi_1^2 - (y - y_1)^2}} \tag{42}$$

After using Eqs. (22) and (25)

$$\phi = -\sigma_2(0, x, t) \tag{43}$$

Therefore

$$\phi_t + M\phi_x = (Mv_0/\pi)\cos^{-1}(t/x) \tag{44}$$

Therefore, there is no difference between parts (1) and (2) in the two-dimensional region [see Eq. (38)].

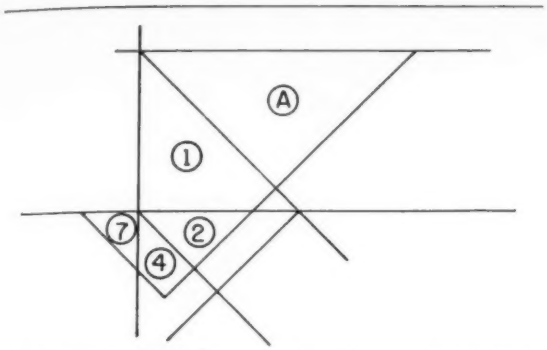

FIG. 5. The second problem—part 2. Diagram for finding ψ_2.

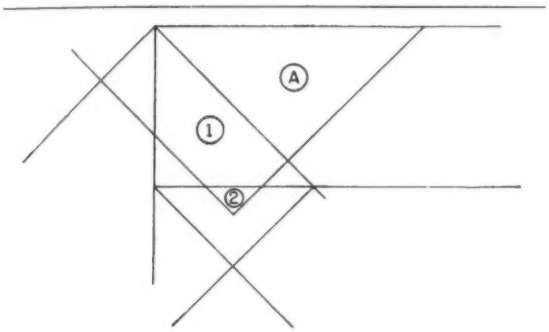

FIG. 6. The second problem—part 2. Diagram for finding ψ_4.

The solutions in regions (A) and (1) are those for a steady two-dimensional and tip region, respectively, since χ_1 is constant. These solutions have been obtained elsewhere [e.g., Eq. (20) of reference 5] and will merely be restated here.

$$\psi_A = v_0(x - \xi)$$

$$\psi_1 = \frac{v_0}{\pi}\left[2\sqrt{y(x - \xi - y)} + 2(x - \xi)\tan^{-1}\sqrt{y/(x - \xi - y)}\right]$$

Letting $\xi = 0$ and differentiating, we find, for $\phi_t + M\phi_x$

$$(\partial\phi_A/\partial t) + M(\partial\phi_A/\partial x) = Mv_0 \tag{45}$$

$$\frac{\partial\phi_1}{\partial t} + M\frac{\partial\phi_1}{\partial x} = \frac{Mv_0}{\pi}\cos^{-1}\left(1 - \frac{2y}{x}\right) \tag{46}$$

We shall now proceed to find the solution in region (2) by the method of reference 9.

Applying the method of reference 9 to the problem shown in Fig. 5 we arrive at the double integral equation

$$\int\int_{(2)} K\frac{\partial}{\partial\xi_1}(\psi_1 - \psi_2)\,d\xi_1\,dy_1 = \frac{\partial}{\partial\xi}(\chi_1 - \chi_2) \tag{47}$$

where

$$K = \pi^{-1}[(\xi - \xi_1)^2 - (y - y_1)^2]^{-1/2} \tag{48}$$

After transforming to "Mach coordinates" and solving each of the double integral equations, we arrive at

$$\frac{\partial}{\partial\xi_1}(\psi_1 - \psi_2) = \frac{1}{\pi}\int\int_{(2)}\frac{(\partial/\partial\xi)(\chi_1 - \chi_2)\,d\xi\,dy}{\sqrt{(\xi_1 - \xi)^2 - (y_1 - y)^2}} \tag{49}$$

Here, the roles of ξ_1, y_1 and ξ, y have changed places. Performing the indicated integration and dropping the subscript on ξ, we arrive at

$$(\partial/\partial\xi)(\psi_1 - \psi_2) = \chi_2 - \chi_1 \tag{50}$$

or

$$\psi_1 - \psi_2 = \sigma_2 - \sigma_1 \tag{51}$$

The analysis for finding ψ_3 yields the relation $\psi_3 = \psi_2$. Hence, for $\xi = 0$, one need not differentiate between regions (2) and (3) but can state, for $\sqrt{x^2 - t^2} < y < x$, $t < 0$,

$$\phi_t + M\phi_x = \frac{Mv_0}{\pi}\left[\cos^{-1}\frac{t}{x} - \cos^{-1}\left(\frac{2y}{x} - 1\right)\right] \tag{52}$$

The analysis for finding ψ_4 leads to the integral equation (see Fig. 6)

$$\int\int_{(4)} K(\psi_4 - \psi_2)\,d\xi_1\,dy_1 = \int\int_{(7)} K(\psi_2 - \psi_1)\,d\xi_1\,dy_1 \tag{53}$$

After considerable manipulation, the solution to this equation is found to be

$$\psi_4 - \psi_2 = \frac{\sqrt{y}}{\pi}\int_{\xi+y}^{\sqrt{x^2-t^2}}\frac{(\sigma_1 - \sigma_2)\,d\xi_1}{(\xi - \xi_1)\sqrt{\xi_1 - \xi - y}} \tag{54}$$

After letting $\xi = 0$ and using Eq. (33), we find

$$\frac{\partial\phi_4}{\partial t} + M\frac{\partial\phi_4}{\partial x} = \frac{Mv_0}{\pi}\left[\cos^{-1}\frac{t}{x} - \cos^{-1}\left(\frac{2y}{x} - 1\right) + \cos^{-1}\left(\frac{2y}{\sqrt{x^2 - t^2}} - 1\right) - \frac{\sqrt{y}}{\pi}\times\int_y^{\sqrt{x^2-t^2}}\frac{\cos^{-1}(t/\sqrt{x^2 - \xi^2})\,d\xi}{\xi\sqrt{\xi - y}}\right] \tag{55}$$

An analysis of region (5) shows that $\psi_5 = \psi_4$. Hence, the Mach line bordering regions (2) and (3) and (4) and (5) does not exist as a demarcation of solutions. Its reflection from the line $y = 0$ cannot exist either, and Fig. 4 should be changed. This changed diagram is shown in Fig. 7.

THE PHYSICAL WING

We shall now recapitulate the multitudinous solutions obtained and interpret them in terms of regions on the physical wing. The line $y = \sqrt{x^2 - t^2}$ becomes, in terms of physical x, t variables,

$$(x - Ut)^2 + y^2 = (ct)^2 \tag{56}$$

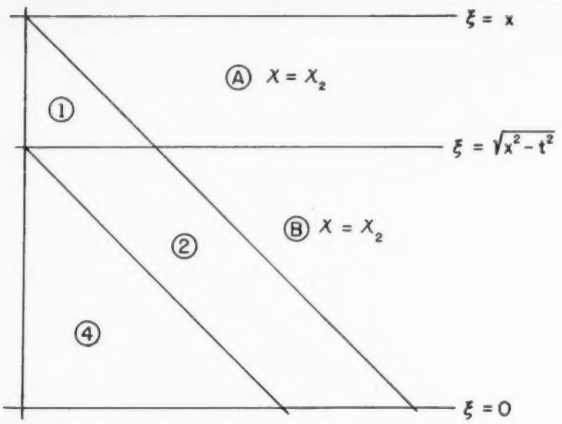

FIG. 7. The second problem—part 2. Extraneous Mach lines removed.

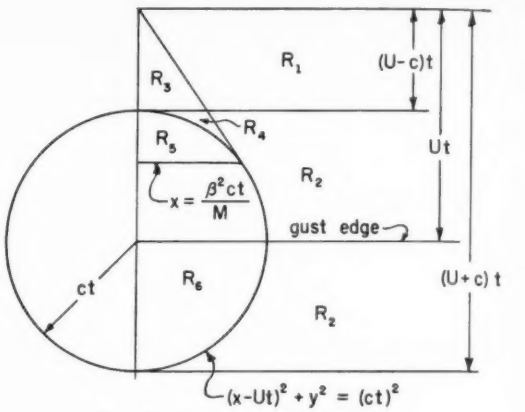

FIG. 8. Regions on physical wing.

This defines an acoustic circle within which the solution is three-dimensional and time dependent; here, the effect of the wing tip and gust edge is completely felt.

The regions on the physical wing are depicted in Fig. 8. The lines are labeled with the physical x, t variables and $\beta = \sqrt{M^2 - 1}$.

As time progresses, the lines $(U - c)t$, Ut, $(U + c)t$ move downstream on the wing; the circle moves downstream also, and its radius increases in such a manner that the Mach cone from the origin is generated tangent to the resulting family of circles. In regions R_1 and R_3 steady flow has been established. In region R_2 the flow is nonsteady but two-dimensional. In regions R_5 and R_6 the flow is three-dimensional nonsteady. In region R_4 the flow consists of two parts—one is three-dimensional steady; the other is two-dimensional nonsteady. These considerations have been arrived at by considering the pressures in each region. From Eq. (16) and the various analyses throughout the paper, one arrives at the following list of the pressures: Here, the subscript number coincides with the numbered regions as depicted on Fig. 8; the number preceding each pressure is the equation number from which the pressure was taken; x and t are transformed variables.

(45) $$p_1 = \rho U v_0/\beta \tag{57}$$

(38), (44) $$p_2 = (\rho U v_0/\pi\beta)\cos^{-1}(t/x) \tag{58}$$

(46) $$p_3 = (\rho U v_0/\pi\beta)\cos^{-1}[1 - (2y/x)] \tag{59}$$

(52) $$p_4 = \frac{\rho U v_0}{\pi\beta}\left[\cos^{-1}\left(1 - \frac{2y}{x}\right) - \cos^{-1}\left(-\frac{t}{x}\right)\right] \tag{60}$$

(55) $$p_5 = \frac{\rho U v_0}{\pi\beta}\left[\cos^{-1}\left(1 - \frac{2y}{x}\right) - \cos^{-1}\frac{|t|}{x} + \frac{\sqrt{y}}{\pi}\int_y^{\sqrt{x^2-|t|^2}} \frac{\cos^{-1}\left(|t|/\sqrt{x^2 - \xi^2}\right) d\xi}{\xi\sqrt{\xi - y}}\right] \tag{61}$$

(41) $$p_6 = \frac{\rho U v_0}{\pi\beta}\left[\cos^{-1}\frac{t}{x} - \frac{\sqrt{y}}{\pi}\int_y^{\sqrt{x^2-t^2}} \frac{\cos^{-1}\left(t/\sqrt{x^2 - \xi^2}\right) d\xi}{\xi\sqrt{\xi - y}}\right] \tag{62}$$

Examination of the pressures in the various regions discloses the character of the solution. Note that the pressure is continuous from region to region. Note also that the pressure reduces to zero along the line $y = 0$. The pressure is conical in all regions—i.e., it is a function of x/t and y/t only. In order to gain greater insight into the behavior of the pressures, they have been determined numerically for $M = 2$, and a diagrammatic drawing of the loading is given in Fig. 9.

THE LIFT AND MOMENT

Although the pressures in regions (5) and (6) cannot be expressed in terms of tabulated functions, if the pressures are integrated in the spanwise (y) direction, the resulting spanwise lift can be expressed in terms of elementary functions. This will now be demonstrated.

The Spanwise Lift

There are three cases to consider. Refer to Fig. 8 and use the transformed x, t variables. Let L_s represent

the spanwise lift, and let $b/2$ be the semispan. Then, case (1) occurs when $t < -x$, and

$$L_{s_1} = 4\left(\int_0^x p_3\,dy + \int_x^{b/2} p_1\,dy\right) \tag{63}$$

Case (2) occurs when $-x < t < 0$ and

$$L_{s_2} = 4\left(\int_0^{\sqrt{x^2-t^2}} p_5\,dy + \int_{\sqrt{x^2-t^2}}^{x} p_4\,dy + \int_x^{b/2} p_2\,dy\right) \tag{64}$$

Case (3) occurs when $x > t > 0$ and

$$L_{s_3} = 4\left(\int_0^{\sqrt{x^2-t^2}} p_6\,dy + \int_{\sqrt{x^2-t^2}}^{b/2} p_2\,dy\right) \tag{65}$$

The factor 4 appears in each of these expressions for the following reasons: A factor of 2 includes both upper and lower surfaces of the wing, and another factor of 2 accounts for the other semispan of the wing. The subscripts on L_s refer to the case. Substituting Eqs. (57)–(62) into Eqs. (63)–(65) leads to the spanwise lift. In order to avoid difficulties with branch points and multivalued functions, it is necessary when integrating p_5 to use the absolute value of t in the expression for p_5 as given in Eq. (61). The results of the integration are

$$L_{s_1} = (2\rho U v_0/\beta)\,(b - x) \tag{66}$$

$$L_{s_2} = L_{s_3} = \frac{2\rho U v_0}{\beta}\left(\frac{b}{\pi}\cos^{-1}\frac{t}{x} + \frac{t}{2} - \frac{x}{2}\right) \tag{67}$$

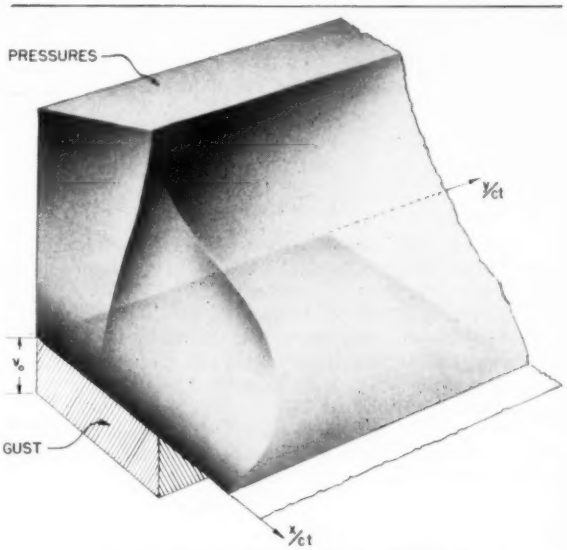

FIG. 9. Pressure distribution in perspective.

Hence, it is not necessary to distinguish between L_{s_2} and L_{s_3}. L_s is equivalent to the γ that Miles[7] obtains and is proportional to it. In order to obtain the lift and leading-edge moment, first transform back to physical x, t variables and then integrate in the chordwise direction with a lever arm x (physical) for the moment and without the lever arm for the lift. The results for the lift are

$$\frac{L}{L_0} = \frac{\beta\tau}{M}\left(1 - \frac{1}{2}\frac{\beta\tau}{M\beta\text{A.R.}}\right) \qquad \left(0 < \tau < \frac{M}{M+1}\right) \tag{68}$$

$$\frac{L}{L_0} = \frac{1}{\pi}\cos^{-1}\left(\frac{M^2 - (M^2-1)\tau}{M}\right) + \frac{\beta\tau}{\pi M}\left(\frac{\pi}{2} + \sin^{-1}\frac{M(1-\tau)}{\tau}\right) + \frac{1}{4\beta\text{A.R.}}\left[\frac{(M-1)\,(M^2-1)\tau^2}{M^2} - \frac{2(M^2-1)\tau}{M} + (M-1)\right] \qquad \left(\frac{M}{M+1} < \tau < \frac{M}{M-1}\right) \tag{69}$$

$$L/L_0 = 1 - (1/2\beta\text{A.R.}) \qquad [(M/M-1) < \tau < \infty] \tag{70}$$

where L_0 ($= 2\rho v_0 bl/\beta$) is the lift on a two-dimensional wing at angle of attack v_0/U, $\tau = Ut/l$ and l is the chord. The results for the leading-edge moment are

$$\frac{M_{LE}}{M_0} = \frac{\beta\tau^2}{M}\left(1 - \frac{2\beta\tau}{3M\beta\text{A.R.}}\right) \qquad \left(0 < \tau < \frac{M}{M+1}\right) \tag{71}$$

$$\frac{M_{LE}}{M_0} = \frac{1}{\pi}\cos^{-1}\left(\frac{M^2 - (M^2-1)\tau}{M}\right) - \frac{\beta\tau}{\pi M^2}\sqrt{\tau^2 - M^2(1-\tau)^2} + \frac{\beta\tau^2}{\pi M}\cos^{-1}\frac{M(\tau-1)}{\tau} + \frac{1}{6\beta\text{A.R.}}\left[\frac{\tau^3(M-1)^3(M+1)}{M^3} - \frac{3(M^2-1)\tau}{M} + 2(M-1)\right] \qquad \left(\frac{M}{M+1} < \tau < \frac{M}{M-1}\right) \tag{72}$$

$$M_{LE}/M_0 = 1 - (2/3\beta\text{A.R.}) \qquad [M/(M-1) < \tau < \infty] \tag{73}$$

where M_0 ($= \rho U v_0 bl^2/\beta$) is the leading edge moment on a two-dimensional wing at angle of attack v_0/U.

These expressions for lift and moment agree with those obtained by Miles.[7]

Discussion

The solution presented here is valid within the assumptions of linear theory. The external regions must not interact, however, and this condition will be met provided βA.R. > 1.

References

[1] Gardner, C. S., *Time-Dependent Linearized Supersonic Flow Past Planar Wings*, Communications on Pure and Applied Mathematics, Vol. III, No. 1, March, 1950.

[2] Schwarz, L., *Ebene instationare Theorie der Tragflache bei Uberschallgeschwindigkeit*, Jahrb. 1943 der deutschen Luftfahrtforschung, IAOIO, Stephan Geibel & Co. (Altenburg/Thur), pp. 1–8. (Available as Translation No. F-TS-934-RE, Air Materiel Command, Wright Field, Dayton, Ohio, March, 1947.)

[3] Miles, John C., *Transient Loading of Airfoils at Supersonic Speeds*, Journal of the Aeronautical Sciences, Vol. 15, No. 10, p. 592, October, 1948.

[4] Heaslet, M. A., and Lomax, H., *Two-Dimensional Unsteady Lift Problems in Supersonic Flight*, N.A.C.A. T.N. No. 1621, June, 1948.

[5] Biot, M. A., *Loads on a Supersonic Wing Striking a Sharp-Edged Gust*, Journal of the Aeronautical Sciences, Vol. 16, No. 5, p. 296, May, 1949.

[6] Watkins, Charles E., *Transient Two-Dimensional Flows at Supersonic Speeds*, Readers' Forum, Journal of the Aeronautical Sciences, Vol. 16, No. 9, p. 569, September, 1949.

[7] Miles, John W., *Transient Loading of Supersonic Rectangular Airfoils*, Journal of the Aeronautical Sciences, Vol. 17, No. 10, p. 647, October, 1950.

[8] Evvard, John C., *Distribution of Wave Drag and Lift in the Vicinity of Wing Tips at Supersonic Speeds*, N.A.C.A. T.N. No. 1382, July, 1947.

[9] Goodman, Theodore R., *The Lift Distribution on Conical and Nonconical Flow Regions of Thin Finite Wings in a Supersonic Stream*, Journal of the Aeronautical Sciences, Vol. 16, No. 6, p. 365, June, 1949.

[10] Goodman, Theodore R., *ibid.*, *Errata*, Journal of the Aeronautical Sciences, Vol. 16, No. 11, p. 703, November, 1949.

Determination of Rocket-Motor Heat-Transfer Coefficients by the Transient Method

(*Continued from page 518*)

Conclusions

(1) Using the rocket-motor injector, motor L^*, and propellant combination reported in this work, nozzle gas-film heat-transfer coefficients can be predicted within the accuracy required for engineering estimates from Eq. (4). Coincidentally, the accepted equation factor for straight pipe heat transfer as given in McAdams[1] is 0.027 in place of 0.029 used above.

(2) Until more accurate high-temperature data become available for the viscosity and thermal conductivity of rocket-motor combustion gas mixtures, satisfactory correlation of rocket-motor heat-transfer data may be achieved by the use of specific heat data in the above type of equation.

(3) The correlation of nozzle heat-transfer data measured under the controlled low-temperature conditions of this report reflected satisfactory operation of the segmented copper nozzle with its attendant instrumentation and has demonstrated the potentiality of the transient method for measurement of rocket-motor gas-film heat-transfer coefficients.

References

[1] McAdams, *Heat Transmission*, 2nd Ed., pp. 171 and 174; McGraw-Hill Book Company, Inc., New York, 1942.

[2] London, A. L., Nottage, H. B., and Boelter, L. M. K., *Determination of Unit Conductances for Heat and Mass Transfer by the Transient Method*, Industrial & Engineering Chemistry, Vol. 33, p. 467, April, 1941.

[3] Schmidt, E. *Einfuhrung In Die Technische Thermodynamik*, Edwards Bros., 1944.

[4] Perry, R. L., and Berggren, W. P., *Transient Heat Conduction in Hollow Cylinders after Sudden Change of Inner-Surface Temperature*, University of California, Publications in Engineering, Vol. 5, No. 3, pp. 59–88, 1944.

[5] Kaye, J., Keenan, J. H., and McAdams, W. H., *Report of Progress on Measurements of Friction Coefficients, Recovery Factors, and Heat Transfer Coefficients for Supersonic Flow of Air in a Pipe*, reprint of a paper delivered at the Heat Transfer and Fluid Mechanics Institute, p. 162, A.S.M.E., June, 1949.

Similarity Laws for Slender Bodies of Revolution in Hypersonic Flows

STANFORD E. NEICE* AND DORRIS M. EHRET†

Ames Aeronautical Laboratory, N.A.C.A.

ABSTRACT

The hypersonic similarity law, as developed by Tsien for bodies of revolution at zero angle of attack, is tested by comparing pressure distributions obtained using the method of characteristics. The results indicate that, in spite of the assumptions made in its development, the hypersonic similarity law is valid for relatively wide ranges of Mach Number and fineness ratio. Similarity laws for hypersonic flow about slender pointed bodies of revolution at angle of attack are also developed. Both the potential flow and the viscous effects of the transverse component of the flow are considered in this development.

INTRODUCTION

SIMILARITY LAWS ARE IMPORTANT to the aerodynamicist because they provide a useful guide for the correlation and extrapolation of data. These laws, for example, show how data for a given body, at a given Mach Number, can be applied to a related body at another Mach Number within the same Mach Number range. Similarity laws of this type have been developed for the different Mach Number ranges. In subsonic flow there is, for example, the familiar Prandtl-Glauert rule. A similar rule is available for low supersonic flow. The validity of these laws has been established through repeated checks with theory and experiment. More recently, similarity laws have been developed for transonic and hypersonic flows. The validity of the transonic law for two-dimensional flow is now being investigated by Liepmann and others.

The hypersonic similarity law is currently under investigation at the Ames Laboratory of the N.A.C.A. The purpose of this investigation is to evaluate the accuracy of the law for nonlifting bodies of revolution and to determine the form of the law for more general three-dimensional flows. The primary emphasis in this investigation to date has been placed on the flow about bodies of revolution. A brief account of our progress is the subject of this paper.

BODIES OF REVOLUTION AT ZERO ANGLE OF ATTACK

The hypersonic similarity law for potential flow about slender nonlifting bodies of revolution was first developed by Tsien.[1] He found that, through the introduction of nondimensional coordinates and a nondimensional perturbation potential into the equation of motion and the boundary conditions, the flow around bodies of a given thickness distribution was a function of a single parameter. This parameter, known as the hypersonic similarity parameter, is the ratio of the free-stream Mach Number to the body fineness ratio. The similarity law for nonlifting bodies of revolution is summarized at the top of Fig. 1. It should be noted that since the pressure ratio is a function of the similarity parameter, K_1, the drag parameter, $M_0^2\ C_D$,* is also a function of K_1 only. An example of conditions where the similarity law would apply is shown in the lower half of Fig. 1.

In view of the simplifying assumptions involved in deriving the similarity law—namely, irrotational flow, slender bodies, and Mach Numbers much greater than 1—the applicability of this law seemed uncertain and therefore was investigated.[2] This investigation was carried out by comparing pressure distributions along several bodies having the same values of the similarity parameter and the same thickness distribution.

The most extensive comparisons were made for ogive cylinders. Although ogives do not have exactly the same thickness distribution, the variation was found to be negligible for the cases considered. Pressure distributions were obtained for these bodies using the method of characteristics for Mach Numbers and fine-

* Force and moment coefficients in this paper are referred to the maximum cross-sectional area and overall length of the body. These coefficients do not consider the effects of pressure forces on the base of the body.

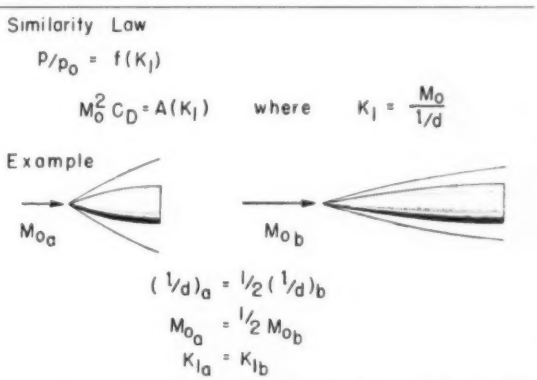

FIG. 1. Hypersonic similarity law for slender nonlifting bodies of revolution.

Presented at the Hypersonic Aerodynamics Session, Nineteenth Annual Meeting, I.A.S., New York, January 29–February 1, 1951.

* Aeronautical Research Scientist.

† Aeronautical Research Scientist.

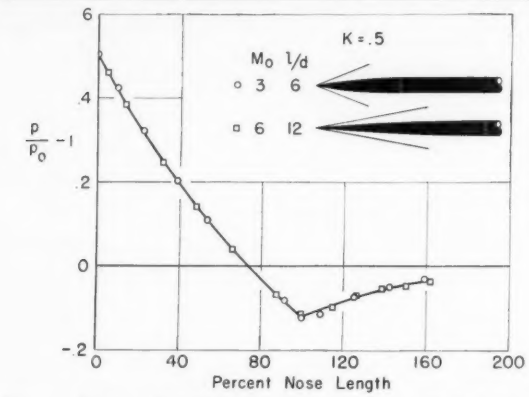

FIG. 2. Pressure distributions along two ogive cylinders at zero angle of attack for $K = 0.5$.

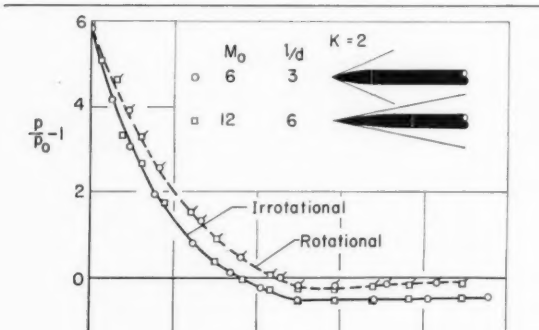

FIG. 3. Pressure distributions along two ogive cylinders at zero angle of attack for $K = 2.0$.

ness ratios varying from 1.5 to 12 in combinations to give values of the similarity parameter from 0.5 to 2.0. Comparisons were made for cases in which the pressure distributions were determined both with and without consideration of rotation—that is, with and without entropy gradients in the flow.

A sample of the results obtained is shown in Fig. 2, which gives the pressure distributions obtained for two ogive cylinders having the same value of K_1 for the nose section. The pressure coefficient $(p/p_0) - 1$ is plotted against per cent nose length. The value of K_1 here is 0.5 with Mach Numbers, M_0, of 3 and 6, and nose fineness ratios, $1/d$, of 6 and 12, respectively. The curve has been faired through the points for both cases. (More points were used in fairing the curve than could be shown here.) It is apparent that within the accuracy of the solution the pressure distributions for these two cases are identical. The similarity in pressure distribution holds on the cylindrical afterbody as well as on the nose section. For the case shown here, the change in the pressure distribution due to rotation is of the same order of magnitude as the scatter of the points for a given solution and, consequently, could not be shown. Fig. 3 gives the pressure distribution for ogive cylinders for $K_1 = 2$; one case is for a Mach Number of 6 and a nose fineness ratio of 3, while the other is for a Mach Number of 12 with a fineness ratio of 6. The solid line is faired through the points obtained by neglecting the effects of rotation, and the dashed line is faired through the points obtained by including the effects of rotation. Again the pressure distributions for the irrotational case are nearly identical. As predicted by Hayes,[3] the pressure distributions are also the same when rotation is considered. It is noteworthy that the effect of rotation is sizable for the case of $K_1 = 2$, whereas it was negligible for the case of $K_1 = 0.5$.

These and other solutions obtained in the investigation demonstrated that the similarity law is applicable to nonlifting bodies within engineering accuracy over a wide range of Mach Numbers and fineness ratios, in spite of the assumptions made in the derivation. More definite limits on the range of applicability were needed. To obtain these limits for ogives, the conditions at the nose, where the body slope was greatest, were considered to give the most severe test of similarity. By following this assumption, the pressure ratios for cones with vertex angles corresponding to the nose angles of the ogives were obtained from Kopal's tables[4] and were plotted against the similarity parameter for the bodies under consideration. A curve was faired through the values obtained for the most slender bodies. The similarity law was considered to be applicable for all cases where the pressure ratios were within 5 per cent of the faired curve. Additional solutions by the method of characteristics were made to substantiate the range of applicability as determined by the foregoing procedure. Fig. 4 shows the range of applicability of the hypersonic similarity law as determined for ogives by

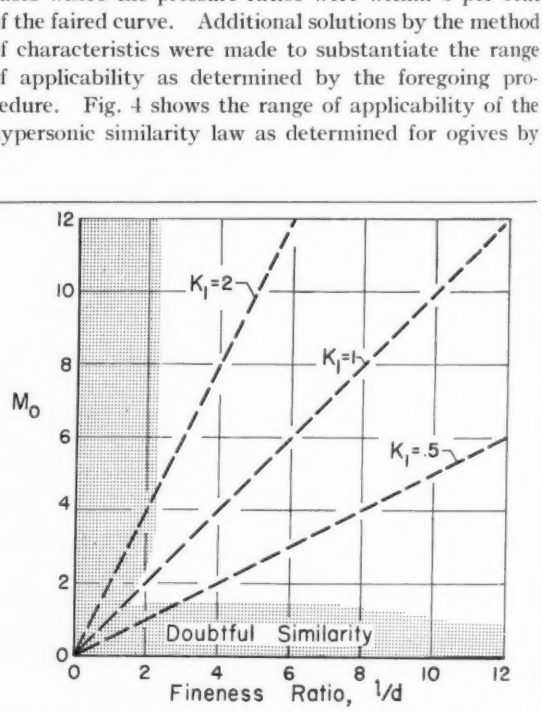

FIG. 4. Estimated range of applicability of the hypersonic similarity laws to nonlifting ogives.

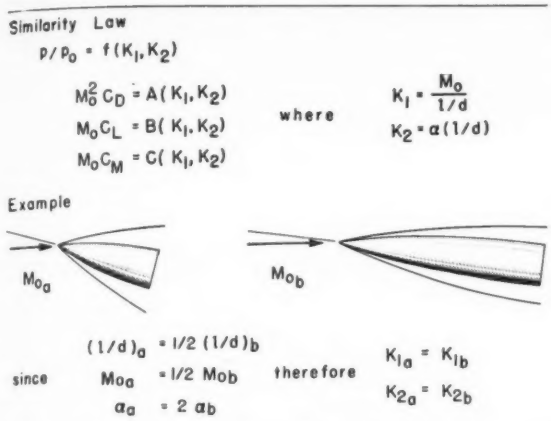

FIG. 5. Hypersonic similarity law for slender inclined bodies of revolution.

this method. Within the unshaded area the hypersonic similarity law should be applicable within 5 per cent.

BODIES OF REVOLUTION AT ANGLE OF ATTACK

Potential Flow Solution

Since the hypersonic similarity law proved to be accurate for nonlifting bodies of revolution, it appeared desirable to determine the form of the law when the angle of attack was not zero. For this analysis, the assumptions made were consistent with those of the previous investigation—that is, slender bodies, small angles of attack, large Mach Numbers, and potential flow. The equation of motion and the boundary conditions were established to the order of the approximations involved in these assumptions and were then reduced to nondimensional form. In this form, flow similarity was indicated for related bodies if K_1, the ratio of the free-steam Mach Number to the fineness ratio, and K_2, the product of the angle of attack and the fineness ratio, remained constant.

This similarity law is summarized in Fig. 5. The pressure ratio for inclined bodies is a function of the parameter, K_2, as well as K_1. It follows then that the drag, lift, and moment parameters are also functions of K_1 and K_2. The two cases illustrated on the lower half of Fig. 5 satisfy the requirements for similarity; hence, the pressure distributions, in terms of p/p_0, and the force and moment parameters for the two bodies should be identical.

Viscous Considerations

Following the suggestion of Allen,[5] it is possible to include certain viscous corrections in the aerodynamic coefficients of slender inclined bodies of revolution. For example, consider a body of revolution at angle of attack. The axial component of the velocity gives rise to surface shear, while the transverse component results not only in surface shear but usually in the separation of the flow. This latter phenomenon has a pronounced effect on the lift, drag, and moment characteristics of an inclined body. It is this phenomenon that was considered.*

If a body of revolution is sufficiently slender, the viscous flow across it may be approximately represented as that over a circular cylinder of infinite length. With this approximation, expressions were obtained for the aerodynamic coefficients resulting from the viscous transverse force. Upon transformation into the nondimensional coordinates previously employed, these expressions become functions of the same parameters obtained for potential flow. As a result, the similarity parameters K_1 and K_2 apply to the viscous cross flow as well as the potential flow. The additional restriction, dictated by the viscous considerations, is that the Reynolds Number of the transverse flow must remain constant.

Experimental Results

As yet we have not been able to make a comprehensive evaluation of the similarity law for inclined bodies of revolution. However, a limited experimental check of the law has been conducted in the Ames 10- by 14-in. supersonic wind tunnel. It will be recalled that the hypersonic similarity law predicts that the ratio of the local pressure to the free-stream static pressure at corresponding points on related bodies is a function of the similarity parameters only. A simple experimental check would then involve measuring the pressures at corresponding points on two cones of different fineness ratios and comparing the results on the basis of the similarity parameters K_1 and K_2. This type of check has been made and is illustrated in Fig. 6.

* R. T. Jones, in N.A.C.A. Report No. 884, 1947, demonstrated that the axial and transverse components of the laminar boundary-layer flow could be considered separately for the case of infinitely long cylinders at angles of yaw.

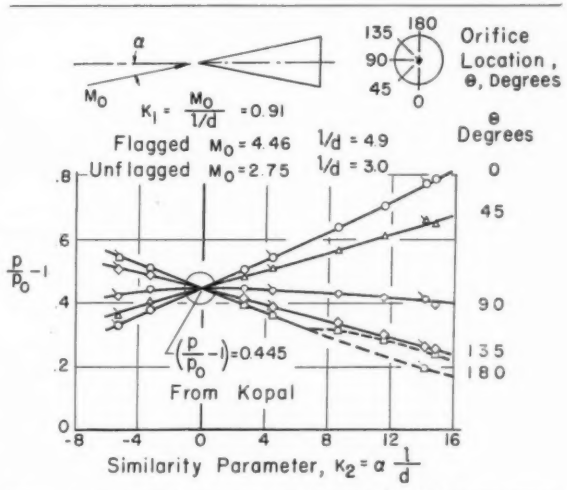

FIG. 6. Variation of pressure coefficient with K_2 for two cones.

Two cones, having fineness ratios of 3.0 and 4.9, were tested at Mach Numbers of 2.75 and 4.46, respectively, and at angles of attack up to 5°. This combination gave a value of K_1 of 0.91 for both bodies. Pressures were measured at five points around the surface in a transverse plane at one-half the body length. In the lower half of Fig. 6, the pressure coefficients for corresponding points are plotted as a function of K_2. Agreement with the hypersonic similarity law can be observed here in that the values of pressure coefficient for corresponding points on both bodies lie essentially along the same curve. A discrepancy at the higher values of K_2 can be noted on the low-pressure side of the cones. This is believed to be a result of dissimilar separation characteristics caused by the fact that we were unable to maintain the same cross-flow Reynolds Number at corresponding values of K_2. Separation phenomenon should be almost identical at the same cross-flow Reynolds Number.

Three-Dimensional Flow

As a result of the success in applying the similarity law to the specific cases previously discussed, it appeared desirable to determine the form of the law for three-dimensional shapes of practical value. In this regard, it has been indicated by Hayes[3] that similarity will be observed in hypersonic flow about slender three-dimensional shapes. His analysis included consideration of the effects of shock waves and rotation; however, it precluded considerations of the form of the law in terms of customary aerodynamic parameters. It was therefore undertaken to determine the law as it would apply to familiar three-dimensional configurations.[6] The assumptions made were the same as those previously employed with one distinct difference: The assumption of slenderness was applied only to the thickness dimension. On this basis, the boundary conditions and equation of motion were transformed into the nondimensional system of coordinates, and flow similarity for related bodies was then observed. The hypersonic similarity law for three-dimensional flow, together with an example of how it may be applied to a wing-body combination, is shown in Fig. 7. In this case, the pressure ratio is a function not only of K_1 and K_2 but also K_3, the ratio of the body thickness to the span. The force and moment parameters are also a function of these three similarity parameters. At present, it appears impractical to further generalize the law to include viscous effects.

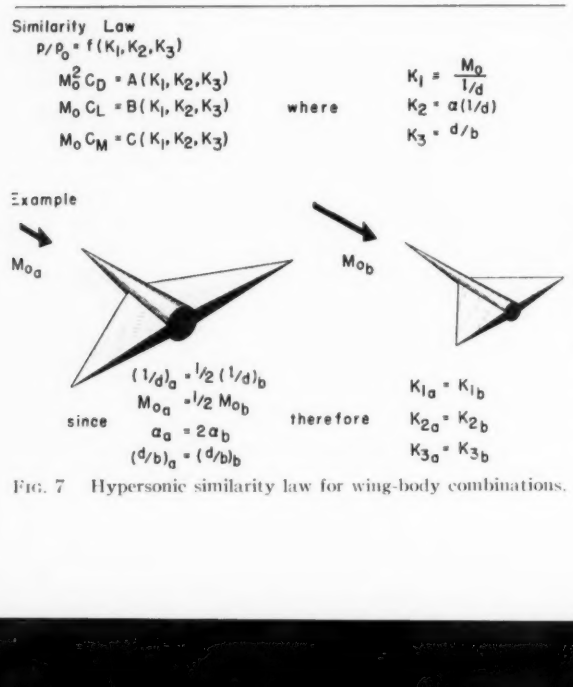

Fig. 7 Hypersonic similarity law for wing-body combinations.

These expressions for three-dimensional similarity apply, as would be expected, to particular cases in addition to the general wing-body combination already illustrated. For example, consider the following cases:

(*1*) *Two-dimensional flow.*—Here, the parameter, K_3, is zero, and therefore the pressure ratio and force and moment parameters are functions of only K_1 and K_2. This result is identical to that developed by Tsien[1] for two-dimensional flow.

(*2*) *Slender body of revolution.*—In this case, the parameter, K_3, has the constant value of 1 and is thus eliminated as a similarity parameter. The resulting expressions due to this consideration are identical to those for the inclined body of revolution previously discussed in this paper. For the zero angle-of-attack case, the value of the similarity parameter, K_2, would, of course, be zero. The similarity law resulting from this consideration (noting the fact that K_3 is constant) would be the axially symmetric case also derived by Tsien.[1]

(*3*) *Finite span wings.*—This is a three-dimensional case involving all the parameters. It should be emphasized, however, that the parameter, K_3, appeared to the second power throughout the equations of motion. It may therefore be concluded that only for wings where the aspect ratio is extremely small will the characteristics differ appreciably from the two-dimensional case. (It has recently been brought to our attention that this rule was also developed by Professor Tsien and, although unpublished, has been presented in the form of lecture notes.)

Concluding Remarks

A final appraisal of the status of our investigation of the hypersonic similarity law may be summarized in three main points. First, it has been shown that in spite of the assumptions made in its derivation, the hypersonic similarity law is applicable to bodies of revolution at zero angle of attack for wide ranges of Mach Number and fineness ratio. Second, limited experimental data presented here indicate that the hypersonic similarity law also applies for bodies of revolution at small angles of attack; however, additional data must be obtained before the range of applicability can be established. Third, the form of the hypersonic

(*Continued on page 568*)

A Superposition Method for Calculating the Aeroelastic Behavior of Swept Wings*

R. B. BROWN,† K. F. HOLTBY,‡ AND H. C. MARTIN**

Boeing Airplane Company and University of Washington

SUMMARY

This paper presents the development and application of a method for solving aeroelastic problems on sweptback wings, primarily suitable for use by aerodynamicists and structural design engineers. This method, called the "superposition method," separates the aerodynamic and structural calculations, making it possible to use either theoretical or experimental determinations of spanwise loading and to account for induction effects. The method has been developed principally for use in design calculations where simplicity and rapidity of solution are primary considerations.

First, certain selected initial twist distributions are applied to the wing. For these, the spanwise loading is determined and the elastic deflections are computed. Any arbitrary loading may then be calculated by a superposition of these initial effects, plus the requirement of equilibrium between elastic and aerodynamic forces.

The superposition method can be used to solve the usual aerodynamic problems arising in longitudinal and lateral stability and control and to provide structural design criteria. Application of the method to these problems is discussed in the second part of this paper. In applying the method, once certain parameters have been calculated, the solution to a large number of specific problems follows at once by application of the superposition principle.

INTRODUCTION

AERODYNAMIC LOADS ON THE WING which cause lift, rolling moment, etc., are dependent on the spanwise distribution of angle of attack. For the nonrigid or flexible wing, this angle-of-attack distribution will be a function of wing deflection. As a result, aerodynamic forces and structural deflections cannot be considered as being independent of each other.

Examples of how structural deflections alter typical aerodynamic parameters are shown in Figs. 1 and 2. These parameters come from the solution for the equilibrium state between aerodynamic and elastic forces. Determination of this equilibrium state constitutes the solution to the flexible wing problem.

In determining the equilibrium state, all deflections that affect the wing angle of attack must be considered. On straight wings, only torsional deflections cause changes in angle of attack along the span. On swept wings, both torsional and bending deflections cause changes in the stream angle of attack.

Aerodynamic loads are a function of dynamic pressure, q, and section lift coefficient, C_l. The lift coefficient is dependent on the wing plan form, angle-of-attack distribution, and the two-dimensional slope of the lift curve, m. For a given plan form and angle-of-attack distribution, structural deflections are directly proportional to qm. Accordingly, qm is a basic parameter that appears throughout this analysis. The variation of m with Mach Number can be taken into account either by use of wind-tunnel data or the usual Glauert relationship

$$m = (m)_{M=0}\,(1/\sqrt{1 - M^2\cos^2\Lambda})$$

The three-dimensional slope of the lift curve for the rigid wing can be used, since two- and three-dimensional values vary in the same manner with Mach Number. In this case span-load distributions must be based on a unit value of the three-dimensional slope for the rigid wing.

Methods of solving the component aerodynamic and structural problems are prerequisite to establishing a solution for equilibrium conditions. For a given angle-of-attack distribution, it must be possible to determine the rigid-wing span-load distribution. Also, for any

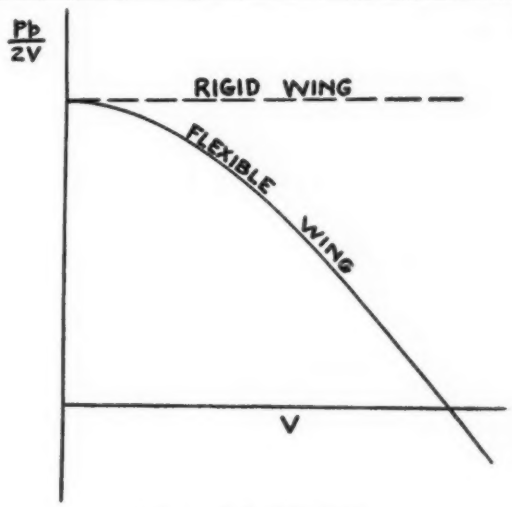

FIG. 1. Roll performance.

Presented at the Aeroelasticity and Structures Session, Annual Summer Meeting, I.A.S., Los Angeles, July 12–14, 1950. Revised and received February 15, 1951.

* Certain parts of this paper are taken from an M.S. Thesis, Department of Aeronautical Engineering, University of Washington, by R. B. Brown.

† Aerodynamics Unit, Boeing Airplane Company.

‡ Aerodynamics Unit, Boeing Airplane Company.

** Associate Professor, University of Washington.

load distribution, it must be possible to calculate the elastic deflection of the wing. Various methods of handling these problems are discussed in succeeding pages of this paper. However, it should be noted that use of the superposition method is independent of the manner in which the individual aerodynamic and structural problems are solved.

Two of the earlier treatments of this problem[1, 2] present solutions based on methods quite different from each other and from that proposed in this paper. In these previous approaches to the problem, the spanwise load calculation is carried out for the elastic wing structure. Thus the span-load problem and the wing-deflection problem both enter more or less simultaneously into the formulation and development of these methods. The significant difference in the superposition method is that the span-load problem is carried out independent of the elastic properties of the wing.

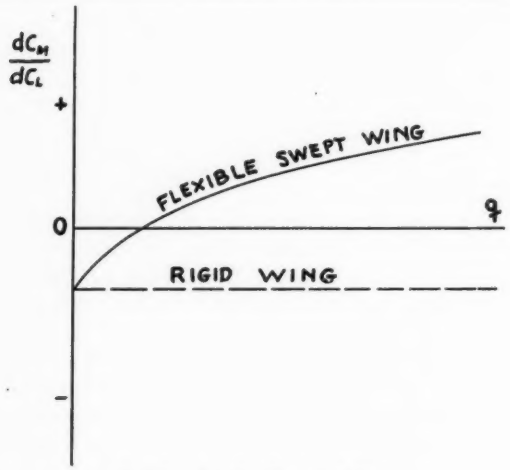

FIG. 2. Longitudinal stability.

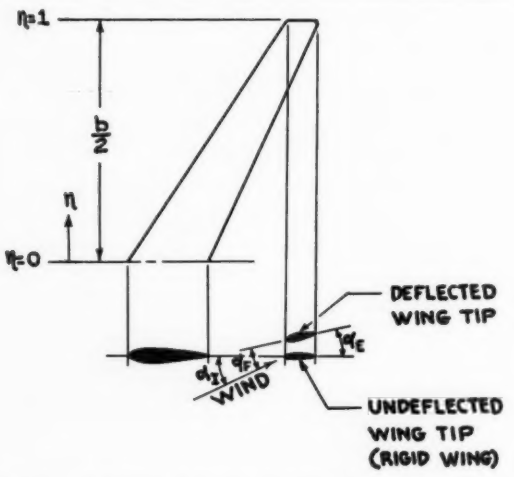

FIG. 3. Deflection of typical sweptback wing due to lifting loading.

PART (I) DEVELOPMENT OF THE SUPERPOSITION METHOD

Equilibrium Condition

As already pointed out, the elastic wing subjected to aerodynamic loading will deflect until equilibrium is established between external aerodynamic and internal elastic forces. Aerodynamic loadings are caused by angle-of-attack distributions; also, angle-of-attack distributions result from structural deflections. Therefore, the relationships upon which the superposition method is based are expressed in terms of angle of attack.

The rigid wing is considered as being subjected to given initial conditions of angle-of-attack distribution α_I and qm. The aerodynamic forces thus initiated will deflect an elastic wing by a spanwise distribution α_E until equilibrium is attained at a final angle-of-attack distribution α_F. These angles are shown in Fig. 3 for the wing with sweepback.

The angles shown in Fig. 3 are defined as follows:

α_I = angle-of-attack distribution initially applied to the wing; hence, α_I refers to the rigid or undeflected wing

α_E = elastic angle-of-attack distribution due to wing deflection (on a swept wing both bending and torsion contribute to α_E)

α_F = angle-of-attack distribution at which equilibrium is established—referred to as the final angle-of-attack distribution

These angles are functions of the spanwise coordinate η and are measured in the direction parallel to the plane of symmetry of the airplane.

The aerodynamic forces due to α_I will be termed the rigid-wing loading. The wing will deflect causing an angle-of-attack distribution, α_E, and the loading corresponding to α_E will be called the "elastic loading." At equilibrium, α_F, the aerodynamic forces will be referred to as either the equilibrium or the final loading. At every station along the span, the three angles are related by

$$\alpha_F = \alpha_I + \alpha_E \tag{1}$$

This relationship is basic to any consideration of the effect of structural deflections on aerodynamic loading and, hence, is basic in the development of the superposition method.

Another important fact is implicit in Eq. (1). Suppose the equilibrium angle of attack α_F is known. Then the equilibrium loading may be found, and, since this is the loading that actually holds the wing in its deflected position, α_E may then be calculated. Knowing α_F and α_E, Eq. (1) gives α_I. Hence, starting with α_F, a complete solution is directly obtainable.

On the other hand, starting with α_I, no such direct determination of the quantities in Eq. (1) is possible. Given α_I, neither α_E nor α_F can be found by direct

means, since they are mutually dependent on each other.

Superposition of Preliminary Cases

Superposition will be based on several solutions determined beforehand for a few selected preliminary cases. For these cases, α_F distributions will be assumed and α_E and α_I calculated by the procedure previously indicated. Since calculation of α_E will depend on wing stiffness and geometry, these initial solutions must be carried out for a specific wing. Information regarding the wing structure must be available if the influence of structural deflection on wing aerodynamic forces is to be predicted.

Let three preliminary solutions be carried out for certain selected Cases 1, 2, and 3, for which α_F is known. Then, all terms in Eq. (1) are known for each of these cases (i.e., α_{I_1}, α_{E_1}, α_{F_1}, for Case 1, etc.). The exact form for the selected values α_{F_1}, α_{F_2}, and α_{F_3} are not important at this point.

Now assume the three known initial values α_{I_1}, α_{I_2}, and α_{I_3} to be multiplied by constants A, B, and C, respectively, and superimposed as shown in Fig. 4.

The superposition of $A\alpha_{I_1}$, $B\alpha_{I_2}$, and $C\alpha_{I_3}$ will yield another angle-of-attack distribution, which will be referred to as α_I. Or

$$A\alpha_{I_1} + B\alpha_{I_2} + C\alpha_{I_3} = \alpha_I$$

Referring to Eq. (1) and

$$A\alpha_{F_1} = A\alpha_{I_1} + A\alpha_{E_1} \tag{2a}$$
$$B\alpha_{F_2} = B\alpha_{I_2} + B\alpha_{E_2} \tag{2b}$$
$$C\alpha_{F_3} = C\alpha_{I_3} + C\alpha_{E_3} \tag{2c}$$

accordingly, elastic α_E and final α_F deflections can be superimposed as follows:

$$A\alpha_{E_1} + B\alpha_{E_2} + C\alpha_{E_3} = \alpha_E$$
$$A\alpha_{F_1} + B\alpha_{F_2} + C\alpha_{F_3} = \alpha_F$$

Hence, by superposition of the three basic cases, a solution α_F to an arbitrary case α_I has been obtained.

The constants A, B, and C must be determined if a specific α_I is to be duplicated. It will be the function of the analytical development of the method to show how these may be calculated. At present, it is of interest to observe that in Eqs. (2a), (2b), and (2c) all terms with the same numerical subscript contain the same constant multiplier. This is necessary if Hooke's Law is to hold and if aerodynamic loads are to be linearly related to the angle of attack. Thus consider α_{F_1}, α_{E_1}, and α_{I_1}, all of which are known. Suppose α_{F_1} is doubled. The loading will then also be doubled. By Hooke's Law, the elastic deflection α_{E_1} will likewise be doubled under these conditions. Finally, by Eq. (1) it is found that α_{I_1} also doubles. Hence, under these conditions of linearity, any factor such as A, B, and C above must appear on each of the three appropriate angles.

Selected Preliminary Cases

The three preliminary cases that are basic to the superposition method as it will be developed in this paper are shown in Fig. 5. These now become the preliminary Cases 1, 2, and 3, respectively, of the previous section. Subscript 1 will then always refer to the linear final angle-of-attack distribution, etc.

It will be noted from Fig. 5 that α_F at the tip has been assumed as 1 rad. for all three cases. This is an arbitrary but convenient assumption.

Having chosen values of α_F for the three preliminary cases ($\alpha_F = \eta, \eta^2, \eta^3$), span-load distributions are es-

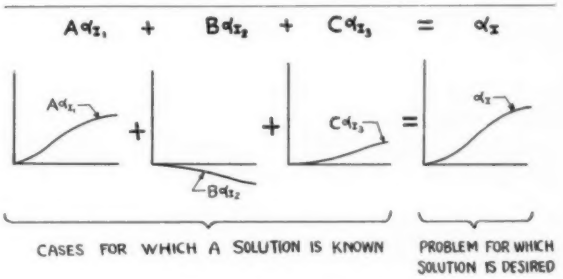

FIG. 4. Superposition of preliminary cases.

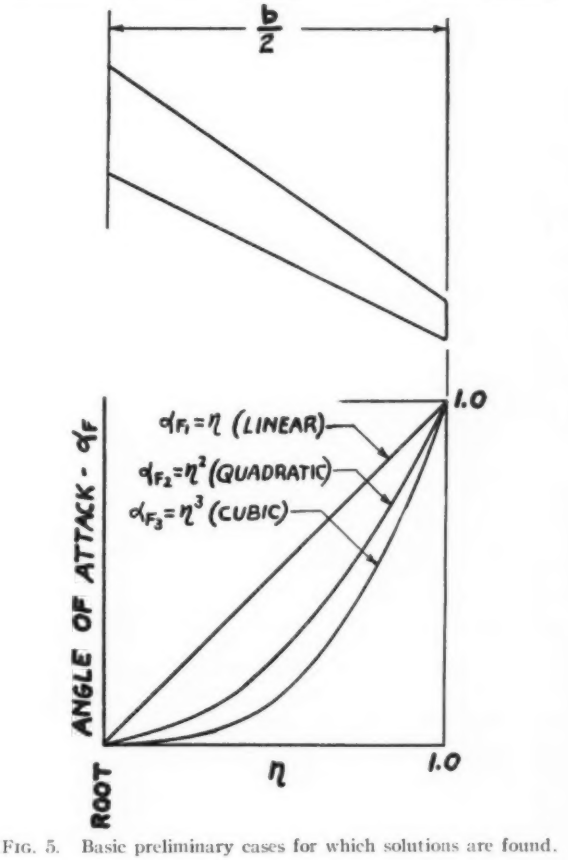

FIG. 5. Basic preliminary cases for which solutions are found.

tablished, and α_E and α_I corresponding to each case are calculated and plotted against η as shown in Fig. 6. These plots can be superimposed as indicated by Fig. 4.

Further Examples of Superposition Procedure

The superposition carried out in Fig. 4 was for a problem in which the initial angle-of-attack distribution α_I could be matched by a superposition of the three preliminary cases (α_{I_1}, α_{I_2}, and α_{I_3}). For problems in which this is not possible, the use of an "*auxiliary diagram*" is introduced. The auxiliary diagram makes the superposition method capable of handling problems in which α_I is completely arbitrary. The following examples cover cases that illustrate the use of the auxiliary diagram:

Example (1) *Constant Angle of Attack.*—The problem to be solved is given by α_I on the right-hand side of Fig. 7. Since $\alpha_I \neq 0$ at the root, it cannot be matched by a simple superposition of α_I's corresponding to linear, quadratic, and cubic α_F's as was possible in Fig. 4.

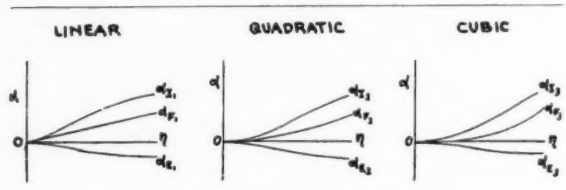

FIG. 6. Solution for basic preliminary cases.

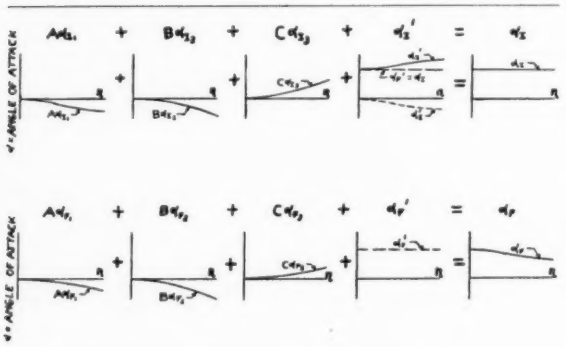

FIG. 7. Superposition procedure for α_I = constant.

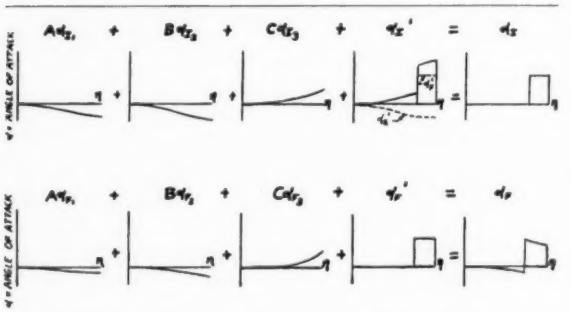

FIG. 8. Superposition procedure for α_I = step.

To overcome this difficulty, another case, represented by the auxiliary diagram, is superimposed, together with the basic linear, quadratic, and cubic cases as illustrated in Fig. 7.

The essential feature of the auxiliary diagram is that it is constructed from the given problem on the basis of putting

$$\alpha_F' = \alpha_I \tag{3}$$

Since α_F' is known, α_E' and α_I' may be calculated precisely in the same manner as already carried out for the linear, quadratic, and cubic cases. It should be noted that this permits the calculation of the spanwise loading as though the wing were rigid. Also, for all arbitrary problems, the four cases shown in Fig. 7 are sufficient to yield an adequate solution. However, the auxiliary diagram must be constructed on the basis of Eq. (3) and, hence, will be different according to the specific problem. Thus, a span-load problem and a solution for the case represented by the auxiliary diagram must be carried out before the superposition method can be applied. This is comparatively simple, since the equilibrium condition is known for the auxiliary diagram because of its construction on the basis of Eq. (3).

Superposition now gives

$$A\alpha_{I_1} + B\alpha_{I_2} + C\alpha_{I_3} + \alpha_I' = \alpha_I \tag{4a}$$
$$A\alpha_{F_1} + B\alpha_{F_2} + C\alpha_{F_3} + \alpha_F' = \alpha_F \tag{4b}$$
$$A\alpha_{E_1} + B\alpha_{E_2} + C\alpha_{E_3} + \alpha_E' = \alpha_E \tag{4c}$$

where $\alpha_{F_1} = \eta$, $\alpha_{F_2} = \eta^2$, and $\alpha_{F_3} = \eta^3$ (see Fig. 3). It should be noted that, for this type of problem, $A\eta + B\eta^2 + C\eta^3$ also equals α_E.

The difficulty with the nonzero value of α_I at the root has now been overcome by introducing the auxiliary diagram. This can be seen by examining Fig. 7.

Example (2) *Step Angle of Attack* (*Aileron, Spoilers, Flaps*).—The solution of the step angle-of-attack distribution is the same as that for the constant angle-of-attack distribution of Example (1). Fig. 8 illustrates the combination of α_I's which can duplicate the step α_I. The solution α_F for any type of α_I may be made if it is possible to establish the rigid-wing-load distributions for α_I.

It is to be emphasized that any other arbitrary problem may be similarly solved with the aid of the three basic cases (linear, quadratic, and cubic) plus the auxiliary diagram.

Function of Auxiliary Diagram

The true function of the auxiliary diagram can best be seen by writing Eq. (4a) as

$$A\alpha_{I_1} + B\alpha_{I_2} + C\alpha_{I_3} = \alpha_I - \alpha_I' \tag{5}$$

Reference to the auxiliary diagram of either Fig. 7 or 8 [and keeping basic Eq. (1) in mind] indicates that

$$\alpha_I - \alpha_I' = \alpha_E' \tag{6}$$

Therefore, the summation of initial values as given by Eq. (4a) is actually made to approximate α_E', rather than α_I, as a result of introducing the auxiliary diagram.

This is significant and makes the superposition method possible. Physically, the wing structure is such that under any applied loading it will deflect in a smooth curve. Thus, α_E' will, in every case, be smooth and zero at the origin. Consequently, a summation as implied by Eq. (4a) becomes entirely possible and reasonable.

Another point is worthy of mention. Other diagrams than those based explicitly on Eq. (3) could serve as the auxiliary diagram. However, there is normally no advantage in deviating from the procedure given above; in fact, Eq. (3) gives an exceptionally convenient means for determining a satisfactory auxiliary diagram.

Analytical Expressions for $\alpha_{I_1}, \alpha_{I_2}, \alpha_{I_3}$

It has already been stated that $\alpha_{E_1}, \ldots$, etc., are known as curves plotted against spanwise coordinate η. These elastic angle-of-attack distributions will now be approximated by cubic equations in η as follows:

$$\alpha_{E_1} = qm(a_1\eta + b_1\eta^2 + c_1\eta^3) \quad (7a)$$
$$\alpha_{E_2} = qm(a_2\eta + b_2\eta^2 + c_2\eta^3) \quad (7b)$$
$$\alpha_{E_3} = qm(a_3\eta + b_3\eta^2 + c_3\eta^3) \quad (7c)$$

where $\alpha_{E_1}, \ldots$, etc., increase with dynamic pressure q and slope of lift curve m. To determine a_1, b_1, and c_1, select three reasonable spanwise values of η and read off the corresponding values of α_{E_1} from the plot of α_{E_1} vs. η. Substituting these into Eq. (7a) will give three equations from which to determine a_1, b_1, and c_1. The other constants can also be found by similar procedure.

Since α_{F_1}, α_{F_2}, and α_{F_3} are linear, quadratic, and cubic, respectively, in η (see Fig. 3), substitution in Eq. (1) gives

$$\alpha_{I_1} = \eta - \alpha_{E_1} = (1 - a_1qm)\eta - b_1qm\eta^2 - c_1qm\eta^3 \quad (8a)$$
$$\alpha_{I_2} = \eta^2 - \alpha_{E_2} = -a_2qm\eta + (1 - b_2qm)\eta^2 - c_2qm\eta^3 \quad (8b)$$
$$\alpha_{I_3} = \eta^3 - \alpha_{E_3} = -a_3qm\eta - b_3qm\eta^2 + (1 - c_3qm)\eta^3 \quad (8c)$$

All coefficients of η in the previous equations are known. Also, qm is now seen to appear as a fundamental parameter in the problem.

Solution for Superposition Coefficients A, B, ***and*** C

Now consider again Eqs. (5) and (6). Actually, α_E' is known as a plot vs. η. Hence, it can be represented also by a cubic in η or

$$\alpha_E' = qm(a\eta + b\eta^2 + c\eta^3) \quad (9)$$

where a, b, and c are known by an analysis similar to that following Eqs. (7). But by Eqs. (5) and (6) it is also seen that

$$\alpha_E' = \alpha_I - \alpha_I' = A\alpha_{I_1} + B\alpha_{I_2} + C\alpha_{I_3}$$

By Eqs. (8), this last result is also seen to be a cubic in η. Hence,

$$qm(a\eta + b\eta^2 + c\eta^3) - (A\alpha_{I_1} + B\alpha_{I_2} + C\alpha_{I_3}) \equiv 0 \quad (10)$$

since the two cubics in η can be made to coincide identically. Substituting from Eqs. (8) into Eq. (10),

$$[aqm - A(1 - a_1qm) + Ba_2qm + Ca_3qm]\eta + [bqm + Ab_1qm - B(1 - b_2qm) + Cb_3qm]\eta^2 + [cqm + Ac_1qm + Bc_2qm - C(1 - c_3qm)]\eta^3 \equiv 0 \quad (11)$$

This last equation can be assured for all values of η only if the coefficients of η are made to vanish. This requires

$$A(1 - a_1qm) - Ba_2qm - Ca_3qm = aqm \quad (12a)$$
$$-Ab_1qm + B(1 - b_2qm) - Cb_3qm = bqm \quad (12b)$$
$$-Ac_1qm - Bc_2qm + C(1 - c_3qm) = cqm \quad (12c)$$

Out of Eqs. (12) a solution can be made for A, B, and C. Then, from Eq. (4b), it is seen that the desired solution for the equilibrium α_F becomes

$$\alpha_F = A\eta + B\eta^2 + C\eta^3 + \alpha_I \quad (13)$$

in which Eq. (3) has been used to put $\alpha_F' = \alpha_I$. Likewise, α_E is known from Eq. (4c), since α_E' has been previously determined.

It should be noted that A, B, and C are the only unknowns in Eq. (12). A specific value for the parameter qm must be assigned. By assuming a series of values for qm, the superposition coefficients A, B, and C can be established for the desired range of qm.

Application of the method to a wide variety of problems has justified the use of a cubic in η for approximating α_E'. A higher degree curve might be used, but this increases the numerical work considerably. In certain cases trial and error may be necessary to find the best form of the cubic used to represent α_E'. However, a solution once found can always be checked. Thus, having determined α_F as from Eq. (13), it is possible to calculate the corresponding loading. Having found the loading, the deflections may be calculated. These must check the value given by Eq. (4c) using A, B, and C.

Part (II) will indicate how the solution for a number of particular quantities follows at once when A, B, and C have been determined for a given problem.

Part (II) Application of Superposition Method

As mentioned in the preceding discussion, the superposition method provides the designer with a rapid means of evaluating the effect of structural flexibility on aerodynamic characteristics and structural design criteria. It has been shown that the superposition method provides a means of solving for equilibrium conditions involving aerodynamic loads and structural deflections. A variety of problems requires solutions

TABLE I BASIC PRELIMINARY INFORMATION

ANGLE OF ATTACK DISTRIBUTION	RIGID WING LOAD DATA				ELASTIC DATA			
	LIFT DISTRIBUTION	LIFT COEFFICIENT	ROLLING MOMENT COEFFICIENT	PITCHING MOM. COEFF. ABOUT ¼ MAC	θ, Φ, AND α_E DISTRIBUTIONS	CUBIC COEFFICIENTS a, b, c	DEFLECTION OF ELASTIC AXIS	BENDING AND TORSIONAL MOMENTS
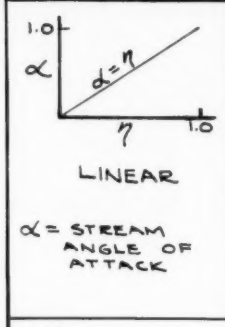 LINEAR α = STREAM ANGLE OF ATTACK	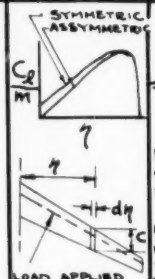	$\frac{C_{L_1}}{m}$ $=\frac{b}{S}\int_0^1 \frac{C_\ell}{m} c\, d\eta$ FROM SYMMETRIC LOAD m = TWO-DIMENSIONAL SLOPE OF THE LIFT CURVE	$\frac{C_{\mathcal{J}_1}}{m}$ $=\frac{b}{2S}\int_0^1 \left(\frac{C_\ell}{m}\right) c\eta\, d\eta$ FROM ASSYMMETRIC OR SEMI-ASSYMMETRIC LOADING, DEPENDING ON TYPE OF CONTROL	$\frac{C_{M_1}}{m}$ $=\frac{\bar{x}}{\bar{c}}\frac{C_{L_1}}{m}$ $\bar{c}$ = M.A.C. $\bar{y}$ = $\frac{C_{\mathcal{J}_1}}{C_{L_1}}$ 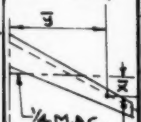	1. APPLY LINEAR LOAD DISTRIBUTION TO THE STRUCTURE FOR $q_m=1$ AND DETERMINE DEFLECTIONS IN TERMS OF α. 2. MATCH THIS α_E DISTRIBUTION BY COMPUTING CUBIC COEFFICIENTS SO THAT, $\alpha_{E_1}=a_1\eta+b_1\eta^2+c_1\eta^3$ 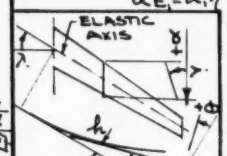	SINCE $q_m=1$, $\frac{\alpha_{E_1}}{q_m}=\alpha_{E_1}$ 	$\frac{h_1}{q_m}=\frac{b}{2}\int\left(\frac{\Theta}{q_m}\right)d\eta$ 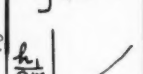	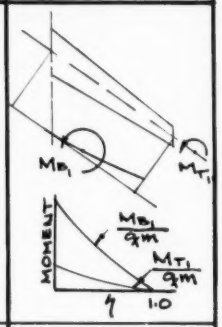
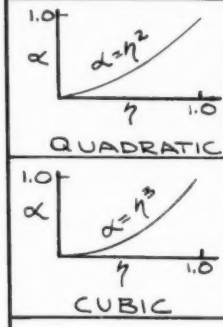 QUADRATIC	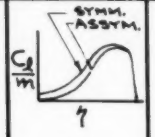	$\frac{C_{L_2}}{m}$	$\frac{C_{\mathcal{J}_2}}{m}$	$\frac{C_{M_2}}{m}$	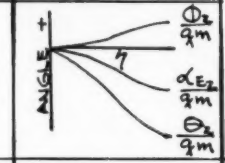	$\frac{\alpha_{E_2}}{q_m}=a_2\eta+b_2\eta^2+c_2\eta^3$	$\frac{h_2}{q_m}$ vs η	$\frac{M_{B_2}}{q_m}$, $\frac{M_{T_2}}{q_m}$ vs η
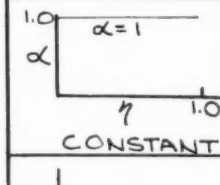 CUBIC		$\frac{C_{L_3}}{m}$	$\frac{C_{\mathcal{J}_3}}{m}$	$\frac{C_{M_3}}{m}$	$\frac{\alpha_{E_3}}{q_m}$, $\frac{\theta_3}{q_m}$, $\frac{\Phi_3}{q_m}$ vs η	a_3, b_3, c_3	$\frac{h_3}{q_m}$ vs η	$\frac{M_{B_3}}{q_m}$, $\frac{M_{T_3}}{q_m}$ vs η
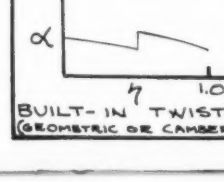 CONSTANT		$\frac{C_{L_\alpha}}{m}$	SYMMETRIC LOAD (NOT REQ'D. FOR ROLL CALCULATIONS)	$\frac{C_{M_\alpha}}{m}$	$\frac{\alpha_{E_\alpha}}{q_m}$, $\frac{\theta_\alpha}{q_m}$, $\frac{\Phi_\alpha}{q_m}$ vs η	$a_\alpha, b_\alpha, c_\alpha$	$\frac{h_\alpha}{q_m}$ vs η	$\frac{M_{B_\alpha}}{q_m}$, $\frac{M_{T_\alpha}}{q_m}$ vs η
BUILT-IN TWIST (GEOMETRIC OR CAMBER)		$\frac{C_{L_T}}{m}$ 	SYMMETRIC LOAD (NOT REQUIRED FOR ROLL CALCULATIONS)	$\frac{C_{M_T}}{m}$	$\frac{\alpha_{E_T}}{q_m}$, $\frac{\theta_T}{q_m}$, $\frac{\Phi_T}{q_m}$ vs η	a_T, b_T, c_T	$\frac{h_T}{q_m}$ vs η	$\frac{M_{B_T}}{q_m}$, $\frac{M_{T_T}}{q_m}$ vs η

TABLE I (CONT'D)

TABLE I (CONT'D)

ANGLE OF ATTACK DISTRIBUTION	RIGID WING LOAD DATA				ELASTIC DATA			
	LIFT DISTRIBUTION	LIFT COEFFICIENT	ROLLING MOMENT COEFFICIENT	PITCHING MOM. COEFF. ABOUT ¼MAC	θ, ϕ, AND α_E DISTRIBUTIONS	CUBIC COEFFICIENTS a, b, c	DEFLECTION OF ELASTIC AXIS	BENDING AND TORSIONAL MOMENTS
NONE (BASIC WING PITCHING MOMENT DUE TO SECTION CAMBER)	NONE	NONE	NONE	$C_{M_0} = \frac{b}{2S}\int_0^1 c_{m_0} c^2 d\eta$ $C_{m_0} = C_m$ @ $c_l = 0$	COMPUTE FOR $q = 1$ AND $C_{m_0} = +1$ $\frac{\alpha'_{E_M}}{q C_{M_0}}$, $\frac{\Phi_M}{q C_{M_0}}$ vs η	$\frac{\alpha'_{E_M}}{q C_{M_0}} = a_M\eta + b_M\eta^2 + c_M\eta^3$	0	$\frac{M_{T_M}}{q C_{M_0}}$ vs η
NONE (WING DEAD WEIGHT)	NONE	NONE	NONE	NONE	COMPUTE FOR $n = 1$ $\frac{\alpha'_{E_n}}{n}, \frac{\theta_n}{n}, \frac{\Phi_n}{n}$ vs η	$\frac{\alpha'_{E_n}}{n} = a_n\eta + b_n\eta^2 + c_n\eta^3$	$\frac{h_n}{n}$ vs η	$\frac{M_{B_n}}{n}$, $\frac{M_{T_n}}{n}$ vs η
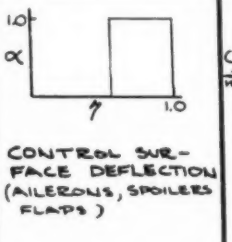 CONTROL SURFACE DEFLECTION (AILERONS, SPOILERS FLAPS)	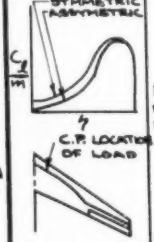	$\frac{C_{L_\delta}}{m}$ NOT REQ'D. FOR ROLL DEVICES	$\frac{C_{\ell_\delta}}{m}$ ASSYMETRIC LOAD USED FOR ASSYMETRIC CONTROL DEFLECTIONS. SPOILERS ARE REPRESENTED BY A LOAD ½ WAY BETWEEN SYMMETRIC AND ASSYMETRIC	$\frac{C_{M_\delta}}{m}$ NOT REQUIRED FOR ROLL DEVICES.	$\frac{\alpha'_{E_\delta}}{qm}, \frac{\theta_{E_\delta}}{qm}, \frac{\Phi_{E_\delta}}{qm}$ vs η	$a_\delta, b_\delta, c_\delta$	$\frac{h_\delta}{qm}$ vs η	$\frac{M_{B_\delta}}{qm}$, $\frac{M_{T_\delta}}{qm}$ vs η
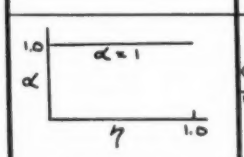 YAWED WING (ANGLE OF ATTACK DUE TO DIHEDRAL EFFECT)		NOT REQUIRED	$\frac{C_{\ell_\psi}}{m}$	NOT REQUIRED	$\frac{\alpha_{E_\psi}}{qm}, \frac{\theta_\psi}{qm}, \frac{\Phi_\psi}{qm}$ vs η	a_ψ, b_ψ, c_ψ	$\frac{h_\psi}{qm}$ vs η	$\frac{M_{B_\psi}}{qm}$, $\frac{M_{T_\psi}}{qm}$ vs η

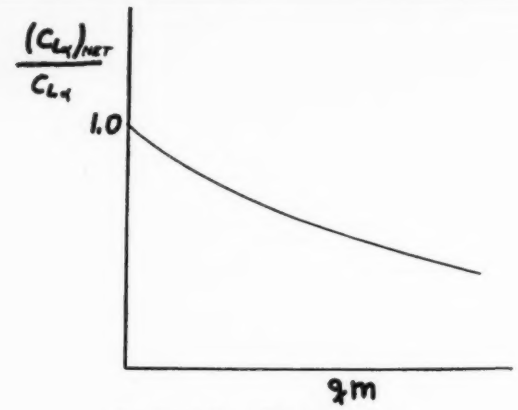

FIG. 9. Lift coefficient variation.

for such conditions. Typical problems for which answers are frequently desired include longitudinal and lateral stability and control characteristics and structural design information on wing loadings, balancing tail loads, structural deflections, gust alleviation, etc.

Preliminary Information Required for Superposition

Since all solutions are obtained by a superposition of known effects, the bulk of the work in using the method is involved in establishing certain basic information. This basic information is used in solving for the superposition coefficients (A, B, and C). Once these constants have been obtained for any given type of loading, a large variety of answers related to that loading becomes immediately available.

As outlined in Part (I), solution for the superposition coefficients A, B, and C is based on combining certain cubic equations that represent various angle-of-attack distributions. The steps involved in obtaining these equations are as follows:

(1) Determine the *rigid-wing* span-load distributions corresponding to linear, quadratic, and cubic angle-of-attack distributions.

(2) Determine the *rigid-wing* span-load distributions corresponding to any angle-of-attack distributions to be considered which cannot be represented by a cubic equation (such as due to level flight, control surface deflection, etc.).

(3) Apply these span-load distributions to the wing structure for a unit value of qm and determine the resulting angular deflections along the span parallel to the plane of symmetry (*without regard to equilibrium conditions*).

(4) Match the angle-of-attack distributions found in step (3) above with cubic equations of the form $a\eta + b\eta^2 + c\eta^3$.

The rigid-wing span-load distributions can be determined by any one of several available methods (e.g., by Weissinger's Method for sweptback wings) or from pressure data obtained on rigid wind-tunnel models for such cases as level flight, yawed flight, control surface deflection, etc.

Calculation of the angular deflections resulting from the application of these load distributions is relatively simple for wings of high aspect ratio. For these wings the selection of a straight elastic axis extending from the wing tip to the body intersection has been found to be reasonable. The structural problem is then reduced to that of a tapered beam subjected to a distributed load. Calculation of structural deflections for this case involves the conventional integration of bending and torsional moment distributions used in conjunction with stiffness values which are known as a function of span. The assumption of a straight elastic axis becomes less valid as aspect ratio is decreased. For such wings, a more complicated means of determining the structural deflections must be used.

Since the fundamental mechanics of the superposition method are independent of the manner in which span-load distributions are obtained and applied to the wing structure, these calculations will not be discussed in further detail in this paper.

Determination of the cubic coefficients a, b, and c is accomplished by solving three simultaneous equations using three points chosen along the semispan; in this way it is possible to represent the angle-of-attack distribution, computed in step (3) above, by a cubic in η. Choice of points to match is dependent on the shape of the elastic deflection curve for the particular problem being considered.

The information listed in steps (1) to (4) is prerequisite to application of the superposition method. Certain additional preliminary data is usually required, depending on the particular problem for which a solution is being sought. For example, if one of the answers desired is lift coefficient C_L, then C_L should be determined for each of the loadings listed in steps (1) and (2) above. Similarly, if bending or torsional moments are desired as a function of span, they should also be computed for each of the various types of loading. Many of these quantities are automatically obtained as by-products in solving for the basic information required in steps (1) to (3).

Table I shows typical preliminary information for linear, quadratic, and cubic angle-of-attack distributions and various other types of loading which are frequently analyzed when carrying out an actual design.

Solution for Level Flight Conditions

Having determined the preliminary data discussed above, solution for equilibrium conditions by superposition is now possible for a variety of specific problems. In order to illustrate use of the method, the solution for level flight conditions will be indicated as an example. The following factors cause structural deflections that affect the level flight lift coefficient: (1) wing angle of attack; (2) built-in twist or camber dis-

tribution; (3) basic wing pitching moment; and (4) wing dead weight.

The lift coefficient for an elastic airplane can be expressed as follows:

$$\frac{nW}{qS} = C_L = (C_{L\alpha})_{\text{net}} + (C_{LT})_{\text{net}} + C_{LM} + C_{Ln} \quad (14)$$

where

$(C_{L\alpha})_{\text{net}}$ = lift coefficient due to wing angle of attack
$(C_{LT})_{\text{net}}$ = increment in C_L due to built-in twist or camber distribution
C_{LM} = increment in C_L resulting from deflections caused by the basic wing pitching moment
C_{Ln} = increment in C_L resulting from deflections caused by wing dead weight

Each of the terms shown above can be solved for as a separate equilibrium condition, and the results can be added to give the net C_L. Basic wing pitching moment, built-in twist, and wing dead weight are usually secondary effects in the above equation. Solution for the lift coefficient due to wing angle of attack generally gives a satisfactory first approximation to the complete result. Fig. 9 shows a typical variation of lift coefficient due to wing angle of attack [i.e., $(C_{L\alpha})_{\text{net}}$] in terms of the value of lift coefficient, $C_{L\alpha}$, for a rigid sweptback wing.

Table II indicates the steps involved in obtaining solutions for each of the terms. Also shown are quantities to plot which will result in single curves to be used in solving for any given flight condition. As indicated, all quantities are a function of qm.

Using values from these curves, Eq. (14) becomes

$$\frac{nW}{qS} = C_L = \frac{(C_{L\alpha})_{\text{net}}}{C_{L\alpha}} C_{L\alpha} + \frac{(C_{LT})_{\text{net}}}{m} m + C_{LM} + \frac{C_{Ln}}{nm} nm$$

For any given flight condition, it is assumed that the following information is known:

n = load factor = L/W
W = airplane gross weight
q = dynamic pressure
S = wing area
M = Mach Number
h = altitude

It is also assumed that the variaton of m with Mach Number is known. The only unknown in the above expression is, then, $C_{L\alpha}$. By solving for $C_{L\alpha}$ and using the relation

$$\alpha_{\text{root}} = C_{L\alpha}/(dC_L/d\alpha)_{\text{rigid}}$$

the value of wing root angle of attack is found which represents the equilibrium attitude of the elastic airplane in level flight. Cases in which the zero lift angle is not zero are automatically taken care of by including the increment in C_L due to built-in twist or effective twist due to camber.

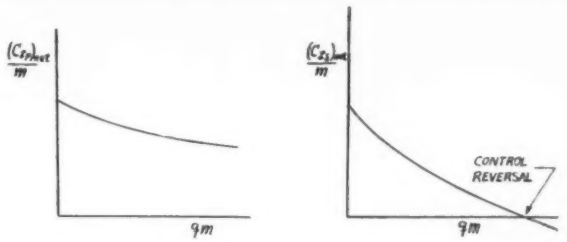

FIG. 10. Lateral control characteristics for the flexible swept wing.

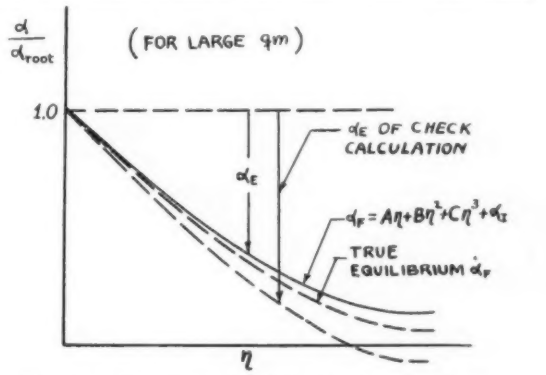

FIG. 11. Checking the solution at large values of qm.

One of the most important elastic effects on swept wings is the shift in spanwise center of pressure caused by deflections. With a sweptback wing in level flight, as speed increases, the center of pressure moves inboard along the quarter chord line and, consequently, forward. This shift is of primary importance in longitudinal stability calculations and structural design for balancing tail loads. The expression for net pitching moment coefficient is analogous to Eq. (14) given previously. It can be written as follows:

$$C_M = (C_{M\alpha})_{\text{net}} + (C_{MT})_{\text{net}} + (C_M)_{\text{net}} + C_{Mn} \quad (15)$$

where

$(C_{M\alpha})_{\text{net}}$ = the pitching moment coefficient about the one-quarter M.A.C. caused by placing the wing at an angle of attack
$(C_{MT})_{\text{net}}$ = the increment in C_M due to built-in twist
$(C_M)_{\text{net}}$ = the increment in C_M due to the basic wing section pitching moment
C_{Mn} = the increment in C_M resulting from the deflection of the wing under the dead weight load

As before, each of the above terms is solved for as a separate equilibrium condition, and the results are added to give the net C_M.

Using values from the plotted curves of Table II, Eq. (15) becomes

TABLE II
SOLUTION FOR LEVEL FLIGHT CONDITIONS

TYPE OF LOADING	KNOWN CUBIC COEFFICIENTS FROM TABLE I	EQUATIONS TO SOLVE FOR COEFFICIENTS A, B & C	SOLUTION FOR C_L & C_M (USING DATA FROM TABLE I)	PLOT	AUXILIARY RESULTS (USING DATA FROM TABLE I)
WING ANGLE OF ATTACK	a_1 b_1 c_1 a_2 b_2 c_2 a_3 b_3 c_3 a_α b_α c_α	$A_\alpha(\frac{1}{qm}-a_1)-B_\alpha a_2-C_\alpha a_3=a_\alpha$ $-A_\alpha b_1+B_\alpha(\frac{1}{qm}-b_2)-C_\alpha b_3=b_\alpha$ $-A_\alpha c_1-B_\alpha c_2+C_\alpha(\frac{1}{qm}-c_3)=c_\alpha$	$(C_{L_\alpha})_{NET}=C_{L_\alpha}+A_\alpha C_{L_1}+B_\alpha C_{L_2}+C_\alpha C_{L_3}$ $(C_{M_\alpha})_{NET}=C_{M_\alpha}+A_\alpha C_{M_1}+B_\alpha C_{M_2}+C_\alpha C_{M_3}$	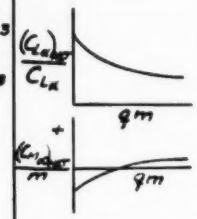	$(\theta_\alpha)_{NET}=\theta_\alpha+A_\alpha\theta_1+B_\alpha\theta_2+C_\alpha\theta_3$ $(\phi_\alpha)_{NET}=\phi_\alpha+A_\alpha\phi_1+B_\alpha\phi_2+C_\alpha\phi_3$ $(h_\alpha)_{NET}=h_\alpha+A_\alpha h_1+B_\alpha h_2+C_\alpha h_3$ $(M_{\theta_\alpha})_{NET}=M_{\theta_\alpha}+A_\alpha M_{\theta_1}+B_\alpha M_{\theta_2}+C_\alpha M_{\theta_3}$ $(M_{T_\alpha})_{NET}=M_{T_\alpha}+A_\alpha M_{T_1}+B_\alpha M_{T_2}+C_\alpha M_{T_3}$ — — — etc. — — —
BUILT-IN TWIST	a_1 b_1 c_1 a_2 b_2 c_2 a_3 b_3 c_3 a_T b_T c_T	$A_T(\frac{1}{qm}-a_1)-B_T a_2-C_T a_3=a_T$ $-A_T b_1+B_T(\frac{1}{qm}-b_2)-C_T b_3=b_T$ $-A_T c_1-B_T c_2+C_T(\frac{1}{qm}-c_3)=c_T$	$(C_{L_T})_{NET}=C_{L_T}+A_T C_{L_1}+B_T C_{L_2}+C_T C_{L_3}$ $(C_{M_T})_{NET}=C_{M_T}+A_T C_{M_1}+B_T C_{M_2}+C_T C_{M_3}$	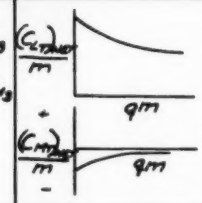	$(\theta_T)_{NET}=\theta_T+A_T\theta_1+B_T\theta_2+C_T\theta_3$ $(\phi_T)_{NET}=\phi_T+A_T\phi_1+B_T\phi_2+C_T\phi_3$ $(h_T)_{NET}=h_T+A_T h_1+B_T h_2+C_T h_3$ — — — etc. — — —
BASIC WING PITCHING MOMENT	a_1 b_1 c_1 a_2 b_2 c_2 a_3 b_3 c_3 a_M b_M c_M	$A_M(\frac{1}{qm}-a_1)-B_M a_2-C_M a_3=\frac{a_M C_{M_0}}{m}$ $-A_M b_1+B_M(\frac{1}{qm}-b_2)-C_M b_3=\frac{b_M C_{M_0}}{m}$ $-A_M c_1-B_M c_2+C_M(\frac{1}{qm}-c_3)=\frac{c_M C_{M_0}}{m}$	$C_{L_M}=A_M C_{L_1}+B_M C_{L_2}+C_M C_{L_3}$ $(C_M)_{NET}=C_{M_0}+\Delta C_{M_0}$ WHERE $\Delta C_{M_0}=A_M C_{M_1}+B_M C_{M_2}+C_M C_{M_3}$	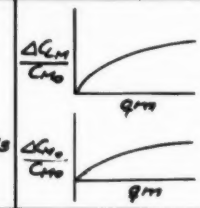	$\theta_M=A_M\theta_1+B_M\theta_2+C_M\theta_3$ $\phi_M=A_M\phi_1+B_M\phi_2+C_M\phi_3$ $h_M=A_M h_1+B_M h_2+C_M h_3$ $M_{\theta_M}=A_M M_{\theta_1}+B_M M_{\theta_2}+C_M M_{\theta_3}$ $M_{T_M}=A_M M_{T_1}+B_M M_{T_2}+C_M M_{T_3}$ — — — etc. — — — —
WING DEAD WEIGHT	a_1 b_1 c_1 a_2 b_2 c_2 a_3 b_3 c_3 a_n b_n c_n	$A_n(\frac{1}{qm}-a_1)-B_n a_2-C_n a_3=\frac{a_n n}{qm}$ $-A_n b_1+B_n(\frac{1}{qm}-b_2)-C_n b_3=\frac{b_n n}{qm}$ $-A_n c_1-B_n c_2+C_n(\frac{1}{qm}-c_3)=\frac{c_n n}{qm}$	$C_{L_n}=A_n C_{L_1}+B_n C_{L_2}+C_n C_{L_3}$ $C_{M_n}=A_n C_{M_1}+B_n C_{M_2}+C_n C_{M_3}$	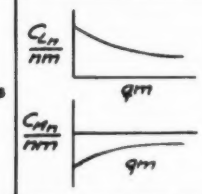	$\theta_n=A_n\theta_1+B_n\theta_2+C_n\theta_3$ $\phi_n=A_n\phi_n+B_n\phi_2+C_n\phi_3$ $h_n=A_n h_1+B_n h_2+C_n h_3$ — — — etc. — — —

$$C_M = \frac{(C_{M\alpha})_{\text{net}}}{m} m + \frac{(C_{MT})_{\text{net}}}{m} m + (C_M)_{\text{net}} + \frac{C_{Mn}}{nm} nm$$

In this case, C_M is the unknown quantity for any given flight condition.

Many other quantities associated with level flight can be determined by combining the proper values with the superposition coefficients A, B, and C. Typical quantities for which solutions are frequently desired are shown on Table II under the heading of "Auxiliary Results."

While this paper is concerned only with wing effects, complete airplane analysis must include the effects of body and tail flexibility. Tail flexibility is analogous to wing flexibility. Wing, body, and tail equilibrium conditions are coupled and must obviously be treated as such for a complete solution. In most cases, however, wing flexibility is the largest contributing factor in any consideration of elastic effects.

Solution of Lateral Control Problem

Determination of steady-state roll conditions will be discussed as an additional example of application of the superposition method.

Steady-state roll occurs when the roll damping moment equals the moment produced by the control device. For rigid wings, the damping load is a function of the roll angle of attack along the semispan $(pb/2v)\eta$. This corresponds to a linear angle-of-attack distribution along the semispan having a value of $pb \div 2v$ at the tip. The helix angle of rolling flight is also equal to $pb/2v$. Consequently, $pb/2v$ becomes the common parameter for comparing roll characteristics. Equations relating damping and control moments are as follows:

$$M_{\text{control}} = (dC_L/d\delta)\ \delta qsb$$

$$M_{\text{damping}} = \frac{dC_L}{d(pb/2v)} \frac{pb}{2v} qsb$$

and defining

$$C_{L_\delta} = \frac{dC_L}{d\delta}, \qquad C_{l_p} = \frac{dC_L}{d(pb/2v)}$$

then, since $M_{\text{control}} = M_{\text{damping}}$ (for steady state),

$$pb/2v = (C_{L_\delta}/C_{l_p})\delta$$

Obviously, only unsymmetric loads can cause roll. Consequently, symmetric loadings due to basic wing angle of attack, dead weight, etc., do not enter into the lateral problem. The problem therefore reduces to solving for C_{L_δ} and C_{L_p} as quantities that are influenced by structural deflections. Typical plots of these terms for a swept wing with an aileron-type control system are shown in Fig. 10.

Table III gives the solution for these terms as separate equilibrium conditions. The rigid value of α_δ =

TABLE III

SOLUTION FOR LATERAL CONTROL PROBLEM

TYPE OF LOADING	KNOWN CUBIC COEFFICIENTS FROM TABLE I	EQUATIONS TO SOLVE FOR COEFFICIENTS A, B & C	SOLUTION FOR C_{L_p} (USING DATA FROM TABLE II)	PLOT	AUXILIARY RESULTS (USING DATA FROM TABLE II)
ROLL DAMPING (LINEAR α DIST.)	a_1 b_1 c_1 a_2 b_2 c_2 a_3 b_3 c_3	$A_p(\frac{1}{qm}-a_1)-B_p a_2-C_p a_3=a_1$ $-A_p b_1+B_p(\frac{1}{qm}-b_2)-C_p b_3=b_1$ $-A_p c_1-B_p c_2+C_p(\frac{1}{qm}-c_3)=c_1$	$C_{L_p}=(1+A_p)C_{l_p}+B_p C_{l_2}+C_p C_{l_3}$	$\frac{C_{L_p}}{m}$ vs qm	$\theta_p=(1+A_p)\theta_1+B_p\theta_2+C_p\theta_3$ $\phi_p=(1+A_p)\phi_1+B_p\phi_2+C_p\phi_3$ $h_p=(1+A_p)h_1+B_p h_2+C_p h_3$ $M_{3p}=(1+A_p)M_{31}+B_p M_{32}+C_p M_{33}$ ——— etc. ———
CONTROL SURFACE DEFLECTION	a_1 b_1 c_1 a_2 b_2 c_2 a_3 b_3 c_3 a_4 b_4 c_4	$A_\delta(\frac{1}{qm}-a_1)+B_\delta a_2-C_\delta a_3=a_\delta$ $-A_\delta b_1+B_\delta(\frac{1}{qm}-b_2)-C_\delta b_3=b_\delta$ $-A_\delta c_1-B_\delta c_2+C_\delta(\frac{1}{qm}-c_3)=c_\delta$	$(C_{L_\delta})_{\text{incr}}=C_{l_\delta}+A_\delta C_{l_1}+B_\delta C_{l_2}+C_\delta C_{l_3}$	$\frac{(C_{L_\delta})_{\text{incr}}}{m}$ vs qm	$(\theta_\delta)_{\text{incr}}=\theta_\delta+A_\delta\theta_1+B_\delta\theta_2+C_\delta\theta_3$ $(\phi_\delta)_{\text{incr}}=\phi_\delta+A_\delta\phi_1+B_\delta\phi_2+C_\delta\phi_3$ $(h_\delta)_{\text{incr}}=h_\delta+A_\delta h_1+B_\delta h_2+C_\delta h_3$ ——— etc. ———

$d\alpha/d\delta$ must be known or estimated for the particular control configuration under consideration.

Concluding Remarks

Having obtained the superposition coefficients A, B, and C for any given type of loading, it is always possible to perform a check to determine whether or not these coefficients actually correspond to equilibrium. When the wing is subjected to the final equilibrium loading corresponding to α_F, it must cause the structure to deflect to α_E. The deflection computed from application of this loading should then equal $A\eta + B\eta^2 + C\eta^3$. If a discrepancy exists, either A, B, and C have been computed incorrectly or the various cubic coefficients used in solving for A, B, and C do not match the deflection curves with sufficient accuracy. On the wings examined to date it has been found that the latter difficulty can be eliminated by careful selection of matching points.

It should be noted that as qm increases it is necessary to increase the accuracy of the computations in order that A, B, and C can be closely checked. However, the closeness of the check does not indicate the accuracy of A, B, and C unless the qm for which they were determined is considered. This is due to the fact that, at high values of qm, slight deviations from the true equilibrium angle of attack, α_F, will produce large loads, which in turn have a big effect on elastic deflections. This is shown by Fig. 11.

Application of the superposition method is not limited to solution of the problems shown as examples on the preceding pages; nor is the method limited to use on swept wings. The relative simplicity of solution makes this method particularly adaptable for use in airplane design.

References

[1] Sears, W. R., and Pai, S. I., *Some Aeroelastic Properties of Swept Wings*, Journal of the Aeronautical Sciences, Vol. 16, No. 2, pp. 105–115, February, 1949.

[2] Miles, John W., *A Formulation of the Aeroelastic Problem for a Swept Wing*, Journal of the Aeronautical Sciences, Vol. 16, No. 8, pp. 477–490, August, 1949.

[3] Diederich, F. W., *Calculation of the Effects of Structural Flexibility on Lateral Control of Wings of Arbitrary Plan Form and Stiffness*, N.A.C.A. Research Memo. No. L8H24a, December, 1948.

[4] Lyon, H. M., *A Method of Estimating the Effect of Aero-elastic Distortion of a Swept-back Wing on Stability and Control Derivatives*, British R.&M. No. 2331.

Nonsteady Supersonic Flow About Pointed Bodies of Revolution

(Continued from page 511)

$$I_1 = \int_{\cosh^{-1}(x/\beta R)}^{0} S'(x - \beta R \cosh u) \cosh u \, du \quad \text{(A1)}$$

$$I_2 = \int_{\cosh^{-1}(x/\beta R)}^{0} S'(x - \beta R \cosh u) \times (x - \beta R \cosh u) \cosh u \, du \quad \text{(A2)}$$

$$I_3 = \int_{\cosh^{-1}(x/\beta R)}^{0} S(x - \beta R \cosh u) \cosh u \, du \quad \text{(A3)}$$

$$I_4 = \int_{\cosh^{-1}(x/\beta R)}^{0} S'(x - \beta R \cosh u) \, du \quad \text{(A4)}$$

When these integrals are differentiated with respect to x, it should be remembered that $S(0) = S'(0) \equiv 0$ for pointed bodies of revolution.

Transient Loading of Wide Delta Airfoils at Supersonic Speeds

JOHN W. MILES*

University of California at Los Angeles

SUMMARY

The indicial admittance of a pointed wing, bounded by two supersonic leading edges and a straight trailing edge and located in an otherwise uniform supersonic flow, is calculated on the basis of linearized theory. This result is applied to the calculation of the lift and moments on a "wide" delta airfoil due to a sudden change of angle of attack, a uniform, sharp-edged gust, an impulsive gust, and sharp-edged and impulsive gusts having antisymmetric linear velocity distributions over the span. The response of a two-dimensional airfoil to an impulsive gust is also calculated. These results are given in the form of algebraic formulas and curves.

NOTATION

A = indicial admittance, Eqs. (2.1) and (2.4)
A_0 = two-dimensional indicial admittance, Eqs. (2.5) and (2.6)
C_L = lift coefficient
C_{L_α} = C_L due to unit increment in angle of attack, Eqs. (3.8) and (3.11)
C_{L_δ} = C_L due to impulsive gust, Eqs. (5.4) and (5.6)
C_{L_1} = C_L due to uniform, sharp-edged gust, Eqs. (4.9) and (4.11)
C_M = pitching moment coefficient
C_{M_α} = C_M due to unit increment in angle of attack, Eqs. (3.9) and (3.12)
C_{M_δ} = C_M due to impulsive gust, Eqs. (5.5) and (5.7)
C_{M_1} = C_M due to uniform, sharp-edged gust, Eqs. (4.10) and (4.12)
C_l = rolling moment coefficient
C_{l_δ} = C_l due to impulsive, antisymmetric gust, Eqs. (6.8) and (6.9)
C_{l_1} = C_l due to sharp-edged, antisymmetric gust, Eqs. (6.5) and (6.6)
G = Green's function for harmonic motion problem, Eq. (1.8)
L = lift force
M_a = pitching moment about a point $ac/2$ aft of the apex
M_x = rolling moment about mid-span
S = surface area
S_n = see Eq. (3.6) and Appendix
T_n = see Eq. (4.6) and Appendix
U = free-stream velocity
a = fraction of root semichord of pitching axis aft of apex; also sonic velocity
c = root chord of delta wing (or simply unit of length in more general use)
f = spanwise weighting function, Eqs. (1.3) and (1.13)
k = reduced frequency, Eq. (1.9)
m = two-dimensional lift curve slope ($= 4 \tan \theta$)
p = gage pressure
t = time
t_0 = see Eq. (1.10)
$\bar{t}$ = dimensionless time, Eq. (1.11)
u = see Eq. (4.3)
$u_{1,2}$ = see Eq. (2.7) and (2.8)
w = dimensionless (i.e., divided by U) downwash at airfoil
x, y, z = coordinates (Fig. 1)
$y_{p,s}$ = port and starboard leading edges
α = angle of attack
δ = Dirac delta function, Eq. (5.2)
ζ_n = see Eqs. (3.17), (3.18), (3.19), and (4.13)
η = running y coordinate
θ = Mach angle, Eq. (1.2)
μ = semiapex angle
ξ = running x coordinate
ρ = air mass density
τ = $(Ut/c)(1 - \sin\theta)$
ϕ = velocity potential
χ = see Eqs. (1.3) and (1.13)
ω = angular frequency
$1(x)$ = Heaviside step function ($= 1$ if $x > 0$; $= 0$ if $x < 0$)

Received June 21, 1950.

* Associate Professor, Department of Engineering. Also, Consultant, U.S. Naval Ordnance Test Station, Inyokern, Calif. Now, Auckland University College, Auckland, New Zealand.

(1) INTRODUCTION

IN A PREVIOUS PAPER[1] we considered the aerodynamic forces on pointed wings, bounded by two supersonic leading edges and a straight trailing edge transverse to the main flow, executing harmonic motion in an otherwise undisturbed, supersonic flow. It was found that the problem could be reduced to an essentially two-dimensional one, which was particularly simple in the case where only the lift, pitching moment, and rolling moment were required. Explicitly, if the main flow (U) is directed along the positive x axis, the nose of the airfoil projects on the origin, and the port and starboard leading edges are specified by $y_p(x)$ and $y_s(x)$, respectively, subject to the restrictions

$$y_p(0) = y_s(0) = 0 \tag{1.1a}$$

$$y_s'(x) > \tan\theta \tag{1.1b}$$

$$y_p'(x) < -\tan\theta \tag{1.1c}$$

$$\theta = \sin^{-1}(a/U) \tag{1.2}$$

θ is the Mach angle, and a is the sonic velocity. If $\phi(x, y, z) \exp(i\omega t)$ is the velocity potential, $w(x, y) \exp(i\omega t)$ is the normal velocity (downwash) at the wing, positive down and referred to U, and $\chi(x)$ is a

weighted spanwise integral of the potential defined by†

$$\chi(x) = U^{-1} \int_{y_p(x)}^{y_s(x)} \phi(x, y, 0^+) f(y)\, dy \qquad (1.3)$$

a solution to the (linearized) boundary-value problem

$$\nabla^2 \phi = \frac{1}{a^2} \left(U \frac{\partial}{\partial x} + \frac{\partial}{\partial t} \right)^2 \phi \qquad (1.4)$$

$$\phi_z(x, y, 0^+) = -Uw(x, y) \mathbf{1}(x) \mathbf{1}[y_s(x) - y] \mathbf{1}[y - y_p(x)] \qquad (1.5)$$

$$\phi(x, y, 0^+) \equiv 0, \qquad x < 0 \qquad (1.6)$$

is given by

$$\chi(x) = \tan\theta \int_0^x d\xi \int_{y_p(\xi)}^{y_s(\xi)} d\eta G(x - \xi, \eta) w(\xi, \eta) \qquad (1.7)$$

$$G(x, y) = \exp(-ikx \sec^2\theta) \mathbf{1}(x) \cdot \frac{1}{\pi} \times \int_0^\pi \cos(kx \sec\theta \tan\theta \sin\varphi) \cdot f(x \cos\varphi + y)\, d\varphi \qquad (1.8)$$

$$k = (\omega c / U) \qquad (1.9)$$

where c is a unit of length, all coordinates being dimensionless and referred to this length, and k is the reduced frequency.

In the present paper, we shall be interested in the response of this same wing for the case where the downwash $w(x, y)$ at (x, y) arises abruptly at $t_0(x, y)$, and is thereafter constant in time, whence the boundary condition, Eq. (1.5), is replaced by

$$\phi_z(x, y, 0^+, t) = -Uw(x, y) \mathbf{1}[t - t_0(x, y)] \times \mathbf{1}(x) \mathbf{1}[y_s(x) - y] \mathbf{1}[y - y_p(x)] \qquad (1.10)$$

where we now introduce the explicit dependence of ϕ on t. Eqs. (1.4) and (1.6) remain as stated.

In considering this problem, we shall find it convenient to introduce the dimensionless time $\bar{t}$, defined by

$$\bar{t} = (Ut/c) \qquad (1.11)$$

noting that $\omega t = k\bar{t}$. Moreover, if c is the wing chord, $\bar{t}$ measures time in chord lengths. In the subsequent sections the use of this dimensionless time will be implicit, and the bar will be dispensed with.

Having found the velocity potential on the upper surface of the wing—i.e., $\phi(x, y, 0^+, \bar{t})$—the gage pressure is given by

$$p(x, y, \bar{t}) = -\rho \frac{D}{Dt} \phi(x, y, 0^+, \bar{t}) = -\rho U^2 \left(\frac{\partial}{\partial x} + \frac{\partial}{\partial \bar{t}} \right) \phi(x, y, 0^+, \bar{t}) \qquad (1.12)$$

† In reference 1 we introduced $\psi(x, \xi)$, defined such that $\chi(x) = \tan\theta \int_0^x \psi(x, \xi)\, d\xi$

and a weighted spanwise integral of this pressure may be expressed in terms of $\chi(x, \bar{t})$ in accordance with

$$-\int_{y_p(x)}^{y_s(x)} p(x, y, \bar{t}) f(y)\, dy = \rho U^2 \left(\frac{\partial}{\partial x} + \frac{\partial}{\partial \bar{t}} \right) \chi(x, \bar{t}) \qquad (1.13)$$

(2) Indicial Admittance

The response of a linear system to the Heaviside excitation $\mathbf{1}(t)$ is designated as the indicial admittance of the system, whereas we may define the response of the same system to the harmonic excitation $\exp(ikt)$ as the transfer function. If these two characteristic functions are denoted by $A(t)$ and $G(k)$, respectively, then A is the Bromwich integral of G—viz.,

$$A(t) = \frac{1}{2\pi} \lim_{\epsilon \to 0^+} \int_{-\infty}^{\infty} dk (\epsilon + ik)^{-1} \exp(ikt) G(k) \qquad (2.1)$$

by virtue of the Fourier representation

$$\mathbf{1}(t) = \frac{1}{2\pi} \lim_{\epsilon \to 0^+} \int_{-\infty}^{\infty} dk (\epsilon + ik)^{-1} \exp(ikt) \qquad (2.2)$$

These relations enable us to transform the solution to Eqs. (1.4), (1.5), and (1.6) given by Eqs. (1.7) and (1.8) to the solution to Eqs. (1.4), (1.10), and (1.6) Thus, if the latter solution is represented by

$$\chi(x, t) = \tan\theta \int_0^x d\xi \int_{y_p(\xi)}^{y_s(\xi)} d\eta A \times [x - \xi, \eta, t - t_0(\xi, \eta)] w(\xi, \eta) \qquad (2.3)$$

the indicial admittance is obtained by substituting Green's function, Eq. (1.8), in Eq. (2.1). The spectrum integrations may be effected directly from Eq. (2.2), and the desired result is

$$A(x, y, t) = \mathbf{1}(x) \cdot \frac{1}{2\pi} \int_0^\pi d\varphi\, f(x \cos\varphi + y) \cdot \{ \mathbf{1}[t - x \sec^2\theta (1 + \sin\theta \sin\varphi)] + \mathbf{1} \times [t - x \sec^2\theta (1 - \sin\theta \sin\varphi)] \} \qquad (2.4)$$

We shall be interested further only in the special cases $f_0(y) = 1$ and $f_1(y) = y$, corresponding to the calculation of the lift and rolling moment, respectively, on the spanwise strip at x. Substituting $f_0 = 1$ in Eq. (2.4) and carrying out the φ integration yields

$$f_0(y) = 1: \qquad A(x, y, t) = A_0(x/t) \qquad (2.5)$$

$$A_0(u) = \mathbf{1}(u) \mathbf{1}(u_1 - u) + \mathbf{1}(u - u_1) \mathbf{1}(u_2 - u) \cdot \frac{1}{\pi} \cos^{-1} \left[\frac{u - u_1 u_2}{(1 - u_1) u} \right] \qquad (2.6)$$

$$u_1 = 1 - \sin\theta \qquad (2.7)$$

$$u_2 = 1 + \sin\theta \qquad (2.8)$$

The result obtained for $f_1 = y$ may be written

$$f_1(y) = y: \qquad A(x, y, t) = yA_0(x/t) \qquad (2.9)$$

The indicial admittance A_0 may be recognized as that for the two-dimensional problem, which has been discussed adequately in the literature,[2–6] including, in particular, physical interpretations of the waves represented by the two step functions in Eq. (2.4). Moreover, in the important special case where t_0 is independent of y, the solution represented by Eqs. (2.3) and (2.4) may be cast in the form

$$\chi_n(x, t) = \tan\theta \int_0^x A_0\left[\frac{x-\xi}{t-t_0(\xi)}\right] w_n(\xi)d\xi \quad (2.10)$$

$$w_n(x) = \int_{y_p(x)}^{y_s(x)} w(x, y)y^n\, dy, \quad n = 0, 1 \quad (2.11)$$

which reduces the problem to an equivalent two-dimensional problem of downwash distribution $w_n(x)$, as was to be expected from the analogous result for harmonic time dependence.[1]

We now proceed to consider important examples that are covered by Eqs. (2.10) and (2.11).

(3) Sudden Change in Angle of Attack

In the case of a sudden change in angle of attack or sudden control surface deflection at time zero, we have

$$t_0(x) \equiv 0 \quad (3.1)$$

We shall consider here only the case of a sudden (unit) change of incidence (*without rotation*) over the entire airfoil, whence

$$w(x, y) \equiv 1 \quad (3.2)$$

Moreover, we shall assume a delta plan form, for which

$$y_s(x) = -y_p(x) = x\tan\mu, \quad \mu \geq \theta \quad (3.3)$$

where μ is the semiapex angle, as shown in Fig. 1.

Because of the symmetry of the downwash distribution [Eq. (3.2)] with respect to mid-span ($y = 0$), we shall be interested only in the lift and pitching moment and require only $\chi_0(x, t)$ [see Eqs. (2.10) and (2.11)]. Substituting $w = 1$ and $t_0 = 0$ in the latter equations yields

$$\chi_0(x, t) = 2\tan\mu\tan\theta\int_0^x A_0\left(\frac{x-\xi}{t}\right)\xi\, d\xi \quad (3.4)$$

Introducing the change of variable $(x - \xi) = tu$, we write

$$\chi_0(x, t) = 2\tan\mu\tan\theta t^2[(x/t)S_0(x/t) - S_1(x/t)] \quad (3.5)$$

$$S_n(z) = \int^z u^n A_0(u)\, du \quad (3.6)$$

In calculating the desired lift and moment coefficients, we choose the root chord† (c) as our unit of length. The surface area is given by

$$S = c^2\tan\mu \quad (3.7)$$

† In reference 1, the average chord ($b = c/2$) was chosen as the unit of length.

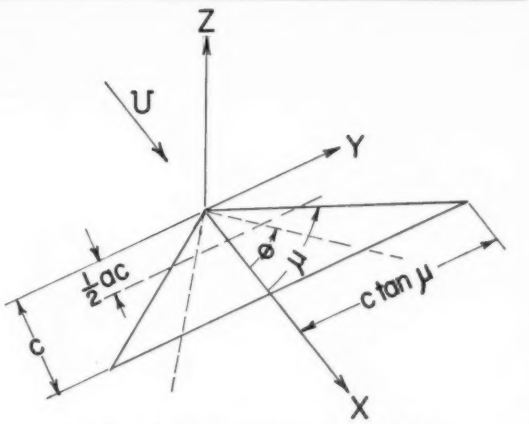

Fig. 1. Wide delta wing in supersonic flow.

By referring to Eq. (1.13), the lift and moment (about an axis $ac/2$ aft of the apex) coefficients can be written

$$C_{L_\alpha}(t) = \left(\frac{\rho U^2}{2}S\right)^{-1} L \quad (3.8a)$$

$$= \left(\frac{\rho U^2}{2}\tan\mu\right)^{-1}\int_0^1 dx\int_{y_p(x)}^{y_s(x)} dy \times [-2p(x, y, 0^+)] \quad (3.8b)$$

$$= 4\cot\mu\int_0^1 dx\left(\frac{\partial}{\partial x}+\frac{\partial}{\partial t}\right)\chi_0(x, t) \quad (3.8c)$$

$$C_{M_\alpha}(t) = \left(\frac{\rho U^2}{2}\cdot S\cdot\frac{c}{2}\right)^{-1} M_a \quad (3.9a)$$

$$= \left(\frac{\rho U^2\tan\mu}{4}\right)^{-1}\int_0^1 dx\left(\frac{1}{2}a - x\right)\times \int_{y_p(x)}^{y_s(x)} dy\,[-2p(x, y, 0^+)] \quad (3.9b)$$

$$= 4\cot\mu\int_0^1 dx(a-2x)\left(\frac{\partial}{\partial x}+\frac{\partial}{\partial t}\right)\chi_0(x, t) \quad (3.9c)$$

where we have used the subscript α to denote the unit increment in incidence. Carrying out the required differentiation of $\chi_0(x, t)$ in Eq. (3.4) yields

$$[(\partial/\partial x) + (\partial/\partial t)]\chi_0(x, t) = 2\tan\mu\tan\theta \times [(x + t)S_0(x/t) - 2tS_1(x/t)] \quad (3.10)$$

which result may be of direct interest in calculating chordwise loading. Substituting Eq. (3.10) in Eqs. (3.8c) and (3.9c) and integrating repeatedly by parts, we may place our results in the form

$$C_{L_\alpha}(t) = m[(1 + 2t)S_0(1/t) - 2t(2 + t)S_1(1/t) + 3t^2S_2(1/t)] \quad (3.11)$$

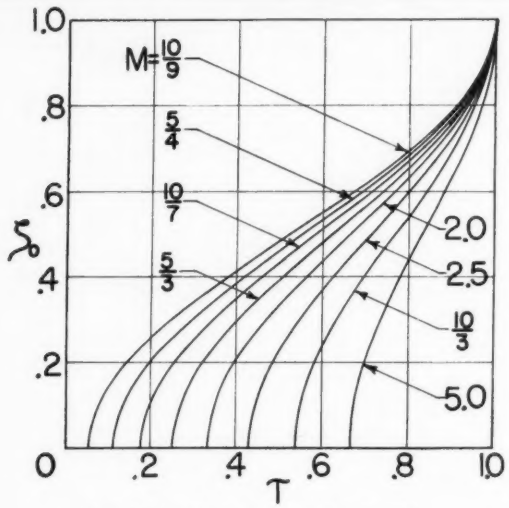

FIG. 2. $\zeta_0(Ut/c)$ vs. τ [see Eq. (3.17)].

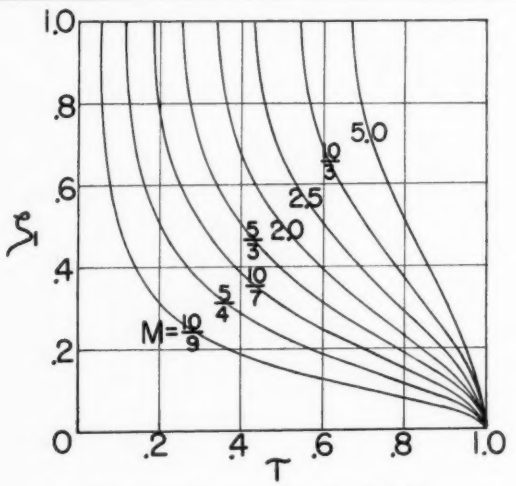

FIG. 3. $\zeta_1(Ut/c)$ vs. τ [see Eq. (3.18)].

$$C_{M_\alpha}(t) = -m\left\{\left[\left(\frac{4}{3} - a\right) + 2(1-a)t\right] \times S_0(1/t) + 2t[at - 2(1-a)]S_1(1/t) - t^2(3a+2t)S_2(1/t) + \frac{8}{3}t^3 S_3(1/t)\right\} \quad (3.12)$$

$$m = 4\tan\theta \quad (3.13)$$

where m is the steady-state, lift curve slope.

The required $S_n(z)$ are evaluated in the appendix, and substitution of the results in Eqs. (3.11) and (3.12) yields

$$\frac{1}{m}C_{L_\alpha}(t) = \zeta_0(t) + \cos\theta\left(1 + \frac{1}{2}t^2\sin^2\theta\right) \times \zeta_1(t) + \frac{1}{2}(3-t)\,\zeta_2(t) \quad (3.14)$$

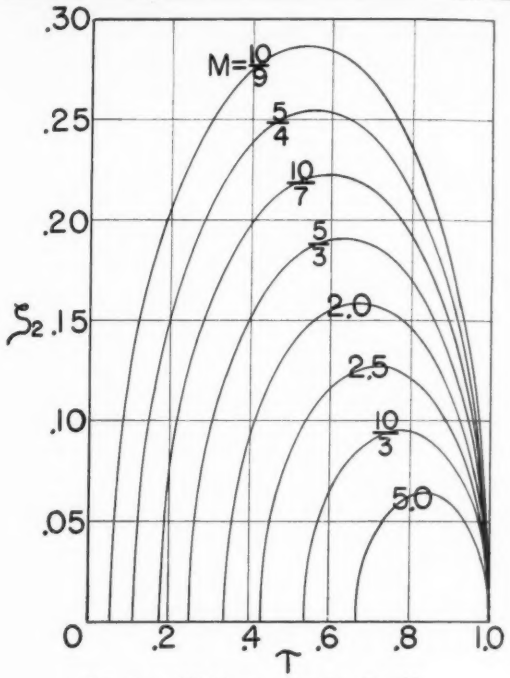

FIG. 4. $\zeta_2(Ut/c)$ vs. τ [see Eq. (3.19)].

$$\frac{1}{m}C_{M_\alpha}(t)\Big|_{a=4/3} = \frac{2}{3}t^2(1-t)\sin^2\theta\cos\theta\,\zeta_1(t) + \frac{2}{9}[(1-t)^2 + 2t^2\sin^2\theta]\zeta_2(t) \quad (3.15)$$

$$C_{M_\alpha}(t) = C_{M_\alpha}(t)\big|_{a=4/3} + \left(\frac{2}{3} - \frac{a}{2}\right)C_{L_\alpha}(t) \quad (3.16)$$

$$\zeta_0(t) = 0, \quad 0 \le t \le (1+\sin\theta)^{-1} \quad (3.17a)$$

$$= \frac{1}{\pi}\cos^{-1}\left(\frac{1 - t\cos^2\theta}{\sin\theta}\right), \quad (1+\sin\theta)^{-1} \le t \le (1-\sin\theta)^{-1} \quad (3.17b)$$

$$= 1, \quad t \ge (1-\sin\theta)^{-1} \quad (3.17c)$$

$$\zeta_1(t) = 1 \quad (3.18a)$$

$$= (1/\pi)\cos^{-1}[(t-1)/(t\sin\theta)] \quad (3.18b)$$

$$= 0 \quad (3.18c)$$

$$\zeta_2(t) = 0 \quad (3.19a)$$

$$= (\cos\theta/\pi)\,[1 - (1-\sin\theta)t]^{1/2} \times [(1+\sin\theta)\,t - 1]^{1/2} \quad (3.19b)$$

$$= 0 \quad (3.19c)$$

where the time intervals in Eqs. (3.18) and (3.19) correspond to those of Eq. (3.17).

In plotting the results, it is convenient to refer them to the time required to reach the steady state—viz., $(1-\sin\theta)^{-1}$. Hence, if t is the real time [see Eq. (1.11)], we introduce the dimensionless time

$$\tau = \bar{l}(1 - \sin\theta) = (Ut/c)\,(1 - \sin\theta) \quad (3.20)$$

The functions ζ_0, ζ_1, ζ_2, $(1/m)C_{L_\alpha}$, and $(1/m)C_{M_\alpha}$, as given by Eqs. (3.14) to (3.19), are plotted as functions of τ in Figs. 2 to 6 for various values of M.

(4) Uniform Gust Entry

As a second application of practical interest, we consider the entry of a sharp-edged uniform gust of unit magnitude. Such a situation is represented by

$$w(x, y) \equiv 1 \quad (4.1a)$$

$$t_0(x, y) = x \quad (4.1b)$$

and is illustrated in Fig. 7.

Substituting $t_0(\xi) = \xi$ and $n = 0$ (since we shall be interested only in the lift and pitching moment) in Eq. (2.10), we have

$$\chi_0(x, t) = 2 \tan\mu \tan\theta \int_0^x A_0\left(\frac{x - \xi}{t - \xi}\right) \xi\, d\xi \quad (4.2)$$

To carry out the required integration, we introduce the change of variable

$$u = (x - \xi)/(t - \xi) \quad (4.3a)$$

$$\xi = (x - tu)/(1 - u) \quad (4.3b)$$

$$t = [x - (1 - u)\xi]/u \quad (4.3c)$$

Because of the singularity in this transformation at $u = 1$ $(t = x)$, some care must be exercised in selecting the limits of integration for u. Referring to Fig. 8, where we have given a graphical representation of the transformation, we observe that the path of integration for u, corresponding to the path $0 < \xi < x$, depends on whether t is greater or less than x.

$$(t/x) > 1 : 0 < \xi < x \longrightarrow (x/t) > u > 0 \quad (4.4a)$$

$$(t/x) < 1 : 0 < \xi < x \longrightarrow (x/t) < u < +\infty \quad (4.4b)$$
$$(-\infty < u < 0)$$

However [see Eq. (2.6)], $A_0(u)$ vanishes for $u > u_2$ and for negative u, and the latter path may be reduced to $(x/t) < u < u_2$.

Accordingly, we may rewrite Eq. (4.2) in the form

$$\chi_0(x, t) = 2 \tan\mu \tan\theta (t - x) \int_{u_2 \mathbf{1}(x-t)}^{x/t} (x - tu) \times (1 - u)^{-3} A_0(u)\, du \quad (4.5)$$

where the lower limit is 0 or u_2 as the upper limit is less or greater than unity. Introducing the integrals

$$T_n(z) = \int_{u_2 \mathbf{1}(z-1)}^{z} (1 - u)^{-n} A_0(u)\, du \quad (4.6)$$

we write

$$\chi_0(x, t) = 2 \tan\mu \tan\theta [t(t - x)T_2(x/t) - (t - x)^2 T_3(x/t)] \quad (4.7)$$

The lift and moment coefficients can now be calcu-

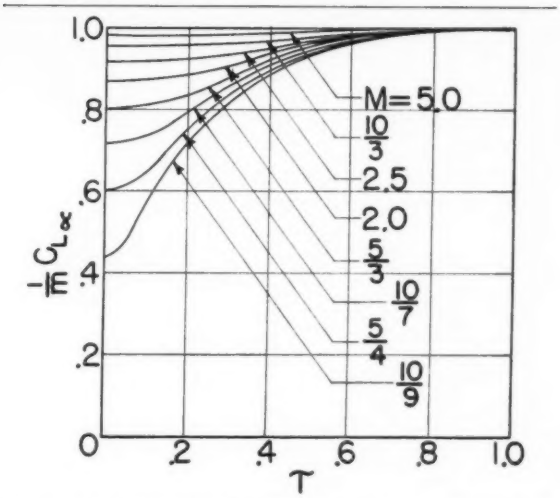

FIG. 5. $C_{L_\alpha}(Ut/c)$, the lift coefficient due to an abrupt unit increment in angle of attack, vs. τ.

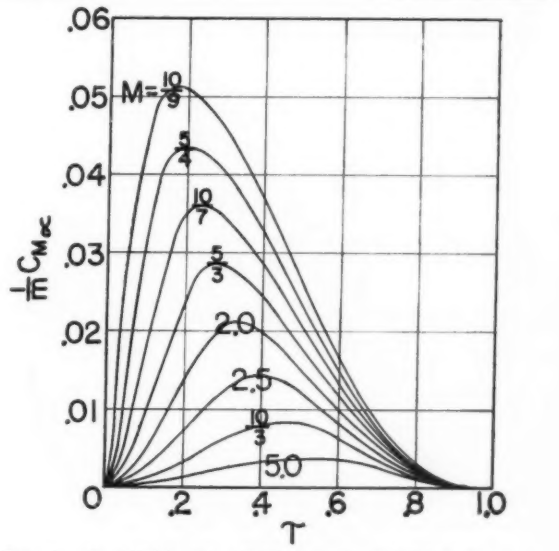

FIG. 6. $C_{M_\alpha}(Ut/c)$, the pitching moment (about the centroidal axis, two-thirds of the root chord from the apex) coefficient due to an abrupt unit increment in angle of attack, vs. τ.

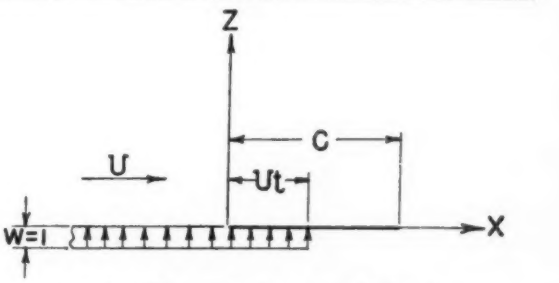

FIG. 7. Wing penetrating sharp-edged gust.

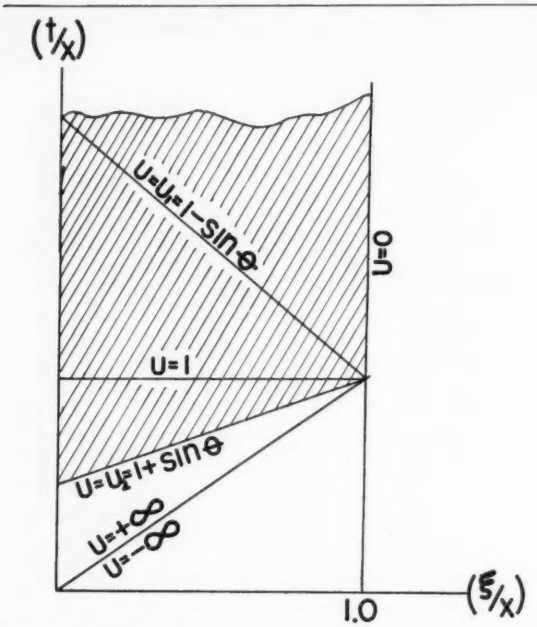

FIG. 8. Graphical representation of the transformation, Eq. (4.3), showing (shaded area) domain of $A_0(u)$.

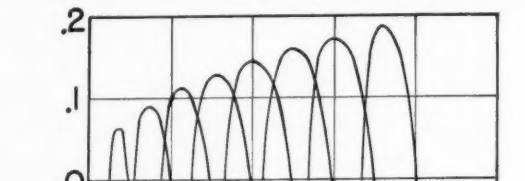

FIG. 9. $\zeta_3(Ut/c)$ vs. τ [see Eq. (4.13)].

lated from Eqs. (3.8) and (3.9). Carrying out the required differentiation of $\chi_0(x, t)$ yields

$$[(\partial/\partial x) + (\partial/\partial t)]\chi_0(x, t) = 2 \tan\theta \tan\mu(t - x)T_2(x/t) \quad (4.8)$$

Substituting this result in Eqs. (3.8c) and (3.9c) and integrating by parts [noting that the discontinuity in the derivative of $T_2(z)$ at $z = 1$ introduces no difficulties due to the factor $(t - x)^2$ which arises in the partial integration], we may express the results in the form

$$(1/m)C_{L_1}(t) = t^2 S_0(1/t) - (1 - t)^2 T_2(1/t) \quad (4.9)$$

$$\frac{1}{m} C_{M_1}(t) = \frac{1}{m}\left(a - \frac{2}{3}t\right)C_{L_1}(t) - \frac{4}{3}\left[t^3 S_1\left(\frac{1}{t}\right) - (1 - t)^2 T_2\left(\frac{1}{t}\right)\right] \quad (4.10)$$

where we have introduced the subscript **1** to denote the unit gust.

The required integrals are evaluated in the appendix, and substitution of the results in Eqs. (4.9) and (4.10) yields

$$\frac{1}{m} C_{L_1}(t) = \zeta_0(t) + t^2 \cos\theta \zeta_1(t) - (1 - t)^2 \zeta_3(t) \quad (4.11)$$

$$\frac{1}{m} C_{M_1}(t) = \frac{4}{3} t^2(1 - t) \cos\theta \zeta_1(t) + \frac{2}{3} t^2 \zeta_2(t) + \frac{2}{3} t(1 - t)^2 \zeta_3(t) \quad (4.12)$$

$$\zeta_2(t) = 0 \quad (4.13a)$$

$$= \frac{(1 - t)\cot\theta}{\pi} \cosh^{-1}\left(\frac{t \sin\theta}{|t - 1|}\right) \quad (4.13b)$$

$$= 0 \quad (4.13c)$$

where the time intervals in Eq. (4.13) are those of Eq. (3.17).

The functions ζ_3, $(1/m)C_{L_1}$, and $(1/m)C_{M_1}$ are plotted vs. τ in Figs. 9 to 11.

(5) Impulsive Gust

The sharp-edged uniform gust dealt with in the preceding section may not be realized with any frequency under actual flying conditions (although it is, of course, true that a gust with any space-time history can be built up by a Duhamel superposition of sharp-edged gusts). A situation that is likely to be realized rather more closely in practice is the impulsive gust. Such a gust is specified by the Dirac delta function—viz.,

$$w(x, t) = \delta[(Ut/c) - x] = \delta(\bar{t} - x) \quad (5.1)$$

$$\int_{-\epsilon}^{\epsilon} \delta(z)\, dz = 1, \quad \epsilon > 0 \quad (5.2a)$$

$$\delta(z) = (d/dz)\mathbf{1}(z) \quad (5.2b)$$

where Eqs. (5.2) define $\delta(z)$. Since w is dimensionless and referred to U, it follows from Eqs. (5.1) and (5.2a) that the velocity time integral (at a fixed point on the airfoil) divided by the chord length is unity—viz.,

$$\frac{1}{c}\int_{-\infty}^{\infty} Uw(x, t)\, dt = \int_{-\infty}^{\infty} \delta(\bar{t} - x)\, d\bar{t} = 1 \quad (5.3)$$

It follows from Eq. (5.2b) that the response of the airfoil to an impulsive gust is obtained from the re-

sponse to a unit gust after differentiation with respect to the dimensionless time $\bar{t}$, which is there denoted by t. Carrying out the differentiation of $C_{L_1}(t)$ and $C_{M_1}(t)$, as given by Eqs. (4.9) and (4.10), yields

$$C_{L_\delta}(t) = m[2tS_0(1/t) + 2(1 - t)T_2(1/t)] \quad (5.4)$$

$$C_{M_\delta}(t) = m[2(a - t)tS_0(1/t) - 4t^2S_1(1/t) + 2(1 - t)(a - 1 - t)T_2(1/t)] \quad (5.5)$$

(The terms involving the derivatives of S_0, S_1, and T_2 cancel identically.) The subscript δ denotes the impulsive gust. Substituting S_0, S_1, and T_2, we obtain

$$\frac{1}{m} C_{L_\delta}(t) = 2t \cos\theta\, \zeta_1(t) + 2\zeta_3(t) \quad (5.6)$$

$$\frac{1}{m} C_{M_\delta}(t) = 4\left(\frac{2}{3}t - t^2\right)\cos\theta\zeta_1(t) + 2t\zeta_2(t) + \frac{2}{3}(1 - 3t)\zeta_3(t) \quad (5.7)$$

These results are plotted in Figs. 12 and 13, respectively.

(6) Antisymmetric (Rolling) Gusts

The previous situations were symmetrical and, therefore, did not give rise to any rolling moments. It is also of some interest to study the response of the wing to an antisymmetric excitation. As a representative (although highly idealized) problem, we shall consider the case

$$w(x, y) = y \cot\mu \quad (6.1a)$$

$$t_0(x, y) = x \quad (6.1b)$$

Viewed spanwise, this distribution is shown in Fig. 7, while a chordwise view is shown in Fig. 14.

Since the antisymmetric gust under consideration does not give rise to any lift or pitching moment, we shall be interested only in the rolling moment and, therefore, only in $\chi_1(x, t)$. Substituting the distribution (6.1) in Eqs. (2.10) and (2.11) and taking $n = 1$ therein yields

$$\chi_1(x, t) = \frac{2}{3}\tan\theta\tan^2\mu\int_0^x A_0\left(\frac{x - \xi}{t - \xi}\right)\xi^3\, d\xi \quad (6.2)$$

Introducing the change of variable (4.3), we obtain

$$\chi_1(x, t) = \frac{2}{3}\tan^2\mu\tan\theta(t - x) \times \int_{u\geq 1(x-t)}^{x/t}(x - tu)^3(1 - u)^{-5}A_0(u)\, du \quad (6.3)$$

This result evidently can be expressed in terms of the $T_n(x/t)$ [see Eq. (4.6)], as can its substantial time derivative.

The rolling moment coefficient is defined by

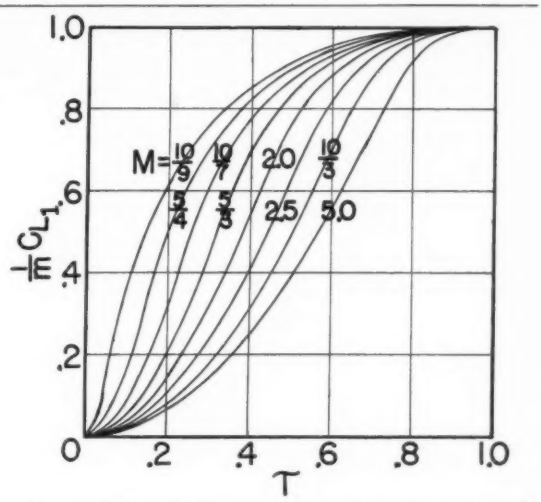

FIG. 10. $C_{L_1}(Ut/c)$, the lift coefficient due to penetration of a uniform sharp-edged gust, vs. τ.

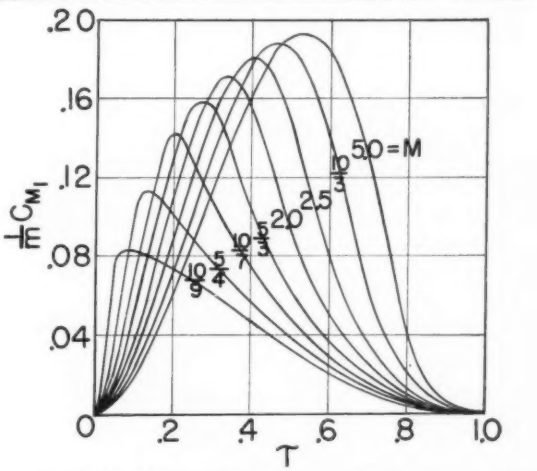

FIG. 11. $C_{M_1}(Ut/c)$, the pitching moment (about the centroidal axis, two-thirds of the root chord from the apex) coefficient due to penetration of a uniform, sharp-edged gust, vs. τ.

$$C_{l_1}(t) = \left(\frac{\rho U^2}{2}\cdot S\cdot 2c\tan\mu\right)^{-1} M_x(t) \quad (6.4a)$$

$$= -(\rho U^2\tan\mu)^{-1}\int_0^1 dx\int_{y_p(x)}^{y_q(x)} y\, dy \times [-2p(x, y, 0^+)] \quad (6.4b)$$

$$= -2\cot^2\mu\int_0^1 dx\left(\frac{\partial}{\partial x} + \frac{\partial}{\partial t}\right)\chi_1(x, t) \quad (6.4c)$$

Substituting $\chi_0(x, t)$ from Eq. (6.3), carrying out the indicated differentiation, and integrating repeatedly by parts yield

$$\frac{1}{m}\,C_{l_1}(t) = -\frac{1}{12}\,t^4 S_0\left(\frac{1}{t}\right) + \frac{1}{2}\,t^2(1-t)^2 T_2\left(\frac{1}{t}\right) + \frac{2}{3}\,t(1-t)^3 T_3\left(\frac{1}{t}\right) + \frac{1}{4}\,(1-t)^4 T_4\left(\frac{1}{t}\right) \tag{6.5}$$

Substituting the required integrals from the appendix, we have

$$-\left(\frac{12}{m}\right) C_{l_1}(t) = \zeta_0(t) + t^4\cos\theta\zeta_1(t) + (1-t)^2\left(1+\frac{5}{2}\,t\right)\csc^2\theta\zeta_2(t) - (1-t)^2\left[(3t^2+2t+1) + \frac{1}{2}\,(1-t)^2\csc^2\theta\right]\zeta_3(t) \tag{6.6}$$

This result is plotted in Fig. 15.

It is also of interest to consider the antisymmetric impulsive gust, specified by

$$w(x, y, t) = y\cot\mu\delta(\bar{l} - x) \tag{6.7}$$

Following the argument of Section (5), the response to this gust can be obtained by time differentiation of the response to the gust (6.1). Differentiating Eq. (6.5) with respect to time yields

$$C_{l_\delta}(t) = -\frac{m}{3}\left[t^3 S_0\left(\frac{1}{t}\right) + 3t(1-t)\,(2t-1)T_2\left(\frac{1}{t}\right) + 2(1-t)^2(4t-1)T_3\left(\frac{1}{t}\right) + 3(1-t)^3 T_4\left(\frac{1}{t}\right)\right] \tag{6.8}$$

$$-\frac{3}{m}\,C_{l_\delta}(t) = t^3\cos\theta\zeta_1(t) - \frac{5}{2}\,t(1-t)\csc^2\theta\zeta_2(t) + (1-t)\left[3t^2 + \frac{1}{2}\,(1-t)^2\csc^2\theta\right]\zeta_3(t) \tag{6.9}$$

This result is plotted in Fig. 16.

(7) Two-Dimensional Gust Problem

For the sake of completeness and in order to find the response to an impulsive gust, we shall consider briefly the two-dimensional gust problem. In this case, we simply set $w_n(\xi) = 1$ and $t_0(\xi) = \xi$ in Eq. (2.10), whence

$$\chi(x, t) = \tan\theta\int_0^x A_0\left(\frac{x-\xi}{t-\xi}\right)d\xi \tag{7.1}$$

Introducing the change of variable (4.3), we have

$$\chi(x, t) = \tan\theta(t-x)\int_{u\le 1(x-t)}^{x/t}(1-u)^{-2}A_0(u)\,du \tag{7.2}$$

FIG. 12. $C_{L_\delta}(Ut/c)$, the lift coefficient due to a unit impulsive gust, vs. τ.

$$\left(\frac{\partial}{\partial x} + \frac{\partial}{\partial t}\right)\chi_0(x, t) = \tan\theta A_0\left(\frac{x}{t}\right) \tag{7.3}$$

The lift and moment coefficients are given by

$$C_{L_1}(t) = [(\rho U^2/2)\cdot c]^{-1}L \tag{7.4a}$$

$$= 4\int_0^1 dx\left(\frac{\partial}{\partial x} + \frac{\partial}{\partial t}\right)\chi(x, t) \tag{7.4b}$$

$$= mtS_0(1/t) \tag{7.4c}$$

$$C_{M_1}(t) = [(\rho U^2/2)\cdot c\cdot c]^{-1}M \tag{7.5a}$$

$$= 4\int_0^1 dx\left(\frac{a}{2} - x\right)\left(\frac{\partial}{\partial x} + \frac{\partial}{\partial t}\right)\chi(x, t) \tag{7.5b}$$

$$= m\left[\frac{a}{2}\,tS_0\left(\frac{1}{t}\right) - t^2 S_1\left(\frac{1}{t}\right)\right] \tag{7.5c}$$

Substituting $S_0(1/t)$ and $S_1(1/t)$ from the appendix, we have

$$(1/m)C_{L_1}(t) = \zeta_0(t) + t\cos\theta\zeta_1(t) \tag{7.6}$$

$$\frac{1}{m}\,C_{M_1}(t)\,|_{a=1} = \frac{1}{2}\,t(1-t)\cos\theta\,\zeta_1(t) + \frac{1}{2}\,t\zeta_2(t) \tag{7.7}$$

where $a = 1$ corresponds to mid-chord.

To obtain the response to an impulsive gust, we differentiate Eqs. (7.4c) and (7.5c) with respect to time, with the results

$$C_{L_\delta}(t) = m[S_0(1/t) - (1/t)A_0(1/t)] \tag{7.8}$$

$$C_{M_\delta}(t) = (m/2)\,[aS_0(1/t) - 4tS_1(1/t) + (2-a)\,(1/t)A_0(1/t)] \tag{7.9}$$

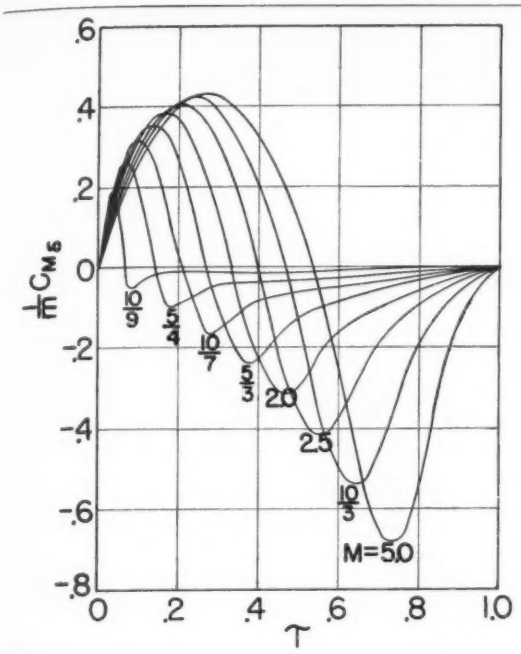

FIG. 13. $C_{M_\delta}(Ut/c)$, the pitching moment coefficient (about an axis two-thirds of the root chord from the apex) due to a unit impulsive gust, vs. τ.

$$(1/m)C_{L_\delta}(t) = \cos\theta\zeta_1(t) \tag{7.10}$$

$$\frac{1}{m}C_{M_\delta}(t)\,|_{a=1} = \left(\frac{1}{2} - t\right)\cos\theta\,\zeta_1(t) + \zeta_2(t) \tag{7.11}$$

The results [Eqs. (7.10) and (7.11)] are plotted in Figs. 17 and 18.

(8) General Downwash Distribution; Pitching Airfoil

The general case of transient motion of an airfoil may be specified by the downwash distribution

$$w(x, y, z) = -\frac{D}{Dt}\,[z(x, y, t)\mathbf{1}(t)] \tag{8.1a}$$

$$= -[z_x(x, y, t) + z_t(x, y, t)]\,1(t) - z(x, y, 0)\delta(t) \tag{8.1b}$$

where t is the dimensionless time of Eq. (1.11). The response to the first two terms in Eq. (8.1b) can be obtained by Duhamel superposition of Eqs. (2.10) and (2.11), assuming $z(x, y, t)$ and $z_t(x, y, t)$ to be continuous in both x and t, while the response to the last term can be obtained by calculating the response to $-z(x, y, 0)\,1(t)$ with the aid of Eqs. (2.10) and (2.11) and then differentiating the result with respect to t, as in the case of the impulsive gust [see Section (5)].

An example of some interest is the suddenly rotated airfoil for which

$$z(x, y, t) = \alpha(a - x) \tag{8.2}$$

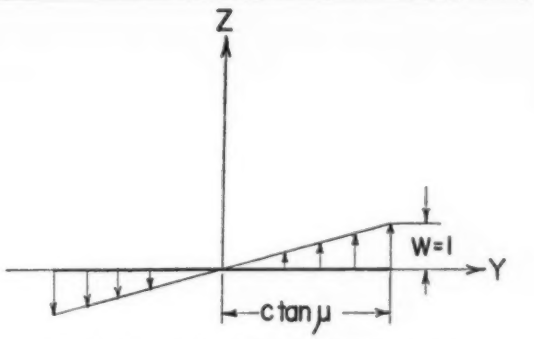

FIG. 14. Chordwise view of antisymmetric gust.

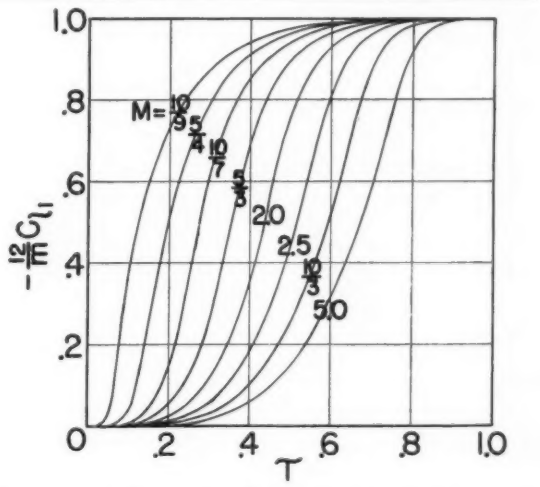

FIG. 15. $C_{l_\delta}(Ut/c)$, the rolling moment coefficient due to antisymmetrical gust of Fig. 14, vs. τ.

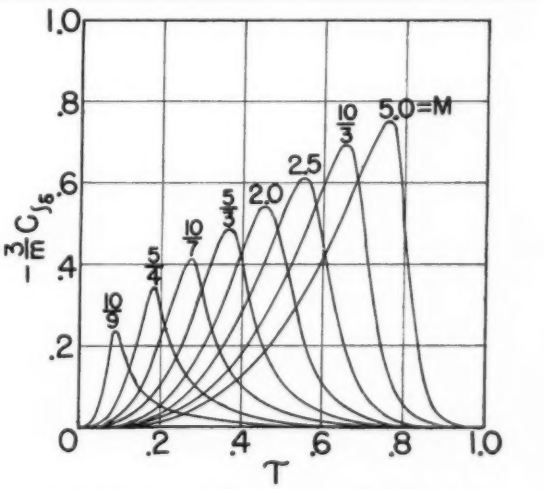

FIG. 16. $C_{l_\delta}(Ut/c)$, the rolling moment coefficient due to an antisymmetrical impulsive gust, vs. τ.

where a specifies the axis of rotation and α the angle. The corresponding downwash distribution is given by

$$w(x, t) = \alpha[\mathbf{1}(t) + (x - a)\delta(t)] \tag{8.3}$$

The response to the first term in Eq. (8.3) has been treated in Section (3). The response to the second term may be obtained by substituting $t_0 = 0$ and $w = (x - a)$ in Eqs. (2.10) and (2.11), taking $n = 0$, and differentiating with respect to t—viz.,

$$\chi_\delta(x, t) = 2\alpha \tan \mu \tan \theta \frac{\partial}{\partial t} \int_0^x A_0\left(\frac{x - \xi}{t}\right) \xi(\xi - a)\, d\xi \Bigg] \tag{8.4}$$

Carrying out the differentiation and then integrating by parts, we have

$$\chi_\delta(x, t) = \frac{2\alpha \tan \mu \tan \theta}{t} \int_0^x A_0\left(\frac{x - \xi}{t}\right) \Big[3\xi^2 - 2(x + a)\xi + ax \Big]\, d\xi \tag{8.5}$$

This must be added to Eq. (3.4) to obtain the overall response. While the result might be reasonably representative of a suddenly deflected control surface (of delta plan form), provided the time for deflection were small relative to $(1 - \sin \theta)^{-1}$, we have not carried out any numerical calculations. However, the final results for the lift and moment coefficients can be expressed in terms of the S_n integrals previously introduced.

Appendix

Evaluation of the Integrals $S_n(z)$ and $T_n(z)$

The required integrals are given by Eqs. (3.6) and (4.6) as

$$S_n(z) = \int_0^z u^n A_0(u)\, du, \qquad n = 0, 1, 2, 3 \tag{A1}$$

$$T_n(z) = \int_{u_2 \mathbf{1}(z-1)}^z (1 - u)^{-n} A_0(u)\, du, \qquad n = 2, 3, 4 \tag{A2}$$

where $A_0(u)$ is given by Eq. (2.6) and can be written

$$A_0(u) = \mathbf{1}(u)\zeta_0(1/u) \tag{A3}$$

$$\zeta_0(1/u) = 1, \qquad 0 < u < u_1, \quad (u_1 = 1 - \sin \theta) \tag{A4a}$$

$$= (1/\pi) \cos^{-1} [(u - \cos^2 \theta)/u \sin \theta], \qquad u_1 < u < u_2 \tag{A4b}$$

$$= 0, \qquad u > u_2, \quad (u_2 = 1 + \sin \theta) \tag{A4c}$$

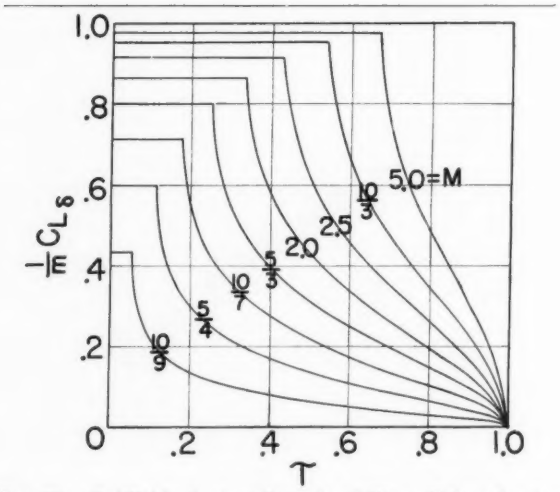

FIG. 17. $C_{L_\delta}(Ut/c)$, the two-dimensional lift coefficient due to an impulsive gust, vs. τ.

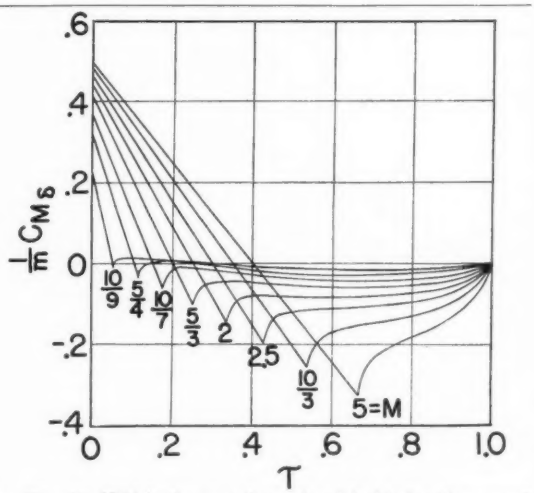

FIG. 18. $C_{M_\delta}(Ut/c)$, the two-dimensional (mid-chord) moment coefficient due to an impulsive gust, vs. τ.

We consider first the $S_n(z)$; substitution of $A_0(u)$ in Eq. (A1) yields

$$(n+1)S_n(z) = z^{n+1}, \qquad 0 < z < u_1 \tag{A5a}$$

$$= I_n(z), \qquad u_1 < z < u_2 \tag{A5b}$$

$$= I_n(u_2), \qquad z > u_2 \tag{A5c}$$

$$I_n(z) = u_1^{n+1} + (n+1)\int_{u_1}^{z} u^n \zeta_0\left(\frac{1}{u}\right) du \tag{A6}$$

Integrating $I_n(z)$ once by parts yields

$$I_n(z) = z^{n+1}\zeta_0(1/z) + \frac{\cos\theta}{\pi}\int_{u_1}^{z} u^n(-\cos^2\theta + 2u - u^2)^{-1/2}\, du \tag{A7}$$

The last integral is elementary;[7] carrying out the evaluation and substituting in Eq. (A5), we obtain

$$S_0(z) = z\zeta_0(1/z) + \cos\theta\zeta_1(1/z) \tag{A8}$$

$$2S_1(z) = z^2\zeta_0(1/z) + \cos\theta\zeta_1(1/z) - z\zeta_2(1/z) \tag{A9}$$

$$3S_2(z) = z^3\zeta_0(1/z) + [1 + (1/2)\sin^2\theta]\cos\theta\zeta_1(1/z) - (1/2)(3+z)z\zeta_2(1/z) \tag{A10}$$

$$4S_3(z) = z^4\zeta_0\left(\frac{1}{z}\right) + \left(1 + \frac{3}{2}\sin^2\theta\right)\cos\theta\zeta_1\left(\frac{1}{z}\right) - \left(\frac{11}{6} + \frac{2}{3}\sin^2\theta + \frac{5}{6}z + \frac{1}{3}z^2\right)z\zeta_2\left(\frac{1}{z}\right) \tag{A11}$$

$$\zeta_1(1/z) = 0, \qquad 0 < z < u_1 \tag{A12a}$$

$$= (1/\pi)\cos^{-1}[(1-z)/\sin\theta], \qquad u_1 < z < u_2 \tag{A12b}$$

$$= 1, \qquad z > u_2 \tag{A12c}$$

$$\zeta_2(1/z) = 0, \qquad 0 < z < u_1 \tag{A13a}$$

$$= \frac{\cos\theta}{\pi}\left[\left(1 - \frac{u_1}{z}\right)\left(\frac{u_2}{z} - 1\right)\right]^{1/2}, \qquad u_1 < z < u_2 \tag{A13b}$$

$$= 0, \qquad z > u_2 \tag{A13c}$$

Turning to the $T_n(z)$, substituting $A_0(u)$ in Eq. (A2) yields

$$(n-1)T_n(z) = (1-z)^{1-n} - 1, \qquad 0 < z < u_1 \tag{A14a}$$

$$= I_n^*(z), \qquad u_1 < z < u_2 \tag{A14b}$$

$$= 0, \qquad z > u_2 \tag{A14c}$$

$$I_n^*(z) = (1-u_1)^{n-1} - 1 + (n-1)\int_{u_1}^{z}(1-u)^{-n}\zeta_0\left(\frac{1}{u}\right)du, \qquad z < 1 \tag{A15a}$$

$$= (n-1)\int_{u_2}^{z}(1-u)^{-n}\zeta_0\left(\frac{1}{u}\right)du, \qquad z > 1 \tag{A15b}$$

Integrating $I_n^*(z)$ once by parts yields

$$I_n^*(z) = (1-z)^{1-n}\zeta_0\left(\frac{1}{z}\right) - \mathbf{1}(1-z) + \frac{\cos\theta}{\pi}\int_{\substack{u_1(z<0)\\ u_2(z>0)}}^{z} u^{-1}(1-u)^{1-n}(-\cos^2\theta + 2u - u^2)^{-1/2}\, du \tag{A16}$$

Introducing the partial fraction expansion

$$u^{-1}(1-u)^{1-n} = u^{-1} + \sum_{m=1}^{n-1}(1-u)^{-m} \tag{A17}$$

we have

$$I_n^*(z) = (1-z)^{1-n}\zeta_0\left(\frac{1}{z}\right) - \mathbf{1}(1-z) + \frac{\cos\theta}{\pi}\int_{1\mp\sin\theta}^{z} u^{-1}(-\cos^2\theta + 2u - u^2)^{-1/2}\,du + \frac{\cos\theta}{\pi}\sum_{m=1}^{n-1}\int_{1\mp\sin\theta}^{z}(1-u)^{-m}(-\cos^2\theta + 2u - u^2)^{-1/2}\,du \quad \text{(A18)}$$

where the upper and lower signs correspond to z less or greater than 1, respectively. Carrying out the first integration[8] and introducing the change of variable

$$u = 1 - \sin\theta\cos\varphi \quad \text{(A19)}$$

in the remaining integrals, Eq. (A18) reduces to

$$I_n^*(z) = [(1-z)^{1-n} - 1]\zeta_0\left(\frac{1}{z}\right) + \frac{\cos\theta}{\pi}\sum_{m=1}^{n-1}(\csc\theta)^m\int_{\pi\mathbf{1}(z-1)}^{\cos^{-1}[(1-z)/\sin\theta]}(\sec\varphi)^m\,d\varphi \quad \text{(A20)}$$

Carrying out the last integrations[9] and substituting the results in Eq. (A14), we obtain

$$T_2(z) = [z/(1-z)]\,[\zeta_0(1/z) - \zeta_3(1/z)] \quad \text{(A21)}$$

$$2T_3(z) = [(1-z)^{-2} - 1]\zeta_0\left(\frac{1}{z}\right) + \frac{z}{1-z}\csc^2\theta\zeta_2\left(\frac{1}{z}\right) - \frac{z}{1-z}\zeta_3\left(\frac{1}{z}\right)$$

$$= \frac{z}{1-z}\left[\frac{2-z}{1-z}\zeta_0\left(\frac{1}{z}\right) + \csc^2\theta\zeta_2\left(\frac{1}{z}\right) - \zeta_3\left(\frac{1}{z}\right)\right] \quad \text{(A22)}$$

$$3T_4(z) = [(1-z)^{-3} - 1]\zeta_0\left(\frac{1}{z}\right) + \frac{1}{2}\frac{z(3-2z)}{(1-z)^2}\csc^2\theta\,\zeta_2\left(\frac{1}{z}\right) - \left(1 + \frac{1}{2}\csc^2\theta\right)\frac{z}{1-z}\zeta_3\left(\frac{1}{z}\right) \quad \text{(A23)}$$

where

$$\zeta_3(1/z) = -[(1-z)/z]\,(\cot\theta/\pi)\cosh^{-1}(\sin\theta/1-z) \quad \text{(A24)}$$

References

[1] Miles, J. W., *On Harmonic Motion of Pointed Supersonic Wings*, Naval Ordnance Test Station Report, Inyokern, Calif., Technical Memorandum RRB-36, 1949.

[2] Biot, M. A., *Loads on a Supersonic Wing Striking a Sharp-Edged Gust*, Journal of the Aeronautical Sciences, Vol. 16, No. 5, pp. 296–301, May, 1949.

[3] Chang, C. C., *The Transient Reaction of an Airfoil Due to a Change in Angle of Attack at Supersonic Speed*, Journal of the Aeronautical Sciences, Vol. 15, No. 11, pp. 635–655, November, 1948.

[4] Heaslet, M. A., and Lomax, H., *Two-Dimensional Unsteady Lift Problems in Supersonic Flight*, N.A.C.A. T.N. No. 1261, June, 1948.

[5] Miles, J. W., *Transient Loading of Airfoils at Supersonic Speeds*, Journal of the Aeronautical Sciences, Vol. 15, No. 10, pp. 592–598, October, 1948.

[6] Schwarz, L., *Ebener instationare Theorie der Tragfläche bei Überschallgeschwindigkeit*, Jahrbuch der deutschen Luftfahrtforschung, pp. 1–8, 1943.

[7] Peirce, B. O., *A Short Table of Integrals*, No. 190; Ginn and Company, Boston, 1929.

[8] *Loc. cit.*, No. 183.

[9] *Loc. cit.*, No. 290.

Comparison of Theoretical and Experimental Results for the Turbulent Boundary Layer in Supersonic Flow Along a Flat Plate*

CARLO FERRARI†

Cornell Aeronautical Laboratory, Inc.

SUMMARY

On the basis of experimental results it is found necessary to restrict previously obtained theoretical data for the boundary layer arising from supersonic flow along a flat plate (placed parallel with the free-stream velocity vector) to an "inner" region, while a different type of solution is formulated for the "outer" region of the boundary layer, the characteristics of which depend appreciably on the distance in the direction of the flow. The theory now conforms with the experimentally determined fact that the drag coefficient decreases with increasing Mach Number.

INTRODUCTION

IN A PREVIOUS REPORT,[1] which was the beginning of an investigation being directed toward a wide understanding of the properties of boundary layers in supersonic flow, the velocity distribution within a cross section of the boundary layer which arises from contact with a flat plate was determined for the case of turbulent flow; also, the resistance coefficient, C_r, was obtained in terms of the Reynolds Number, R_x. These deductions depend upon a parameter that had been considered as a universal constant and which was denoted by β. In the above-mentioned first report of this series, the presumed value of β was also given. This value was based on the assumption that for the same Reynolds Numbers, the friction coefficients, at least up to Mach Number = 2, would be equal or approximately equal. Recent experiments by Young and Wilson have shown, on the contrary, that there is an appreciable decrease in C_r with increasing M_a. With use of these results as a starting point, the value of β is now recalculated. Furthermore, from the same experimental evidence, it appears that the assumption upon which the preceding investigation was based—i.e., that the variables characterizing the physical and kinematical state of the fluid are independent of the x-coordinate along the plate—is far from being verified for the range of Reynolds Numbers within which the experiments were conducted. The investigation, therefore, is now extended by rejecting this restrictive assumption. To accomplish this purpose, a method is applied which is similar to that described in another report[2] of this series concerning the turbulent boundary layer. When this extension is carried out for the cases investigated here, the calculated results agree satisfactorily with the experimental ones.

Received July 5, 1950.

* This research project was conducted under Navy BuOrd sponsorship.

† Member of Cornell Aeronautical Laboratory consulting staff. Professor, Laboratorio di Aeronautica, Politecnico di Torino.

SYMBOLS

R_x = Reynolds Number of the undisturbed stream ($R_x = \bar{U}_a x/\nu_a$)
T = absolute temperature
U = component of the velocity along the x-axis
V = component of the velocity along the y-axis
W = $\sqrt{U^2 + V^2}$
ρ = density of the fluid
μ = viscosity coefficient
ν = kinematic viscosity
p = pressure
τ = tangential friction stress
τ_p = tangential friction stress at the wall
U^* = friction velocity [$U^* = (\tau_p/\rho_p)^{1/2}$]
V_l = limit velocity of the undisturbed stream when expanded into a vacuum
u_a = $\bar{U}_a/V_l$
f = $\bar{U}/U^*$
f_a = $\bar{U}_a/U^*$
σ = $\bar{U}/\bar{U}_a = f/f_a$
u^* = U^*/V_l
M = Mach Number
γ = T_0/T_p
δ = thickness of the boundary layer
t = time
c_f = coefficient of local friction drag [$c_f = \tau_p/(1/2)\,\rho_a \bar{U}_a^2$]
C_r = coefficient of total friction drag for a plate of length x
h = factor of proportionality relating friction stress to the product of the parameters $\bar{\rho}$, δ, $\bar{U}_a$, and $\partial\bar{U}/\partial y$
ξ = x/L; $\eta = y/L$, x being taken in the direction of the wetted surface and where L = reference length
$\bar{\rho}_a$ = density in the external stream at a cross section of the layer having an abscissa equal to x
z = [see Eq. (9) of text]
$\bar{U}_a$ = velocity of the external stream (its magnitude is taken to be equal to the component in the direction of the x-axis of the actual vector)
Z = [see Eqs. (6′) and (6″) of text]
ψ = $\rho\bar{U}y$ = stream function (dimensions of a viscosity coefficient)
ψ_1 = $\psi/\rho_a U_a L$
$\bar{\delta}$ = δ/L

$$\delta^* = \delta \int_0^1 \left(1 - \frac{\bar{\rho}}{\bar{\rho}_a}\frac{\bar{U}}{\bar{U}_a}\right) d\,\frac{y}{\delta}$$

$\bar{\delta}^*$ = δ^*/L

$$\delta^{**} = \delta \int_0^1 \frac{\bar{\rho}}{\bar{\rho}_a}\frac{\bar{U}}{\bar{U}_a}\left(1 - \frac{\bar{U}}{\bar{U}_a}\right) d\,\frac{y}{\delta}$$

$\bar{\delta}^{**}$ = δ^{**}/L

Bars and primes will be used to denote, respectively, the mean values of the above quantities and their fluctuations about their mean values due to turbulence. The subscripts 0, p, and a correspond, respectively, to stagnation of the undisturbed stream, the wall, and the undisturbed stream.

(A) Determination of the Law of Velocity Distribution Within the Boundary Layer

(*A-1*) *Turbulent Friction Stress*

Through reference to the first report[1] of this series on the turbulent boundary layer, it appears that the turbulent friction stress within the region of the boundary layer close to the wetted wall may be written as

$$\tau = \bar{\rho} l \frac{\partial \bar{U}}{\partial y} U_p^* + \beta \frac{U_p^*}{V_t} \rho_p U_p^* \bar{U} \tag{1}$$

while, for the region of the boundary close to the undisturbed flow, it is true that

$$\tau = \bar{\rho} h \delta \bar{U}_a (\partial \bar{U}/\partial y) \tag{2}$$

as was explained in the second report[2] of this investigation of the turbulent boundary layer.

The replacement of Eq. (2) by Eq. (1) may be justified in the following way:

(1) While in the neighborhood of the wall the scale of the turbulence must essentially depend on the distance, y, from the wall on which the friction is operative, in proximity to the external stream it seems likely that this scale is dependent on the thickness, δ, of the boundary layer.

(2) For small values of y, the characteristic velocity upon which the correlation among the turbulent fluctuations of the main velocity itself depends is U_p^*, but for values of y close to δ, this characteristic velocity is likely to be $\bar{U}_a$.

(3) In proximity to the external stream it is likely that τ vanishes along with $\partial \bar{U}/\partial y$; on the other hand, for this same region, the variation of the several physical quantities is certainly always related in some perceptible way with the x-coordinate. At the wall, on the contrary, at least starting from some suitable value of x, it seems likely that this dependence on the x-coordinate is negligible in comparison to that related to the y-coordinate. In this latter region close to the wall, therefore, the considerations still hold that lead one to assume that β is a constant for the "inside" of the boundary layer. However, within the "external" region (which is external to the "inside" layer), this assumption is no longer acceptable.

(*A-2*) *Velocity in the "Inside" of the Boundary Layer in Proximity to the Wall*

For sufficiently small values of y, $\partial p/\partial x$ is equal to zero, and it is permissible to write $\partial \tau/\partial y = 0$. Consequently, the distribution of velocity within this region of the boundary layer is still given by Eq. (22) of the first report[1] of this series. The relationship is rewritten here.

$$\frac{\alpha_0}{c}\left\{ - \frac{1}{(f_1+f_2)\,[\sqrt{\gamma}\,(u^*/c) - f_1]} \log \frac{f_1 - \sqrt{\gamma}\,u^* f}{f_1} + \frac{1}{(f_1+f_2)\,[\sqrt{\gamma}(u^*/c) + f_2]} \log \frac{\sqrt{\gamma}\,u^* f + f_2}{f_2} + \frac{1}{[\sqrt{\gamma}(u^*/c) + f_2]\,[\sqrt{\gamma}(u^*/c) - f_1]} \log (1 - cf) \right\} = \log y^* + B \tag{3}$$

In the simpler case of a thermally insulated system, Eq. (3) may be reduced and becomes, upon reduction,

$$\frac{\alpha_0}{c}\left\{ - \frac{1}{2}\frac{1}{[(u^*/c) - 1]} \log (1 - fu^*) + \frac{1}{2}\frac{1}{[(u^*/c) + 1]} \log (1 + fu^*) + \frac{1}{[(u^{*2}/c^2) - 1]} \log (1 - cf) \right\} = \log y^* + B \tag{3'}$$

where $c = \beta u^*$.

(*A-3*) *Velocities Within the Boundary Layer in the Neighborhood of the External Stream*

The equation of motion for the boundary-layer flow in the neighborhood of the external stream is

$$(\partial/\partial\xi)\,(\bar{\rho}\bar{U}^2) + (\partial/\partial_\eta)\,(\bar{\rho}\bar{U}\bar{V}) = (\partial/\partial\eta)\tau$$

where τ is given by Eq. (2). Employing ξ and ψ_1 as independent variables, one obtains

$$\bar{\rho}\bar{U}\,(\partial/\partial\xi)\bar{U} = (\bar{\rho}\bar{U}/\bar{\rho}_a\bar{U}_a)\,(\partial\tau/\partial\psi_1) \tag{4}$$

On the other hand, it is true that

$$\frac{\partial \tau}{\partial \psi_1} = \frac{\partial}{\partial \psi_1}\left(\bar{\rho} h\, \bar{\delta} \bar{U}_a{}^2 \frac{\partial}{\partial \eta} \frac{\bar{U}}{\bar{U}_a} \right) = \frac{\partial}{\partial \psi_1}\left(\bar{\rho}_a h \bar{\delta} \bar{U}_a{}^2 \frac{\bar{\rho}^2}{\bar{\rho}_a{}^2} \frac{\bar{U}}{\bar{U}_a} \frac{\partial}{\partial \psi_1} \frac{\bar{U}}{\bar{U}_a} \right)$$

Thus, it follows that

$$\frac{\bar{\rho}^2}{\bar{\rho}_a{}^2}\frac{\bar{U}}{\bar{U}_a}\frac{\partial}{\partial\psi_1}\frac{\bar{U}}{\bar{U}_a} = \frac{1-u_a{}^2}{2u_a{}^2}\frac{\partial Z}{\partial\psi_1} \tag{5}$$

provided one sets therein

$$Z = 2u_a{}^2\int_0^{\bar{U}/\bar{U}_a}\frac{\bar{\rho}^2}{\bar{\rho}_a{}^2}\frac{\bar{U}}{\bar{U}_a}\,d\,\frac{\bar{U}}{\bar{U}_a} = 2u_a{}^2\,(1-u_a{}^2)\gamma^2\int_0^{\sigma}\frac{\sigma d\sigma}{[1-u_a{}^2\,\gamma\sigma^2+(\gamma-1)\sigma]^2} \tag{6}$$

For a thermally insulated system ($\gamma = 1$), one has simply

$$Z = \bar{\rho}/\bar{\rho}_a \tag{6'}$$

For $\gamma \neq 1$, one obtains

$$Z = (\bar{\rho}/\bar{\rho}_a) + (\gamma-1)\mathfrak{F}(\sigma) \tag{6''}$$

where

$$\mathfrak{F} = \frac{-1}{2\{u_a{}^2\gamma+[(\gamma-1)^2/4]\}}\left[\frac{(\gamma-1)/2-u_a{}^2\,\gamma\sigma}{1-u_a{}^2\,\gamma\sigma^2+(\gamma-1)\sigma}-\frac{\gamma-1}{2}\right]+\frac{u_a{}^2\,\gamma}{u_a{}^2\gamma+[(\gamma-1)^2/4]}\times$$
$$\frac{1}{2\sqrt{u_a{}^2\gamma+[(\gamma-1)^2/4]}}\left\{\log\frac{\sqrt{u_a{}^2\gamma+[(\gamma-1)^2/4]}-(\gamma-1)/2+u_a{}^2\,\gamma\sigma}{\sqrt{u_a{}^2\gamma+[(\gamma-1)^2/4]}+(\gamma-1)/2-u_a{}^2\,\gamma\sigma}-\right.$$
$$\left.\log\frac{\sqrt{u_a{}^2\gamma+[(\gamma-1)^2/4]}-(\gamma-1)/2}{\sqrt{u_a{}^2\gamma+[(\gamma-1)^2/4]}+(\gamma-1)/2}\right\} = \frac{-1}{2\{u_a{}^2\gamma+[(\gamma-1)^2/4]\}}\left[\frac{\gamma-1'}{2}\left(\frac{\bar{\rho}}{\bar{\rho}_p}-1\right)-u_a{}^2\,\gamma\sigma\,\frac{\bar{\rho}}{\bar{\rho}_p}\right]+$$
$$\frac{u_a{}^2\,\gamma}{2\{u_a{}^2\gamma+[(\gamma-1)^2/4]\}^{3/2}}\left\{\log\frac{\sqrt{u_a{}^2\gamma+[(\gamma-1)^2/4]}-(\gamma-1)/2+u_a{}^2\,\gamma\sigma}{\sqrt{u_a{}^2\gamma+[(\gamma-1)^2/4]}+(\gamma-1)/2-u_a{}^2\,\gamma\sigma}-\right.$$
$$\left.\log\frac{\sqrt{u_a{}^2\gamma+[(\gamma-1)^2/4]}-(\gamma-1)/2}{\sqrt{u_a{}^2\gamma+[(\gamma-1)^2/4]}+(\gamma-1)/2}\right\} \tag{7}$$

It results that

$$\partial\tau/\partial\psi_1 = \bar{\rho}_a h\bar{\delta}\,(\bar{U}_a{}^2/2u_a{}^2)\,(1-u_a{}^2)\,(\partial^2 Z/\partial\psi_1{}^2)$$

On the other hand, it is true that

$$\bar{U}(\partial/\partial\xi)\bar{U} = (\bar{U}_a{}^2/2u_a{}^2)\,(\bar{\rho}_a{}^2/\bar{\rho}^2)\,(1-u_a{}^2)\,(\partial Z/\partial\xi)$$

so that one has

$$\frac{\bar{\rho}}{\bar{\rho}_a}\,\bar{U}_a{}^2\frac{\bar{\rho}_a{}^2}{\bar{\rho}^2}\frac{\partial Z}{\partial\xi} = \frac{\bar{\rho}}{\bar{\rho}_a}\frac{\bar{U}}{\bar{U}_a}\,h\bar{\delta}\bar{U}_a{}^2\frac{\partial^2 Z}{\partial\psi_1{}^2} \tag{8}$$

that is,

$$\partial Z/\partial\xi_1 = (\bar{\rho}^2/\bar{\rho}_a{}^2)\,(\bar{U}/\bar{U}_a)\,(\partial^2 Z/\partial\psi_1{}^{*2}) \tag{8'}$$

where $\psi_1{}^*$ is set equal to $\psi_1/\sqrt{h}$ and $\xi_1 = \int_0^{\xi}\bar{\delta}d\xi$.

Also, if one writes

$$z = Z_0 - Z \tag{9}$$

where $Z_0 = 1+\gamma(\gamma-1)\mathfrak{F}(1)$, then,

$$\frac{\partial z}{\partial\xi_1} = \frac{\bar{\rho}^2}{\bar{\rho}_a{}^2}\frac{\bar{U}}{\bar{U}_a}\frac{\partial^2 z}{\partial\psi_1{}^{*2}} \tag{9'}$$

which is formally analogous to Eq. (23) of the second report[2] of this series.

(A-4) *Solution of von Mises Eq. (9')*

For the region of the boundary layer close to the external stream, within which "outer" region $\rho \cong \bar{\rho}_a$ and $\bar{U} \cong \bar{U}_a$, one has

$$\partial z_e/\partial\xi_1 = \partial^2 z_e/\partial\psi_1{}^{*2} \tag{9''}$$

together with the following boundary conditions: For $\psi_1{}^* = \infty$, $z_e = 0$; for $\psi_1{}^* = 0$, $z_e = H$. Here, H denotes a function of ξ_1 only, which will be specified

shortly. It will be presumed that it varies so slightly that one may assume it to be constant. The solution of Eq. (9″), satisfying the above conditions, is given by

$$z_e = H \operatorname{erfc} (\psi_1^*/2\sqrt{\xi_1}) \tag{10}$$

If it is now assumed that the "external" solution, Eq. (10), is a first approximation solution of Eq. (9′) itself, at least within a certain region, the exact solution of Eq. (9′) can be obtained by means of the method of successive approximations[3] in an analogous manner to the procedure suggested by von Kármán[4] in carrying out the study of the laminar boundary layer along a flat plate for the case of incompressible flow.

Let the variable $\psi_1^*/2\sqrt{\xi_1}$ be denoted now by means of the symbol ξ. Also, note that Eq. (9′) can be written in the *normal* form,

$$\frac{\partial z}{\partial \xi_1} = \frac{\partial^2 z}{\partial \psi_1^{*2}} - \left[\frac{1}{A(z)} - 1\right]\frac{\partial z}{\partial \xi_1}$$

where $A(z) = (\bar{\rho}^2/\bar{\rho}_a{}^2)\,(\bar{U}/\bar{U}_a)$.

In addition, let z_n be the solution of Eq. (9′) which corresponds to the $(n-1)$th approximation, so that z_n is defined by the following equation:

$$\frac{\partial z_n}{\partial \xi_1} = \frac{\partial^2 z_n}{\partial \psi_1^{*2}} - \left[\frac{1}{A(z_{n-1})} - 1\right]\frac{\partial z_{n-1}}{\partial \xi_1}$$

If, in addition, one now sets $\Delta_n z = z_n - z_{n-1}$ and $A_{n-1} = A(z_{n-1})$, then it follows that

$$\frac{\partial}{\partial \xi_1}\Delta_n z = \frac{\partial^2}{\partial \psi_1^{*2}}\Delta_n z - \left(\frac{1}{A_{n-1}} - 1\right)\frac{\partial z_{n-1}}{\partial \xi_1} + \left(\frac{1}{A_{n-2}} - 1\right)\frac{\partial z_{n-2}}{\partial \xi_1}$$

But, if z_n is only a function of ζ, $z_n = z_n(\zeta)$ (and because it is true that

$$\partial z_n/\partial \xi_1 = -(\zeta/2\xi_1)\,(dz_n/d\zeta)$$
$$\partial^2 z_n/\partial \psi_1^{*2} = (1/4\xi_1)\,(d^2 z_n/d\zeta^2)$$
$$\partial z_{n-1}/\partial \xi_1 = -(\zeta/2\xi_1)\,(dz_{n-1}/d\zeta)$$

etc.), it may be inferred that

$$\frac{d^2}{d\zeta^2}\Delta_n z + 2\zeta\frac{d}{d\zeta}\Delta_n z + \Delta_{n-1}G = 0$$

where

$$\Delta_{n-1}G = 2\zeta\left(\frac{1}{A_{n-1}} - 1\right)\frac{dz_{n-1}}{d\zeta} - 2\zeta\left(\frac{1}{A_{n-2}} - 1\right)\frac{dz_{n-2}}{d\zeta}$$

Thus one obtains

$$\Delta_n z = C_n\int_0^\zeta e^{-\zeta^2}d\zeta - \int_0^\zeta e^{-\zeta^2}d\zeta \times \int_0^{\zeta_1}\Delta_{n-1}Ge^{\zeta_1^2}d\zeta_1 + C_n'$$

Remembering that it is true that $\Delta_n z = 0$ for $\zeta = 0$, one has $C_n' = 0$; while from the equation $\Delta_n z = 0$ for $\zeta = \infty$ it is inferred that

$$C_n = \frac{2}{\sqrt{\pi}}\int_0^\infty e^{-\zeta^2}d\zeta\int_0^\zeta \Delta_{n-1}Ge^{\zeta_1^2}d\zeta_1 = \int_0^\infty \Delta_{n-1}Ge^{\zeta_1^2}\operatorname{erfc}\zeta_1 d\zeta_1$$

Furthermore, one finds

$$\int_0^\zeta e^{-\zeta^2}d\zeta\int_0^\zeta \Delta_{n-1}Ge^{\zeta_1^2}d\zeta_1 = \frac{\sqrt{\pi}}{2}\int_0^\zeta \Delta_{n-1}Ge^{\zeta_1^2}(\operatorname{erf}\zeta - \operatorname{erf}\zeta_1)d\zeta_1$$

and thus,

$$\Delta_n z = \frac{\sqrt{\pi}}{2}\left[\operatorname{erf}\zeta\int_0^\infty \Delta_{n-1}Ge^{\zeta_1^2}\operatorname{erfc}\zeta_1 d\zeta_1 - \int_0^\zeta \Delta_{n-1}Ge^{\zeta_1^2}(\operatorname{erf}\zeta - \operatorname{erf}\zeta_1)d\zeta_1\right] \tag{11}$$

This equation allows one to evaluate the nth approximation if the $(n-1)$th is known.

The sequence of the functions $z_1 = z_e$, z_2, etc., certainly converges,[3] at least for values of ζ confined within a suitable interval. Accordingly, the limit function of this sequence gives within this suitable interval the exact solution of Eq. (9′). The value of the function H, for each ξ_1, is to be determined by keeping in mind that the solution of Eq. (9′) which has just been obtained must produce velocity profiles for the series of cross sections along the boundary layer, which may be joined to the equivalent profiles afforded by Eq. (3) for the "inside" region of the boundary layer. One can easily see that a satisfactory "join" or connection and a satisfactory agreement with the experimental results may be achieved by assuming for H values that, though changing from cross section to cross section along the boundary layer, vary so slowly as to justify the assumption made at the beginning of this Section.

(B) Law of Variation of the Thickness of the Boundary Layer and of the Friction Coefficient

(B-1) *Law of Variation of the Thickness of the Boundary Layer*

From the velocity profiles for the cross sections of the boundary layer, the thickness δ of the layer can at once be inferred. It is worth pointing out that, even assuming the velocity distribution to be the one corresponding to the external solution [Eq. (10)], one obtains, at least in the case of a thermally insulated system, a variation of δ which is approximately linear with ξ. In fact, it is true that

$$\eta = \int_0^{\psi_1} \frac{\bar{\rho}_a}{\bar{\rho}} \frac{\bar{U}_a}{\bar{U}} d\psi_1 = 2\sqrt{\xi_1}\sqrt{h} \times \int_0^{\psi_1^*} \frac{\bar{\rho}_a}{\bar{\rho}} \frac{\bar{U}_a}{\bar{U}} d \frac{\psi_1^*}{2\sqrt{\xi_1^*}} \quad (12)$$

In addition, according to Eq. (6′), one has

$$\bar{\rho}/\bar{\rho}_a = 1 - z = [1 - (\bar{U}_a^2/V_l^2)]/[1 - (\bar{U}^2/V_l^2)]$$

whence

$$\bar{U}/\bar{U}_a = \sqrt{(u_a^2 - z)/[u_a^2(1 - z)]}$$

if $u_a^2 = U_a^2/V_l^2$, and, consequently,

$$(\bar{\rho}_a/\bar{\rho})\,(\bar{U}_a/\bar{U}) = u_a/\sqrt{(1 - z)\,(u_a^2 - z)}$$

Because of the assumption that H varies but slightly with ξ, one can consider the value ζ_0 of $\psi_1^*/2\sqrt{\xi_1}$ for which z reaches a value corresponding, for instance, to $\bar{U}/\bar{U}_a = 0.995$ to be independent of ξ. Consequently,

$$\delta = 2\sqrt{\xi_1}\sqrt{h}\,u_a \int_0^{\zeta_0} \frac{d\zeta}{\sqrt{(1 - z)(u_a^2 - z)}} = 2\sqrt{\xi_1}\sqrt{h}\,u_a B(H, u_a) \quad (13)$$

wherein the following definition of B is employed:

$$B(H, u_a) = \int_0^{\zeta_0} \frac{d\zeta}{\sqrt{(1 - z)\,(u_a^2 - z)}} \quad (14)$$

Substituting in place of ξ_1 the integral form of this quantity, squaring Eq. (13), and differentiating (still assuming H = const.), one infers that

$$\left.\begin{aligned} d\delta/d\xi &= 2u_a^2 h B^2 \\ \text{or} \qquad \delta &= 2u_a^2 h B^2 \xi \end{aligned}\right\} \quad (15)$$

Because of the slowness of variation of B with ξ, this equation demonstrates what has been stated above concerning the linearity of δ.

(B-2) *Friction Coefficient*

The value of the total friction coefficient is given by the relation

Table 1
Velocity Distribution at Station 7

$\bar{U}/\bar{U}_a$	y^*	y	η
0.6	73.75	0.1907 mm.	0.0002384
0.7	250.70	0.6483 mm.	0.0008106
0.8	922.10	2.3850 mm.	0.0029810
0.85	1,835.00	4.7460 mm.	0.0059330

$$C_f = \frac{2\delta^{**}}{\xi} = \frac{2}{\xi}\int_0^\infty \frac{\bar{\rho}\bar{U}}{\bar{\rho}_a\bar{U}_a}\left(1 - \frac{\bar{U}}{\bar{U}_a}\right) d\eta = \frac{4\sqrt{\xi_1}}{\xi}\int_0^\infty \left(1 - \frac{\bar{U}}{\bar{U}_a}\right) d\,\frac{\psi_1}{2\sqrt{\xi_1}} \quad (16)$$

which, in the case of a thermally insulated system, becomes

$$C_f = \frac{4\sqrt{h}\sqrt{\xi_1}}{\xi}\int_0^\infty \left[1 - \sqrt{\frac{u_a^2 - z}{u_a^2(1 - z)}}\right] d\zeta \quad (16')$$

(C) Numerical Application: Comparison Between the Theoretical Formulas and the Experimental Results by Young and Wilson

For the purpose of checking the formulas given in the preceding Sections, they have been applied to the determination of the velocity distribution within the boundary layer along a flat plate under the same conditions as existed in the experiments performed by Young and Wilson.[5] The final results are presented below. The intermediate steps through which the value of the constants appearing in the formulas was obtained may be determined in a straightforward manner and are not reproduced here.

At the 7th Station along the plate used in the experiments, where the abscissa x = 31.49 in. = 799.8 mm., one has (assuming $\gamma = 1$) $M_a = 1.695$; $R_x = 17.7 \times 10^6$; $\beta = 0$; $c_f = 0.0019$. Then one finds

$$u_a = \bar{U}_a/V_l = 0.6041$$

$$\bar{U}_p^*/\bar{U}_a = 0.03868$$

$$\frac{\bar{U}_p^*}{\nu_p} = \frac{\bar{U}_p^*}{\bar{U}_a}\frac{\bar{U}_a}{\nu_a}\frac{\nu_a}{\nu_p} = 0.03868\,\frac{17.7 \times 10^6}{79.98}\,(0.6351)^{1.75} = \frac{1}{0.02586 \times 10^{-2}\ \text{cm.}}$$

hence, $y = 0.02586 \times 10^{-2}\, y^*$ cm.

The universal constant B is taken to be 2.2, since this is the value it assumes from the relation $\log(1 + by^*) = \log y^* + B$ as y^* becomes large and upon selection of the value 8.93 for b (see the first report[1] of this series). From Eq. (3′) and with the aid of the above data, Table 1 may be constructed.

The values in Table 1 are plotted on the graph of Fig. 1; the experimental results by Young and Wilson are also given. It may be seen that, for $\bar{U}/\bar{U}_a \leq 0.82$, the agreement between the theoretical and experimental results is fairly good, while the curve corresponding to Eq. (3′) departs more and more from the experi-

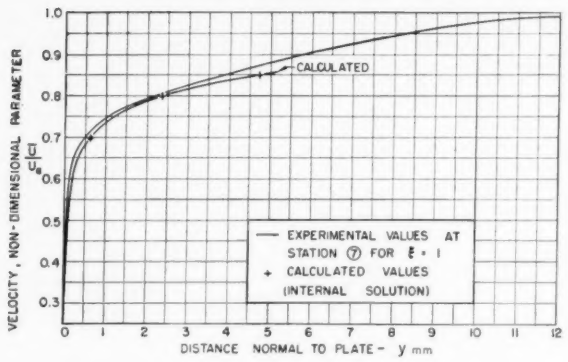
VELOCITY, NON-DIMENSIONAL PARAMETER
DISTANCE NORMAL TO PLATE - y mm
CALCULATED
EXPERIMENTAL VALUES AT STATION ⑦ FOR ξ = 1
CALCULATED VALUES (INTERNAL SOLUTION)

FIG. 1. Velocity distribution at Station 7 for $\xi = 1$.

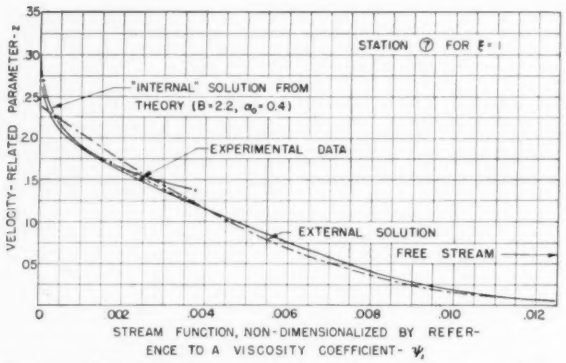
VELOCITY-RELATED PARAMETER - z
STREAM FUNCTION, NON-DIMENSIONALIZED BY REFERENCE TO A VISCOSITY COEFFICIENT - ψ1
STATION ⑦ FOR ξ = 1
"INTERNAL" SOLUTION FROM THEORY (B = 2.2, a0 = 0.4)
EXPERIMENTAL DATA
EXTERNAL SOLUTION
FREE STREAM

FIG. 2. Variation of the stream function upon traverse of the boundary layer, as related to a velocity parameter.

mental one for $\bar{U}/\bar{U}_a$ exceeding the above-mentioned limit. In the following equations,

$$\left.\begin{aligned} \psi_1 \int_0^\eta \frac{\bar{\rho}}{\bar{\rho}_a}\frac{\bar{U}}{\bar{U}_a}\,d\eta &= \int_0^\eta \frac{1-u_a^2}{1-u_a^2\,(\bar{U}^2/\bar{U}_a^2)}\,\frac{\bar{U}}{\bar{U}_a}\,d\eta \\ z &= u_a^2\,\frac{1-(\bar{U}^2/\bar{U}_a^2)}{1-u_a^2\,(\bar{U}^2/\bar{U}_a^2)} \end{aligned}\right\} \quad (17)$$

let $u_a^2 = 0.3649$. By use of the experimentally determined values of $\bar{U}/\bar{U}_a$, Fig. 2 is plotted, giving z as a function of ψ_1. Now because the experimental data for δ equal to the value of y for which $\bar{U}/\bar{U}_a = 0.995$ yield the relation $10^2\,\delta = 0.04 + 1.545\,\xi$, one obtains

$$\xi_1^* = 10^2 \quad \xi_1 = 0.04 \quad \xi + 1.545\,(\xi^2/2) \qquad (18)$$

whence $\xi_1^* = 0.8123$, for $\xi = 1$, and $2\sqrt{\xi_1^*} = 1.804$. Consequently, it may be inferred that (upon selection of the value 2 for $\zeta = 10\psi_1/\sqrt{h}\;2\sqrt{\xi_1^*}$, which implies the value 0.016 for ψ_1) the following value for $\sqrt{h}$ applies:

$$\sqrt{h} = 0.16/1.804\;(2) = 0.04435$$

Then, assuming $H = 0.24$, one obtains Table 2 through use of Eq. (10).

The values in Table 2 are also plotted in Fig. 2 as a graph of z versus ψ_1. The agreement between this plot and the experimental curve appears to be satisfactory. It also joins up satisfactorily with the graph produced by the "internal" solution, so that it seems unnecessary to push the approximation any further by following the method described in Section (A-4).

By use of the experimental values of z, as well as through aid of the calculated points on the graph of z versus ψ_1—which together describe the solution for the "internal" and "external" equations of the boundary layer (the theoretical and experimental data curves are joined together as indicated in Fig. 2)—the friction coefficient has been evaluated from Eq. (16′). It is found that, for the experimental curve, $C_r = 0.0024$ and that, for the theoretical curve, $C_r = 0.00235$.

At Station 2, located on the plate so that the abscissa $x = 11.92$ in. $= 302.8$ mm., one has

$$\xi = 0.3785; \quad M_a = 1.695; \quad R_x = 6.78 \times 10^6$$

(and still assuming $\gamma = 1$)

$$\beta = 0; \quad \bar{U}_a/V_t = 0.6041$$

If it is assumed that the local friction coefficient is $c_r = 0.00211$, it follows that

$$U_p^*/\bar{U}_a = 0.04076; \quad y = 0.02425 \times 10^{-2}\,y^* \text{ cm.}$$

Through reference to Eq. (3′), Table 3 follows.

TABLE 3
Velocity Distribution at Station 2

$\bar{U}/\bar{U}_a$	y^*	y	η
0.6	52.9	0.128 mm.	0.0001605
0.7	169.0	0.410 mm.	0.000513
0.8	581.5	1.411 mm.	0.001764
0.85	1,117.0	2.711 mm.	0.003390

The values in Table 3 of $\bar{U}/\bar{U}_a$ are plotted as a function of y on the graph of Fig. 3. The experimental results are also given. Again it can be seen that the agreement is good for $\bar{U}/\bar{U}_a \leq 0.8$ and that, for larger

TABLE 2
Data Required for Calculating Friction Coefficient at Station 7

ζ	0	0.05	0.10	0.15	0.20	0.25	0.30
ψ_1	0	0.0004	0.0008	0.0012	0.0016	0.0020	0.0024
z	0.2400	0.2265	0.2130	0.1997	0.1865	0.1736	0.1611
ζ	0.35	0.40	0.50	0.60	0.70	0.80	0.90
ψ_1	0.0028	0.0032	0.0040	0.0048	0.0056	0.0064	0.0072
z	0.1489	0.1372	0.1151	0.0951	0.0773	0.0619	0.0487
ζ	1.00	1.20	1.40	1.60	1.80	2.00	
ψ_1	0.0080	0.0096	0.0112	0.0128	0.0144	0.0160	
z	0.03775	0.02152	0.01145	0.00568	0.00262	0.00112	

values of $\bar{U}/\bar{U}_a$, the departure of the theoretical from the experimental results progresses somewhat more rapidly than was true in the preceding case for Station 7.

Following the same procedure as used in treating the data for Station 7, the values of ψ_1 and z, based on the experimental data, have been calculated. Then, from Eq. (18), one has $\xi_1^* = 0.1258$ and $2\sqrt{\xi_1^*} = 0.7094$. Let $\xi_{1,0}^*$ be the value of ξ_1^* that corresponds to $\xi = 1$ and set

$$\bar{\psi}_1 = \psi_1 \sqrt{\xi_{1,0}^*/\xi_1^*} \tag{19}$$

By use of this equation, into which the above-mentioned values are inserted, one obtains $\bar{\psi}_1 = 2.5421\ \psi_1$. This $(z, \bar{\psi}_1)$-curve is drawn in Fig. 4 to stand as a representation of the experimental results.

Now, taking $H = 0.26$ for the station under consideration, Eq. (10) yields Table 4.

The graph of z_1 versus $\bar{\psi}_1$, which depicts the values just calculated, is plotted on Fig. 4. Again, for this station, the agreement with experimental results, within the "external" region of the boundary layer, is satisfactory; the "join" with the previously evaluated "internal" solution is also good.

The friction coefficients obtained from Eq. (16′) are now found to be

$$(C_f)_{\text{exp.}} = 0.0028; \quad (C_f)_{\text{calc.}} = 0.0026$$

A typical velocity profile has also been determined by a reversal of these procedures and the use of presently established data. A hypothetical station along the plate has been selected for which M_a is still to be equal to 1.695 and for which $R_x = 10^6 \times 30$; hence, $\xi = 1.695$. For this station, however, no experimental data are available. As a consequence of the investigation pursued in the first report[1] of this series, it was found that, for the asymptotic solution of the problem concerning the turbulent flow along a flat plate, c_f and R_x are related to each other by an equation of the type

$$1/\sqrt{c_f} = A \log (c_f R_x) + B$$

If one accepts the validity of this relation and if use is made of the assumed values of c_f for the two values of Reynolds Number ($R_x = 6.78 \times 10^6$ and $R_x = 17.7 \times 10^6$) obtained previously, one is led to the conclusion in the present case that $c_f = 0.00176$. Corresponding to this value of c_f are the quantities

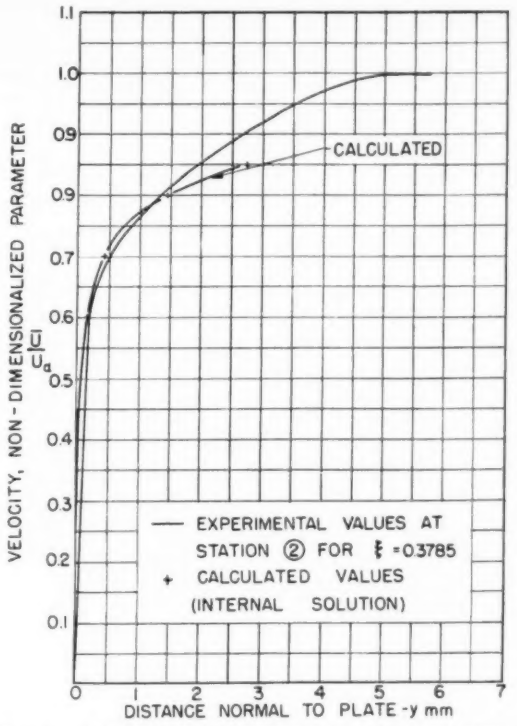
VELOCITY, NON-DIMENSIONALIZED PARAMETER U/U_a
DISTANCE NORMAL TO PLATE - y mm
CALCULATED
EXPERIMENTAL VALUES AT STATION ② FOR ξ =.03785
CALCULATED VALUES (INTERNAL SOLUTION)

FIG. 3. Velocity distribution at Station 2 for $\xi = 0.3785$.

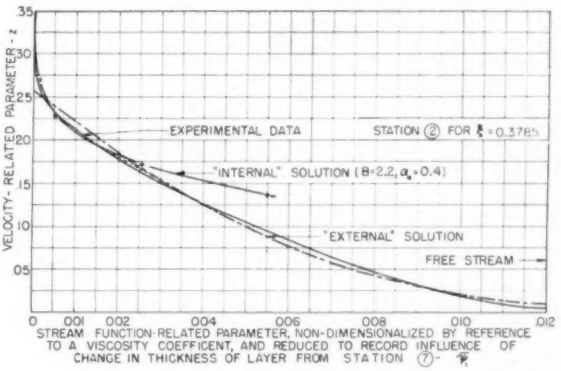
VELOCITY-RELATED PARAMETER - z
EXPERIMENTAL DATA
STATION ② FOR ξ =0.3785
"INTERNAL" SOLUTION (B=2.2, α_a=0.4)
"EXTERNAL" SOLUTION
FREE STREAM
STREAM FUNCTION-RELATED PARAMETER, NON-DIMENSIONALIZED BY REFERENCE TO A VISCOSITY COEFFICENT, AND REDUCED TO RECORD INFLUENCE OF CHANGE IN THICKNESS OF LAYER FROM STATION ⑦

FIG. 4. Variation of the nondimensionalized and "reduced" stream function as related to a velocity parameter.

$$U_p^*/U_a = 0.03722$$

$$y = 0.02687 \times 10^{-2}\, y^* \text{ mm.}$$

Table 5 results.

TABLE 4

Data Required for Computing Friction Coefficient at Station 2

ζ	0	0.10	0.15	0.20	0.25	0.30	0.35
$\bar{\psi}_1$	0.0004	0.0008	0.0012	0.0016	0.0020	0.0024	0.0028
z	0.2453	0.2307	0.2163	0.2021	0.1882	0.1746	0.1614
ζ	0.40	0.50	0.60	0.70	0.80	0.90	1.00
$\bar{\psi}_1$	0.0032	0.0040	0.0048	0.0056	0.0064	0.0072	0.0080
z	0.1486	0.1247	0.1030	0.0838	0.0670	0.0528	0.0409
ζ	1.20	1.40	1.60	1.80	2.00		
$\bar{\psi}_1$	0.0096	0.0112	0.0128	0.0144	0.0160		
z	0.02332	0.01241	0.00609	0.00284	0.00122		

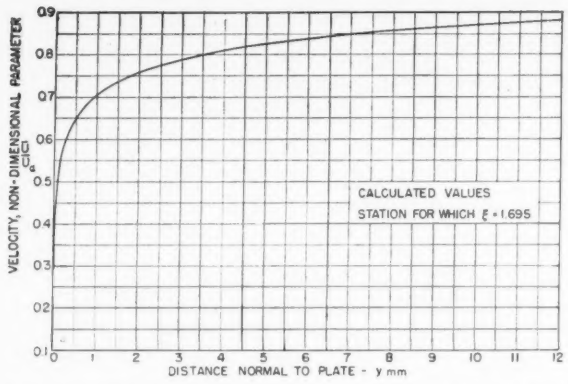

FIG. 5. Velocity distribution at the station for which $\xi = 1.695$

TABLE 5
Velocity Distribution at Station Where $\xi = 1.695$

$\bar{U}/\bar{U}_a$	y^*	y	η
0.6	95.0	0.2554 mm.	0.000319
0.7	338.9	0.9104 mm.	0.001138
0.8	1,311.0	3.5232 mm.	0.004405
0.85	2,681.0	7.2019 mm.	0.009004
0.9	5,651.0	15.1830 mm.	0.018980

The graph of $\bar{U}/\bar{U}_a$ versus y is constructed on the basis of these calculations giving the curve depicted in Fig. 5. By a procedure analogous to that previously used, the value of ξ_1^* is determined to be $\xi_1^* = 2.287$ and $2\sqrt{\xi_1^*} = 3.024$. It follows that

$$\bar{\psi}_1 = \psi_1 \sqrt{\xi_{1,0}^*/\xi_1^*} = 1.804\psi_1/3.024 = 0.5964\psi_1$$

From the above given values of $\bar{U}/\bar{U}_a$ and y, the evaluation of $\bar{\psi}_1$ and z has been carried out, and the resulting graph is plotted in Fig. 6. This curve of z vs. $\bar{\psi}_1$ is drawn in as a solid line.

The values for the solution of the "external" equation, given in Table 6, have been obtained by taking $II = 0.23$.

The graph that describes the relationship existing between these quantities also has been plotted on Fig. 6 (represented by a long-dashed line); the two solutions—i.e., the "internal" and the "external" ones—join together well. The joining curve is drawn in as a dotted line. The value of the total friction coefficient was calculated and found to be $C_f = 0.00222$.

Finally, Fig. 7 presents the graph of C_f versus R_x, drawn on a logarithmic scale. It is derived from the three pairs of values of C_f and R_x which were given above. From this graph one infers, at least within the restrictions of the approximation being considered, that it may be stated that

$$1/\sqrt{C_f} = A^* \log (R_x C_f) + B_0^* \qquad (18')$$

and it is evident that the value $A^* = 1.697$ may be deduced from those data. On the other hand, upon calculation of the local friction coefficient [by means of the equation, $1/\sqrt{c_f} = A \log (R_x c_f) B_0$], one finds that the following approximate formulas hold:

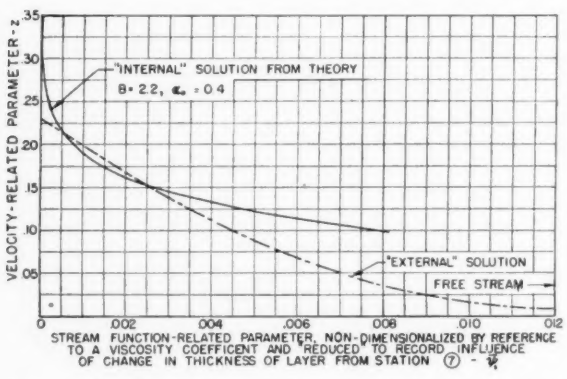
VELOCITY-RELATED PARAMETER - z
"INTERNAL" SOLUTION FROM THEORY
B = 2.2, ε = 0.4
"EXTERNAL" SOLUTION
FREE STREAM
STREAM FUNCTION-RELATED PARAMETER, NON-DIMENSIONALIZED BY REFERENCE TO A VISCOSITY COEFFICENT AND REDUCED TO RECORD INFLUENCE OF CHANGE IN THICKNESS OF LAYER FROM STATION ⑦ - $\bar{\psi}_1$

FIG. 6. Variation of the nondimensionalized and "reduced" stream function as related to a velocity parameter.

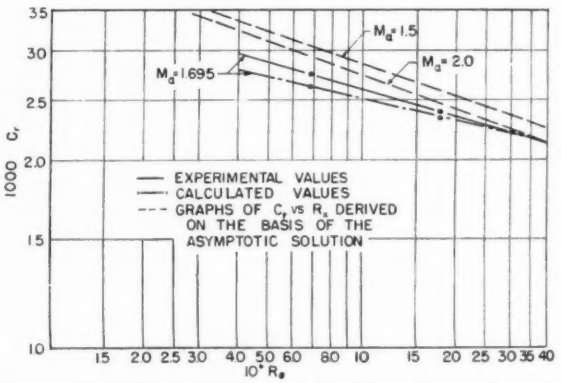

FIG. 7. Plot of the total friction coefficient versus Reynolds Number for various Mach Numbers.

TABLE 6
Data Required for Calculating Friction Coefficient at Station Where $\xi = 1.695$

ζ	0	0.05	0.10	0.15	0.20	0.25	0.30
$\bar{\psi}_1$	0	0.0004	0.0008	0.0012	0.0016	0.0020	0.0024
z	0.2300	0.2170	0.2041	0.1914	0.1788	0.1664	0.1544
ζ	0.35	0.40	0.50	0.60	0.70	0.80	
$\bar{\psi}_1$	0.0028	0.0032	0.0040	0.0048	0.0056	0.0064	
z	0.1427	0.1315	0.1103	0.0911	0.0741	0.0593	
ζ	0.90	1.00	1.20	1.40	1.60	1.80	
$\bar{\psi}_1$	0.0072	0.0080	0.0096	0.0112	0.0128	0.0144	
z	0.04671	0.03618	0.02063	0.01097	0.00544	0.00251	
			ζ	2.00			
			$\bar{\psi}_1$	0.0160			
			z	0.00108			

$$\left.\begin{aligned} c_f &\cong \frac{C_f}{1 + 2A\sqrt{c_f}} \cong C_f(1 - 2A\sqrt{C_f}) \\ A &= A^*\sqrt{1 + 2A^*\sqrt{C_f}} \cong A^*(1 + A^*\sqrt{C_f}) \end{aligned}\right\} \quad (19')$$

Consequently, from these relationships one obtains $A = 1.823$.

These results permit one to check whether the values assumed for c_f in the three cases considered above agree with the values of C_f derived on the basis of the above assumptions.

Introducing into Eq. (19′) the value of A just obtained, one finds: for $C_f = 0.0022$,

$$c_f = 0.0022\ (1 - 3.645 \times 0.0472) = 0.00184 \text{ (instead of } 0.00176)$$

for $C_f = 0.0024$,

$$c_f = 0.0024\ (1 - 3.645 \times 0.0490) = 0.00197 \text{ (instead of } 0.0019)$$

for $C_f = 0.00276$,

$$c_f = 0.00276\ (1 - 3.645 \times 0.0525) = 0.00223 \text{ (instead of } 0.00211)$$

The asymptotic equation, Eq. (55), deduced in the first report[1] of this series may now be tested. It is repeated here as

$$A = (1/\sqrt{2})\ (1/\sqrt{1 - u_a^2})\ (1/F)$$

where

$$F = \frac{\alpha_0}{u_a}\left[-\frac{1}{2(1-\beta)}\log(1 - u_a) + \frac{1}{2(1+\beta)}\log(1 + u_a) + \frac{\beta}{1+\beta^2}\log(1 - \beta u_a)\right]$$

It is interesting to note that, if β is assumed equal to 0 and $\alpha_0 = 0.394$, the asymptotic solution yields the value $F = 0.5050$ or, thus, $A = 1.925$. As far as the calculation of the thickness of the boundary layer is concerned, it may be easily determined through use of Eq. (15). Since the value of z which corresponds to $\bar{U}/\bar{U}_a = 0.995$ is $z = 0.00571$, it may be seen from the tables that, in all of the three cases studied, this value implies that the magnitude of ζ_0 is close to $\zeta_0 = 0.16$. The value of z which applies to Station 7 is first selected, and then making use of it in the evaluation of the coefficient B of Eq. (15), one infers that $u_aB = 1.979$; hence,

$$\bar{\delta} = 2 \times 1.979^2 \times 0.001967\xi = 1.5404 \times 10^{-2}(\xi)$$

This proportionality factor is in good agreement with the previously given value.

(D) Application of the Method Just Described to the Prediction on a Theoretical Basis of the Velocity Profile in the "Inside" of the Boundary Layer and Determination of the Related Drag Coefficient

For the practical application of the above formulas, not to the analysis of the experimental results but to the theoretical prediction of the velocity profiles within the boundary-layer cross sections, as well as to the prediction of the related friction drag coefficients, it is necessary to make use of the method of successive approximations. As first approximation values for c_f one may take, for instance, those that are evolved, for given Mach Numbers and Reynolds Numbers, by use of the asymptotic solution, provided these results are diminished in the same ratio as in the cases considered in Section (C).

Analogously, in order to predict the law of variation of the thickness of the boundary, one may take as the first approximation $\bar{\delta} = 0.332\sqrt{c_f}\,\xi$. This relation is formally analogous to that corresponding to the asymptotic solution, as well as to Eq. (15). The coefficient of ξ has been deduced by taking into account the results of the calculations performed in Section (C). It should be remarked that u_aB does not depend appreciably upon u_a. By following the method suggested and applied in Section (C), the assumptions just discussed afford the means of computing the velocity profiles for the various cross sections of the boundary layer. The construction of such profiles permits one, in turn, to determine the value of the coefficient C_f and the thickness $\bar{\delta}$ of the boundary layer. It will then be possible to obtain a second approximation for c_f and for $\bar{\delta}$; consequently, such an approximation will enable one to determine the corrections to be applied to the previously obtained results—that is, these corrections are to be taken as the differences between the assumed and the calculated coefficients.

(E) Graph of the Drag Coefficients Derivable from the Asymptotic Solution

The experiments by Young and Wilson clearly show a decrease in the drag coefficient with increasing Mach Number, and a comparable theoretical check on this coefficient may be obtained by use of the asymptotic equations of the flow. In addition, it appears from the preceding paragraphs that, in order to bring the theoretical equations and the experimental results into satisfactory agreement (as far as the determination of the velocity in the region of the boundary layer close to the wall is concerned), it is necessary to set $\beta = 0$. With this provision in mind, a calculation has been carried through by means of the asymptotic equations [Eqs. (12) of the first report[1] of this series] in order to obtain the values of the coefficients A and B_0 which define the asymptotic drag law,

TABLE 7
Calculations for Obtaining Drag Coefficients from the Asymptotic Solutions

	F		A		$0.4342B$	
M_a	$\beta = 0$	$\beta = -0.2$	$\beta = 0$	$\beta = -0.2$	$\beta = 0$	$\beta = -0.2$
0	0.394	0.394	1.795	1.795	1.647	1.647
0.5	0.400	0.392	1.809	1.849	1.638	1.657
1.0	0.418	0.402	1.851	1.928	1.614	1.649
1.5	0.445	0.420	1.915	2.027	1.580	1.628
2.0	0.476	0.444	1.995	2.138	1.540	1.599

$$1/\sqrt{c_f} = A \log (R_x c_f) + B - A \log 2A$$

The calculation was carried out for several Mach Numbers, as well as for two values of β—i.e., for $\beta = 0$ and for $\beta = -0.2$. The values for the experimentally determined constants α_0 and b are taken to be equal to *0.394* and *11.7*, respectively. With the use of these values, the asymptotic formulas giving A and B (which, for $M_a = 0$, become formally equal to the equations suggested by von Kármán as applicable in the case of an incompressible fluid) turn out to be, when $M_a = 0$, identically the same thing as the von Kármán formula. The results of these calculations are given in Table 7.

REFERENCES

[1] Ferrari, C., *Study of the Boundary Layer at Supersonic Speeds in Turbulent Flow: Case of Flow Along a Flat Plate*, Quarterly of Applied Mathematics, Vol. VIII, No. 1, April, 1950.

[2] Ferrari, C., *The Turbulent Boundary Layer in a Compressible Fluid with Positive Pressure Gradient*, Journal of the Aeronautical Sciences, Vol. 18, No. 7, pp. 460–477, July, 1951.

[3] Gevrey, M., *Sur les Équations aux Dérivées Partielles du Type Parabolique*, Thesis presented to the Faculté des Sciences de Paris, pp. 90–93; Gauthier Villars (Imprimeur Libraire de l'École Polytechnique), Paris, 1913.

[4] von Kármán, Theodore, and Millikan, C. B., *On the Theory of Laminar Boundary Layers Involving Separation*, N.A.C.A. T.R. No. 504, 1934.

[5] Young, E. C., and Wilson, R. E., *First Interim Report on Experimentally Determined Turbulent Boundary Layer Characteristics at Supersonic Speeds*, Bumblebee CF-1095, Defense Research Lab. No. 181, Univ. of Texas No. 1-AA-9, September 25, 1948.

Readers' Forum

BRIEF REPORTS of investigations in the aeronautical sciences and discussions of papers published in the JOURNAL are presented in this special department. The publication will be completed approximately 8 to 10 weeks after receipt of the material. The Editorial Committee does not hold itself responsible for the opinions expressed by the correspondents. Contributions should not exceed 800 words in length.

Turbulent Diffusion from a Source in Turbulent Shear Flow

J. O. Hinze
Royal Dutch/Shell Laboratory, Delft, Holland
March 22, 1951

IN THIS JOURNAL, Dr. Corrsin[1] explained the observed skewness in transverse temperature distributions close behind a fine, heated wire set perpendicular to both mean flow and direction of the greatest gradient by assuming that this transverse temperature distribution is simply equal to the probability density of the lateral velocity fluctuations. His hypothesis was that the skewness in this density is the result of the lateral gradient in lateral turbulence intensity.

However, there is another aspect, not hitherto considered, in diffusion by continuous movements. It is not entirely correct to put the transverse distribution equal to the probability density of the lateral velocity fluctuations. It is better to assume this transverse distribution to be equal to the probability density $Y(y)$ of the lateral distances y covered by the fluid particles that have passed the source (provided the effect of molecular diffusion may be neglected).

Let Γ be a transportable quantity; then, according to this assumption

$$\Gamma(y)/\Gamma(0) = Y(y)/Y(0) \tag{1}$$

According to the Lagrangian method for describing the path of a particle, the coordinates of the particles at time t are

$$y = vt$$
$$x = (U + u)t$$

whence

$$\eta = y/x = v/(U + u) \tag{2}$$

If we assume $u/U < 1$, Eq. (2) may be written

$$\eta = \frac{v}{U}\left(1 - \frac{u}{U} + \frac{u^2}{U^2} - \frac{u^3}{U^3} + \dots\right)$$

If the average value of y for a large number of particles is taken, the result is

$$\bar{\eta} = -\frac{\overline{uv}}{U^2} + \frac{\overline{u^2v}}{U^3} - \frac{\overline{u^3v}}{U^4} + \dots \tag{3}$$

If, in this expression the effect of the triple- and higher order correlations is negligibly small, the value of $\bar{\eta}$ must be proportional to the shearing stress in the flow at the point of the source,

$$\bar{\eta} \simeq -(\overline{uv}/U^2) = \tau/\rho U^2 \tag{4}$$

Since by definition

$$\bar{\eta} = \int_{-\infty}^{+\infty} \frac{Y(\eta)}{Y(0)}\,\eta\,d\eta = \int_{-\infty}^{+\infty} \frac{\Gamma(\eta)}{\Gamma(0)}\,\eta\,d\eta$$

the average value of $\bar{\eta}$ is identical with the ordinate of the centroid of the Γ-distribution surface.

The skewed Γ-distribution is determined by the probability density $Y(y)$. Let $F(u, v)$ be the probability density of the joint distribution u, v. According to the relation [Eq. (2)] between y and the turbulence velocities u and v, the probability density $Y(y)$ apparently is obtained by taking from $F(u, v)$ all those values for which the relation [Eq. (2)] holds, or we must integrate $F(u, v)$ along a path $v/(U + u) = \eta$ = constant. Thus,

$$Y(\eta) = \frac{1}{U}\int_{-\infty}^{+\infty} F(u, v)\,ds$$

along the path $v/(U + u) = \eta$.

Since

$$ds = \sqrt{1 + (dv/du)^2}\,du = \sqrt{1 + \eta^2}\,du$$

the expression for $Y(\eta)$ becomes

$$Y(\eta) = \sqrt{1 + \eta^2}\,\frac{1}{U}\int_{-\infty}^{+\infty} F[u, \eta(U + u)]\,du \tag{5}$$

The function $F(u, v)$ has to satisfy the conditions

$$\bar{u} = \frac{1}{U^2}\int\int_{-\infty}^{+\infty} F(u, v)\,u\,du\,dv = 0$$

$$\bar{v} = \frac{1}{U^2}\int\int_{-\infty}^{+\infty} F(u, v)\,v\,du\,dv = 0$$

$$\frac{1}{U^2}\int\int_{-\infty}^{+\infty} F(u, v)\,u^2\,du\,dv = \overline{u^2}$$

$$\frac{1}{U^2}\int\int_{-\infty}^{+\infty} F(u, v)\,v^2\,du\,dv = \overline{v^2}$$

$$\frac{1}{U^2}\int\int_{-\infty}^{+\infty} F(u, v)\,du\,dv = 1$$

At the present juncture, nothing is known about the function $F(u, v)$. But a function that satisfies all the above conditions is the normal correlation function,

$$F(u, v) = \frac{U^2}{2\pi u' v'\sqrt{1 - R^2}} \times \exp\left[\frac{-1}{2(1 - R^2)}\left(\frac{u^2}{u'^2} - \frac{2R\,uv}{u'v'} + \frac{v^2}{v'^2}\right)\right] \tag{6}$$

where

$$R = \overline{uv}/u'v', \quad u' = \sqrt{\overline{u^2}}, \quad v' = \sqrt{\overline{v^2}}$$

If we assume the turbulence velocities to be normally correlated, though this implies that the marginal distributions or the probability densities of u and v separately are Gaussian, the expression for $Y(\eta)$ becomes

$$Y(\eta) = U\sqrt{\frac{1 + \eta^2}{2\pi(v'^2 - 2R\eta\,u'v' + \eta^2u'^2)}} \times \exp\left[\frac{-U^2\eta^2}{2v'^2\left(1 - 2R\,\frac{u'}{v'}\,\eta + \frac{u'^2}{v'^2}\,\eta^2\right)}\right]$$

Using Eq. (1), one obtains for the Γ-distribution

$$\frac{\Gamma(\eta)}{\Gamma(0)} = \sqrt{\frac{1 + \eta^2}{1 + 2\frac{\tau}{\rho}\frac{U^2}{U^2v'^2}\,\eta + \frac{u'^2}{v'^2}\eta^2}} \times \exp\left[\frac{-U^2\eta^2}{2v'^2\left(1 + 2\,\frac{\tau}{\rho}\frac{U^2}{U^2v'^2}\,\eta + \frac{u'^2}{v'^2}\eta^2\right)}\right] \tag{7}$$

if at the same time

$$\tau = -\rho\,\overline{uv} = -\rho\,R\,u'v'$$

is introduced in the expression for Γ.

It may be interesting to see to what expression (7) reduces when the turbulence is isotropic. In this case, $\tau = 0$ and $u' = v'$.

$$\Gamma(\eta)/\Gamma(0) = \exp\{-U^2\eta^2/[2v'^2(1+\eta^2)]\} \qquad (8)$$

According to this result, the spread for great values of η is greater than according to the Gaussian error law. This difference is caused by the fact that the effect of the turbulence velocity u on the spread has not been neglected as it had been hitherto.

It is intended to present the results of applying the above considerations to measurements of the local diffusion of heat from a heated wire located in the turbulent mixing zone of a plane free jet to the general discussion on heat transfer and related fluid mechanics at the meeting of the Institution of Mechanical Engineers and the American Society of Mechanical Engineers to be held in London, September, 1951.

Reference

[1] Corrsin, S., *Hypothesis for Skewness of the Probability Density of the Lateral Velocity Fluctuations in Turbulent Shear Flow*, Journal of the Aeronautical Sciences, Vol. 17, No. 7, p. 396, July, 1950.

Note on Sphere Drag Data

Frederick S. Sherman
University of California at Berkeley
May 4, 1951

In his recent report[1] on sphere drag data at supersonic speeds and low Reynolds Numbers, Kane remarks that the experimental drag coefficients obtained may have been fictitiously low because of interference between the cross-stream support rod and the sphere boundary layer. To investigate this matter, his tests were repeated (again under the sponsorship of O.N.R.-O.A.R.) last summer, using the same wind-tunnel facilities but employing a rear sting support arrangement for the sphere models. The principal results of these tests are shown in Fig. 1, in which Kane's results are indicated by the curve that best fits his data.

The drag coefficients obtained with the rear sting support method differ strongly from those obtained with a cross-stream support only for Reynolds Number <100. Below this value the discrepancy becomes large, reaching about 20 per cent at the lowest Reynolds Numbers encountered. Contrary to the expectations that prompted these supplementary tests, the new drag coefficients were smaller than those presented in reference 1. It might appear, then, that the interference initiated in the flow about the sphere by a rear sting support is at least equally as serious as that caused by the cross-stream rod. To date no optimum support technique has been developed here.

Also apparent in the more recent drag results are certain discrepancies between drag-coefficient values obtained at a given Reynolds Number, but with different size spheres. These discrepancies were identifiable because of an improvement in pressure-measuring instrumentation which reduced experimental scatter considerably. They have not been explained satisfactorily in terms of the small variations of Mach Number involved but may be due to these, in combination with such factors as the nonuniformity and limited extent of the free jet, nonsimilarity of support geometries, and variations of sphere surface condition.

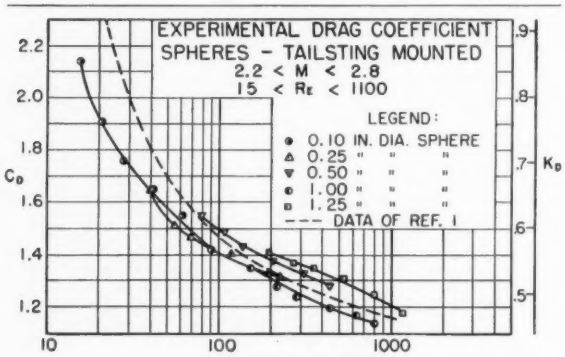

FIG. 1

Reference

[1] Kane, E. D., *Sphere Drag Data at Supersonic Speeds and Low Reynolds Numbers*, Journal of the Aeronautical Sciences, Vol. 18, No. 4, pp. 259-270, April, 1951.

Effective End Restraint of Columns by Frequency Measurements

Harold Lurie
The RAND Corporation
April 24, 1951

In a recent investigation, I came across a paper by Stephens in this Journal[1] which is based on a fallacious argument, and apparently his erroneous analysis has not been pointed out subsequently. Stephens proposed that the end restraint of a beam could be found by measuring the natural vibration frequency of the beam, where the end restraint is defined as the coefficient c in the basic Euler buckling equation

$$P_{cr} = c\pi^2 EI/l^2$$

To correlate the degree of end fixity with the natural frequency, Stephens used the value of c for the following four different types of end restraint: (a) one end fixed, one end free ($c = 1/4$); (b) both ends pinned ($c = 1$); (c) one end fixed, one end pinned ($c = 2.047$); and (d) both ends fixed ($c = 4$).

The frequency equations for these four types of restraint were then calculated, and the first eigenvalue determined for each case. The square of the eigenvalue was called the "frequency constant," denoted by K. The values for K are 3.516, 9.870, 15.421, and 22.373, respectively, for the above four cases. By plotting K against c, Stephens obtained a single curve. Thus, to determine the degree of end restraint, he stated that it was only necessary to determine the natural vibration frequency by test, after which K could be determined from the equation

$$f = (K/2\pi\, l^2)\,\sqrt{EI/\rho}$$

The corresponding value of c, which is the measure of the end fixity, could then be found from the curve of K against c.

However, his proposed relationship between K and c is not unique, since there may be more than one value of K corresponding to each value of c. This might be suspected from the physics of the problem. It is feasible for two identical bars with differently restrained ends to have the same resultant fixity coefficient c. However, different modes of vibration and, hence, different frequencies would be anticipated.

A simple example will illustrate this. Consider a strut elastically restrained at each end, and suppose the restraint is such as to give an end fixity coefficient equal to 2.047 (the same as for one end fixed, one end pinned). The value of K for such a beam

can be calculated. Suppose the spring constant at each end is the same, and denote it by α. Taking the origin of coordinates at the center of a beam of length $2L$, the boundary conditions are

$$\left.\begin{aligned} v &= 0 \qquad \text{at } x = \pm L \\ EIv'' &= \alpha v' \qquad \text{at } x = \pm L \end{aligned}\right\} \tag{1}$$

The general solution of the buckling problem is[2]

$$v = A \cos \beta x + B \sin \beta x + Cx + D$$

where $\beta^2 = P/EI$.

As

$$P = c\pi^2 EI/4L^2$$

therefore,

$$\beta = \pi\sqrt{c}/2L \tag{2}$$

Putting in the boundary conditions [Eqs. (1)],

$$(EI/\alpha)\beta = \tan \beta L$$

Substituting the value for β from Eq. (2),

$$\alpha = (\pi EI\sqrt{c}/2L) \cot (\pi\sqrt{c}/2) \tag{3}$$

The general solution for free vibrations is[3]

$$v = A \cos \lambda x + B \sin \lambda x + C \cosh \lambda x + D \sinh \lambda x$$

where

$$\lambda^2 = \omega\sqrt{\rho/EI}$$

Putting in the boundary conditions [Eqs. (1)],

$$\alpha = 2\ EI\lambda/(\tan \lambda L + \tanh \lambda L) \tag{4}$$

As the value of α is to be the same for buckling and vibrations, Eqs. (3) and (4) may be equated. Therefore,

$$\frac{2\lambda L}{\tan \lambda L + \tanh \lambda L} = \frac{\pi\sqrt{c}}{2} \cot \frac{\pi\sqrt{c}}{2} \tag{5}$$

By taking $c = 2.047$ as for the fixed-pinned strut, Eq. (5) becomes

$$2\lambda L/(\tan \lambda L + \tanh \lambda L) = -1.8052$$

Therefore,

$$2\lambda L = 3.776$$

$$K = (2\lambda L)^2 = 14.258$$

Hence, for a symmetric strut with elastically restrained ends, an end fixity coefficient of 2.047 corresponds to a frequency constant of 14.258; whereas for a fixed-pinned strut with the same end fixity coefficient, the frequency constant is 15.421. It may be concluded that Stephen's single curve relating c to K is not justifiable.

In the same paper, Stephens derives the relation between end thrust and vibration frequency as

$$P = m\ P_{cr}\ [1 - (f/f_0)^2]$$

where m is a constant depending on the end restraint. He lists m for various end conditions. This again is incorrect, since m is actually a function of P if the ends are not pinned. The constant m was determined by the energy method, which makes it dependent upon the approximation used. According to the above formula, $P \neq P_{cr}$ when $f = 0$. However, using exact methods, it can be shown that as P is increased, f decreases until it finally vanishes at $P = P_{cr}$.

References

[1] Stephens, B. C., *Natural Vibration Frequencies of Structural Members As an Indication of End Fixity and Magnitude of Stress*, Journal of the Aeronautical Sciences, Vol. 4, No. 2, 1936.

[2] Lurie, Harold, *A Note on the Buckling of Struts*, Journal of the Royal Aeronautical Society, Vol. 55, March, 1951.

[3] Timoshenko, S., *Vibration Problems in Engineering*, D. Van Nostrand Company, Inc., 1937.

Comment on the Calculation of Deflections of Indeterminate Structures

Carlos Thalau
Instituto Aerotécnico, Córdoba, Argentina

May 8, 1951

WITH REFERENCE TO *Note on the Calculation of Deflections of Indeterminate Structures* by Bruno A. Boley and Roland H. Moore, published in the JOURNAL OF THE AERONAUTICAL SCIENCES, August, 1950, and the considerations of H. F. Michielsen in the same publication, April, 1951, concerning the same item, the following remarks may be of interest.

The fact that in calculating a deflection $\delta_{i'k'}$ of an indeterminate structure it is possible to write

$$\delta_{i'k'} = \delta_{i'k_0} = \delta_{i_0k'}$$

i.e., to substitute for the indeterminate structure a conveniently chosen determinate structure in *one* of the two loading systems by applying the principle of virtual displacements (prime for the indeterminate structure and sub zero for the determinate structure) has been known as the "law of reduction" (Reduktionssatz) for a number of years.

As I remember, Mueller-Breslau, in his *Graphische Statik der Baukonstruktionen* (published by Kroener, Leipzig), and Kammer, in his *Statisch unbestimmte Hauptsysteme* (published by Springer, Berlin), have already treated this fact in detail. Still other sources probably exist.

In our book *Aufgaben aus der Flugzeugstatik* [Thalau-Teichmann (published by Springer, Berlin, 1933)], which I had the honor to present to your Institute at that time, we treated the law of reduction with a few examples on pages 202 and 285, since it belongs among the tools of every engineer concerned with statics of indeterminate structures.

In agreement with the wishes of the authors of the note, the "law of reduction" already has found its way into a few books.

◆

Note on "Heat Transfer by Laminar Flow from a Rotating Plate"*

Arthur N. Tifford
The Ohio State University, Columbus

May 8, 1951

THE RECENT ABSTRACT[1] of an exact solution of the energy equation in the case of laminar flow along an isothermal rotating plate is interesting. It is related to an exact solution of the energy equation in the case of flow near a forward stagnation point obtained here last summer in work supported by the Office of Air Research, U.S.A.F. The latter analysis resulted from a desire to investigate the influence upon boundary-layer solutions of extremely large surface temperature variations. Since, under such conditions, Prandtl's order-of-magnitude arguments do not significantly simplify the equations, the exact equations were analyzed. The detailed results will be reported soon.

Our earlier exact solution suggests that the rotating plate being considered need not necessarily be isothermal in order for the complete energy equation to be tractable. A little thought on the matter reveals that the form of solution given in reference 1 may, in fact, be interpreted in such a manner as to be applicable when the surface temperature distribution is parabolic. This is only a special case, however, of the more general surface temperature distribution

* Work supported by the Office of Air Research, U.S.A.F.

$$T_w = T_{\text{ref.}} + a_0 + a_2 r^2 + a_4 r^4 + \ldots a_{2n} r^{2n}$$

that may be subjected to an exact analysis. The associated general solution may be written as,

$$T - T_{\text{ambient}} = \bar{g}(z) + a_0 g_0(z) + a_2 g_2(z) + a_4 g_4(z) + \ldots a_{2n} g_{2n}(z) + r^2[\bar{s}(z) + a_2 s_2(z) + a_4 s_4(z) + \ldots a_{2n} s_{2n}(z)] + r^4[a_4 t_4(z) + \ldots a_{2n} t_{2n}(z)] + \ldots + r^{2n} a_{2n} \gamma_{2n}(z)$$

where all functions are simply related to universal functions (for a given Prandtl Number) and where the barred functions completely account for the contribution of frictional heating. It would be of additional interest for Drs. Millsaps and Pohlhausen to consider some of the facets† of the more general solution in their forthcoming paper.

† For example, as in the case of an isothermal spinning surface,[2] there is an analogy, when the Prandtl Number is unity, between the rate of heat transfer and the power expenditure required to overcome frictional resistance to rotation. In the case of the rotating plate, however, the analogy applies even when the surface temperature distribution is parabolic.

REFERENCES

[1] Millsaps, Knox, and Pohlhausen, Karl, *Heat Transfer by Laminar Flow from A Rotating Plate*, Readers' Forum, Journal of the Aeronautical Sciences, Vol. 18, No. 5, pp. 354–355, May, 1951.

[2] Tifford, Arthur N., *Letter to the Editor*, Journal of the Aeronautical Sciences, Vol. 15, No. 5, pp. 280–281, May, 1948.

Similarity Laws for Slender Bodies of Revolution in Hypersonic Flows

(*Continued from page 530*)

similarity law for three-dimensional flow has been presented, including its application to finite span wings and wing-body combinations. However, the accuracy and range of applicability has not as yet been established. It seems clear from these results that future effort should be directed toward further verification of the law in its various forms and toward determination of its range of applicability.

REFERENCES

[1] Tsien, Hsue-shen, *Similarity Laws of Hypersonic Flows*, Journal of Mathematics and Physics, Vol. 25, No. 3, October, 1946.

[2] Ehret, Dorris M., Rossow, Vernon J., and Stevens, Victor I., *An Analysis of the Applicability of the Hypersonic Similarity Law to the Study of Flow About Bodies of Revolution at Zero Angle of Attack*, N.A.C.A. T.N. No. 2250, 1950.

[3] Hayes, Wallace D., *On Hypersonic Similitude*, Quarterly of Applied Mathematics, Vol. V, No. 1, April, 1947.

[4] Massachusetts Institute of Technology, Department of Electrical Engineering, Center of Analysis, *Tables of Supersonic Flow Around Cones*, by the Staff of the Computing Sections, Center of Analysis under the direction of Zdenek Kopal, Technical Report No. 1, Cambridge, 1947.

[5] Allen, H. Julian, *Pressure Distribution and Some Effects of Viscosity on Slender Inclined Bodies of Revolution*, N.A.C.A. T.N. No. 2044, 1950.

[6] Hamaker, Frank M., Neice, Stanford E., and Eggers, A. J., Jr., *The Similarity Law for Hypersonic Flow About Slender Three-Dimensional Shapes*, Prospective N.A.C.A. publication.